A uniform search for thermonuclear burst oscillations in the RXTE legacy dataset

Anna V. Bilous<sup>1</sup> and Anna L. Watts<sup>1</sup>

Anton Pannekoek Institute for Astronomy, University of Amsterdam, Science Park 904, 1098 XH Amsterdam

## Submitted to ApJS

#### ABSTRACT

We describe a blind uniform search for thermonuclear burst oscillations (TBOs) in the majority of Type-I bursts observed by RXTE (2118 bursts from 57 neutron stars). We examined 2–2002 Hz power spectra from the Fourier transform in sliding 0.5–2s windows, using fine-binned light curves in 2-60 keV energy range. The significance of the oscillation candidates was assessed by simulations which took into account light curve variations, dead time and sliding time windows. Some of our sources exhibited multi-frequency variability at  $\lesssim 15\,\mathrm{Hz}$  that cannot be readily removed with light-curve modeling and may have an astrophysical (non-TBO) nature. Overall, we found that the number and strength of potential candidates depends strongly on the parameters of the search. We found candidates from all previously known RXTE TBO sources, with pulsations that had been detected at similar frequencies in multiple independent time windows, and discovered TBOs from SAX J1810.8-2658. We could not confirm most previously-reported tentative TBO detections or identify any obvious candidates just below the detection threshold at similar frequencies in multiple bursts. We computed fractional amplitudes of all TBO candidates and placed upper limits on non-detections. Finally, for a few sources we noted small excess of candidates with powers comparable to fainter TBOs, but appearing in single independent time windows at random frequencies. At least some of these candidates may be noise spikes that appear interesting due to selection effects. The potential presence of such candidates calls for extra caution if claiming single-window TBO detections.

Keywords: burst oscillations; LMXB

## 1. INTRODUCTION

Thermonuclear burst oscillations (TBOs) are fast (typically, with a frequency of a few hundreds of Hz), relatively faint (fractional amplitude of a few percent) oscillations of photon count rate, detected in about 20% of known Type I X-ray bursts<sup>1</sup>. The phenomenon of TBOs is attributed to the development of bright patches during thermonuclear explosions on the surface of accreting neutron stars. Several theories of patch formation have been proposed: flame spreading from the ignition point of the bursts (e.g. Strohmayer et al. 1997b), cooling wakes (Mahmoodifar & Strohmayer 2016), convective patterns (Garcia et al. 2018), or largescale (magneto)hydrodynamical oscillations in the burning material, induced by the spreading flame (e.g. Hevl 2004). However, none of them can explain all of the observed TBO properties, motivating the development of

Corresponding author: Anna Bilous A.Bilous@uva.nl, hanna.bilous@gmail.com

better physical models for the ignition and progression of thermonuclear reactions on the neutron star surface (see the review by Watts 2012).

From the observational side, it is important to establish as complete a picture of TBOs as possible. Finding TBOs and constraining their properties is not always straightforward: although oscillations are highly coherent, their frequencies can drift (or jump) by a few Hz during the typical few-second duration of the TBO, with oscillations sometimes disappearing and reappearing throughout the burst (Muno et al. 2002a,b). The standard TBO search method relies on the Fourier transform (or calculation of  $Z^2$ -statistics) in a series of closely overlapping windows covering the burst duration (e.g. Strohmayer et al. 1998). Blind searches assume a constant frequency within a single time window, since searching for frequency derivatives adds an extra dimension to parameter space and is thus computationally expensive.

Estimates of signal significance are traditionally done analytically, based on simple photon counting statistics (Groth 1975; van der Klis 1989). At the same time, it has been recognized that the distribution of noise powers

<sup>&</sup>lt;sup>1</sup> http://www.sron.nl/~jeanz/bursterlist.html, see also Galloway et al. (2008), Watts (2012), and references therein.

in real spectra is more complicated, being influenced by the burst envelope and dead time of the detector (van der Klis 1989; Zhang et al. 1995). Using overlapping time windows and custom data filters complicates calculations of the number of independent trials, and thus estimates of TBO candidate significance. Some previous studies addressed these issues by discarding low frequencies affected by variation of the photon count rate due to the burst envelope (e.g. Ootes et al. 2017), directly measuring the dead time-affected average noise power (e.g. Thompson et al. 2005), using a conservative number of trials (e.g. Bhattacharyya 2007), or estimating candidate significance with the simulation of data for a small number of bursts (e.g. Kaaret et al. 2007).

Searching for TBOs requires a sensitive instrument, operating in hard  $(1\text{--}30\,\text{keV})$  X-rays and capable of providing  $\mu\text{s}$  time resolution. So far, the majority of TBO studies have been performed using the large set of observations from the Rossi X-ray Timing Explorer (RXTE, Jahoda et al. 2006), although other telescopes such as Swift (Strohmayer et al. 2008) and AstroSat (Verdhan Chauhan et al. 2017) have also been used to search for TBOs. The relatively quiet period that followed the termination of RXTE's mission in Dec 2011 ended with the recent launch of NICER (Arzoumanian et al. 2014) in 2017; and ongoing studies for the next generation of instruments, such as eXTP (Zhang et al. 2019) and STROBE-X (Ray et al. 2018), are also providing new impetus for TBO studies.

Previous TBO searches explored relatively small subsets of data and were conducted using different methods or search parameters. In order to prepare for searches with new satellites and to provide a uniform picture for theoretical modeling of TBOs, we have undertaken the first comprehensive blind search for TBOs across almost the entire archival RXTE burst data set, using the 2015 pre-release version of the Multi-INstrument Burst ARchive (MINBAR<sup>2</sup>, Galloway et al., in prep). We use the standard approach of constant frequency and overlapping windows, but estimate the significance of candidates through data simulation that takes into account lightcurve (LC) variations, dead time and number of trials. This more realistic noise model allows us to search for TBOs in the regions of parameter space that were omitted or poorly examined before, such as low TBO frequencies ( $\nu \lesssim 200\,\mathrm{Hz}$ ) or TBOs at very high count rates. We also search for clusters of candidates just below our detection threshold. We pay special attention to bursts with reported TBO candidates, which were afterwards deemed as tentative or controversial, and prepare our own list of potentially interesting candidates for subsequent follow-up with upcoming missions. Finally, the obtained frequencies and fractional amplitudes of TBOs or the upper limits on FAs of non-detections will provide

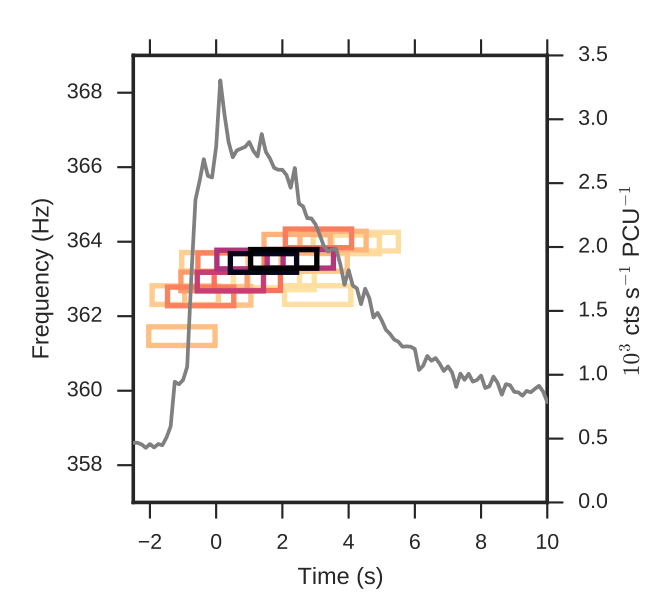


Figure 1. An example of TBOs from the burst observed on MJD 50711.4 from 4U 1728-34. The grey line shows photon count rate binned into 0.125-s bins. Color boxes show the TBO candidates from the Fourier power spectrum in a series of 2-s sliding windows, with the start time of each window shifted every time by 0.25 s. The size of the boxes matches the length of the time window and the frequency resolution. A small random jitter was added to the central frequency of the boxes for better visual clarity. Box colors reflect Leahy-normalized power, running from 15 (lightest) to 190 (darkest).

important input for the TBO mechanisms (see e.g. Heyl (2004) and Piro & Bildsten 2005).

# 2. SIGNIFICANCE ESTIMATE OF PS FOR IDEALIZED LIGHT CURVES

Burst oscillations are very coherent pulsations which typically last for several seconds. During this time the oscillation frequency may jump or drift by several Hz. The search for TBOs is therefore usually conducted in separate, but often heavily overlapping time windows of about 0.25-5 s. Within each window, the photon arrival times are binned into sub-ms bins, then the Fast Fourier Transform (FFT) is taken from the number of photons versus time and the obtained power spectrum (PS) is examined for outliers. An example of such spectrum is shown in Fig. 1. An alternative to a FFT PS is to use  $Z^2$  statistics (Buccheri et al. 1983), which do not require binning of photon arrival times, and can be computed on a finer grid of frequencies (including variable frequency).  $\mathbb{Z}^2$  statistics are more computationally expensive than FFTs, so they are usually used to search for TBOs from sources with known oscillations in a narrow range of frequencies (e.g. Watts et al. 2005).

<sup>&</sup>lt;sup>2</sup> https://burst.sci.monash.edu/minbar/

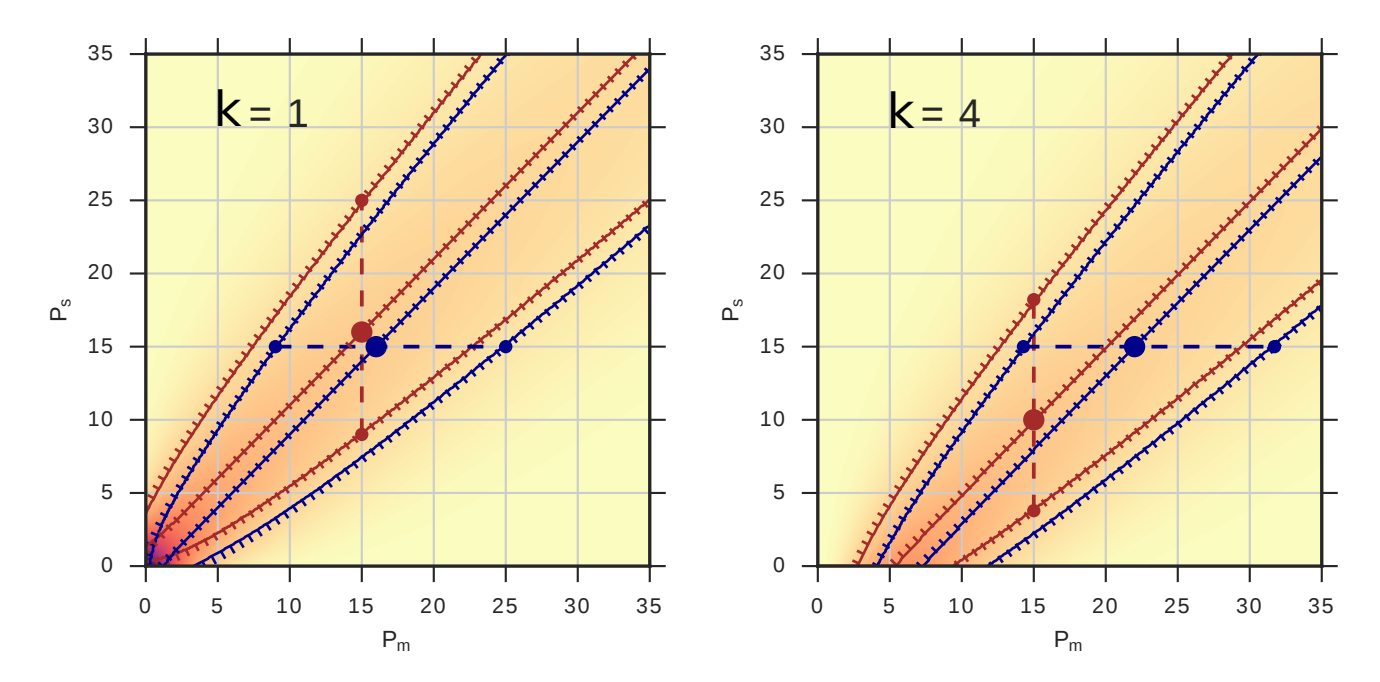


Figure 2. Color: probability density  $p_k(P_{\rm m}, P_{\rm s})$  from Groth (1975) for two different values of number of averaged harmonics, k. The color scale is the same for both plots, with the lightest and darkest colors corresponding to  $p_k \approx 0$  and  $p_k = 0.5$ , respectively. Solid lines show the numerically calculated median and [0.159, 0.841] percentiles for  $p_k(P_{\rm s}|P_{\rm m})$  (light brown) and  $p_k(P_{\rm m}|P_{\rm s})$  (dark blue). Fine-dashed lines show the median and mean  $\pm$  standard deviation from Table 1. The vertical and horizontal lines mark the median and 68% confidence interval of  $P_{\rm s}$  given  $P_{\rm m} = 15$  and  $P_{\rm m}$  given  $P_{\rm s} = 15$ , respectively. For k > 1 the probability density of  $P_{\rm s}$  at  $P_{\rm m} \lesssim 2(k - \sqrt{k})$  has a very sharp peak close to 0, so the median and percentiles of  $p(P_{\rm s}|P_{\rm m})$  become progressively locked at  $\approx 0$  with decreasing  $P_{\rm m}$ .

# 2.1. Probability of false detection and the distribution of intrinsic signal power

Once the PS has been computed, potential oscillation candidates are identified as harmonics exceeding a certain threshold. Two questions immediately emerge: (a) for a given candidate, what is the probability of obtaining this power purely due to noise fluctuations, and (b) given the recorded power, what is the distribution of true signal power? The answers to both questions were given in the work of Groth (1975). Below, we repeat the author's derivations in a somewhat modified form, using a different (nowadays, standard) normalization for the power spectrum.

In Groth (1975) the data time series is assumed to be composed of signal and noise:

$$N_{\rm m}(t) = N_{\rm s}(t) + N_{\rm n}(t),$$
 (1)

where N is the number of photons in a given time bin and the subscripts correspond to measurement (m), signal (s) and noise (n). The coefficients of the Fourier transform of N(t), R for real and I for imaginary, are the sum of the corresponding coefficients for signal and noise:

$$R_{\rm m}(\nu) = R_{\rm s}(\nu) + R_{\rm n}(\nu),$$
  
 $I_{\rm m}(\nu) = I_{\rm s}(\nu) + I_{\rm n}(\nu).$  (2)

If  $N_{\rm n}$  has a Poisson distribution, then both  $R_{\rm n}$  and  $I_{\rm n}$  have normal distributions. For the so-called Leahynormalized  $P_{\rm n}$  (Leahy et al. 1983):

$$P_{\rm n} = \frac{2}{\sum N_{\rm n}} (R_{\rm n}^2 + I_{\rm n}^2),\tag{3}$$

normal distributions are standard, with mean of 0 and variance of 1. In this case  $P_n$  will have a  $\chi^2$  distribution with 2 degrees of freedom.

Assuming that the signal is deterministic, Groth derived an analytical expression for the joint probability distribution of the measured power  $P_{\rm m}$  and the signal of power  $P_{\rm s}$ :

$$p_k(P_{\rm m}, P_{\rm s}) = \frac{1}{2} \left( \frac{P_{\rm m}}{P_{\rm s}} \right)^{(k-1)/2} \exp\left[ -\frac{P_{\rm m} + P_{\rm s}}{2} \right] \times \times I_{k-1} \left( \sqrt{P_{\rm m} P_{\rm s}} \right), \tag{4}$$

where in this equation I is a modified Bessel function of the first kind and k is the number of PS samples summed. Here, both  $P_{\rm m}$  and  $P_{\rm s}$  are Leahy-normalized and the whole derivation is valid if the total number of noise photons in the time window,  $\sum N_{\rm n}$ , is larger than approximately ten.

Eq. 4 can be used to estimate the probability distribution of  $P_{\rm s}$  as a function of the measured power  $P_{\rm m}$ ,

**Table 1.** Moments of the 1-D distributions from Eq. 4. The moments for  $p_k(P_{\rm s}|P_{\rm m})$  and median for  $p_k(P_{\rm m}|P_{\rm s})$  are approximations that are not valid for  $P_{\rm m} \lesssim 2k + 3\sqrt{n}$ .

	$P_{\rm m}$ given $P_{\rm s}$	$P_{\rm s}$ given $P_{\rm m}$
Median	$P_{\rm s} + 2k - 1$	$P_{\rm m} - 2k + 3$
Mean	$P_{\rm s} + 2k$	$P_{\rm m}-2k+4$
Standard deviation	$2\sqrt{P_{\rm s}+k}$	$2\sqrt{P_{\rm m}-k+2}$

 $p_k(P_{\rm s}|P_{\rm m})$ , or alternatively the probability distribution of measured power  $P_{\rm m}$  as a function of the signal power  $P_{\rm s},\,p_k(P_{\rm m}|P_{\rm s})$ . Fig. 2 shows an example of the 2D probability density  $p_k(P_{\rm m},P_{\rm s})$  for k=1 and k=4, together with the median and [0.159, 0.841] percentiles for  $p_k(P_{\rm m}|P_{\rm s})$  and  $p_k(P_{\rm s}|P_{\rm m})$ .

Table 1 gives expressions for the median, mean and standard deviation of 1-D distributions  $p_k(P_{\rm m}|P_{\rm s})$  and  $p_k(P_{\rm s}|P_{\rm m})$ . The mean and standard deviation of  $p_k(P_{\rm m}|P_{\rm s})$  were given in Groth (1975) and are exact. The rest of the moments are useful approximations, obtained using numerically computed values for  $1 \leq k \leq 20$  and both  $P_{\rm m}$  and  $P_{\rm s}$  smaller than 200. For  $p_k(P_{\rm s}|P_{\rm m})$ , the approximations are valid when  $P_{\rm m} \gtrsim 2(k+\sqrt{k})$ . For these  $P_{\rm m}$  the absolute value of discrepancies between the approximation and the numerically computed moments are  $\lesssim 0.2k, \lesssim 0.02k$  and  $\lesssim 0.03k$ , for the median, mean, and standard deviation, respectively. For  $p_k(P_{\rm m}|P_{\rm s})$ , the median value deviates from  $P_{\rm s} + 2k - 1$  by  $\lesssim 0.1k$  for  $P_{\rm s} > k$ .

For  $P_{\rm s}=0$ , Eq. 4 expresses the probability of obtaining  $P_{\rm m}$  without any signal, due to noise alone. This is used to estimate the significance of a potential signal detection. For k=1, Eq. 4 reduces to:

$$p_1(P_{\rm m}, 0) = \frac{1}{2} \exp[-P_{\rm m}/2],$$
 (5)

which is the probability density function (pdf) for the  $\chi^2$  distribution with two degrees of freedom. It can be also shown that for k > 1 the pdf is the  $\chi^2$  distribution with 2k degrees of freedom.

## $2.2.\ Fractional\ amplitudes$

Besides oscillation frequency, power spectra contain information about the amplitude of pulsations. For example, for a Leahy-normalized PS, the rms fractional amplitude (FA) is defined as:

$$A = \left(\frac{P_{\rm s}}{\sum N_{\rm m}}\right)^{1/2}.\tag{6}$$

Let us show that for the simplest case of a purely sinusoidal wave on a constant-rate background, described

by a measured photon count of  $N_{\rm m}={\rm Poisson}(C)+B\sin(2\pi\nu t)$ , the fractional amplitude calculated from Eq. 6 is, on average, equal to  $B/(C\sqrt{2})$ . In this specific case the noise count rate is described by the Poisson process with a mean rate of C, and the signal is  $N_{\rm s}=B\sin(2\pi\nu t)$ . The Leahy-normalized power spectrum of the signal is, by definition:

$$P_{\rm s} = \frac{2}{\sum N_{\rm n}} (R_{\rm s}^2 + I_{\rm s}^2). \tag{7}$$

Here, the average total number of noise photons is equal to its average rate times the number of time bins:  $\sum N_{\rm n} = C N_{\rm bin}$ . Since  $\sum N_{\rm s} \approx 0$ ,  $\sum N_{\rm n} \approx \sum N_{\rm m} = C N_{\rm bin}$ . For a sine wave with amplitude B, scipy DFT<sup>3</sup> yields PS harmonic with an amplitude of  $R_{\rm s}^2 + I_{\rm s}^2 = B^2 N_{\rm bin}^2/4$ . Thus, the Leahy-normalized  $P_{\rm s} = B^2 N_{\rm bin}/(4C)$  and  $A = B/(C\sqrt{2})$ .

In the limit of very small noise, A approaches  $A=1/\sqrt{2}\approx 70\%$ . However, formal calculation of fractional amplitudes may result in arbitrarily large A. If there is no signal present, B=0,  $P_{\rm s}=0$ , and  $P_{\rm m}$  is distributed as  $\chi^2$  with 2n degrees of freedom. The formally estimated  $P_{\rm s}$  given observed  $P_{\rm m}$ , regardless of its actual probability, yields a median value of  $P_{\rm s}=P_{\rm m}-2k+3$  (Table 1). For sufficiently large  $P_{\rm m}$ ,  $P_{\rm s}$  can be such that A>1.

Rms fractional amplitude is not a uniformly accepted way of describing oscillation amplitude. Some authors quote a full fractional amplitude (2B/C) or a half fractional amplitude (B/C).

For the actual burst observations, the noise level has a contribution from background unrelated to the observed low-mass X-ray binary (both astrophysical and instrumental), and the persistent emission from the source itself. The fractional amplitudes are usually calculated for photons in the burst only:

$$A = \left(\frac{P_{\rm s}}{N_{\rm m}}\right)^{1/2} \frac{N_{\rm m}}{N_{\rm m} - N_{\rm bkg}},\tag{8}$$

with  $N_{\text{bkg}}$  being an estimate of the number of background photons collected during the burst interval.

While analyzing fractional amplitudes one should bear in mind that there may be additional complications biasing the obtained values: the persistent emission may increase during the burst (Worpel et al. 2013, 2015) and there may be pulsed background, unrelated to TBOs, such as accretion-powered pulsations (APPs) or a pulsed reflection component from the accretion disk.

## 2.3. Complications and caveats

The standard approach described above provides a simple and relatively fast method for searching for

 $<sup>^3</sup>$  https://docs.scipy.org/doc/numpy-1.13.0/reference/routines.fft.html

TBOs. However, there exist some complications and caveats:

- (a): The burst count rate may vary significantly within the typical time window (e.g. during the burst rise). This results in excess power at low frequencies, and biases estimates of  $P_{\rm s}$  and its significance.
- (b): Because of dead time (time during which the detector is busy processing the current event and cannot record the next one), noise statistics deviate from  $\chi^2$ . The influence of dead time is larger at higher count rates.
- (c): Searching for TBOs in overlapping windows complicates the assessment of the number of independent trials, and thus the significance of  $P_s$ .
- (d): Abrupt variations of the burst count rate cause covariance between harmonics in the PS spectra. This may create the illusion of rapid drift or splitting of the TBO frequency.

In the following sections we are going to address caveats (a)-(c), complementing the traditional approach with more realistic noise modeling. The influence of rapid count variation on the recorded TBO frequency will be explored in a subsequent work (Bilous & Watts, in prep).

## 3. RXTE DATA SET

The observations were performed in 1996–2011 with the proportional counter array (PCA, Jahoda et al. 1996) on board the RXTE telescope. The PCA consists of five identical co-aligned proportional counter units (PCUs), each with a  $r = 1^{\circ}$  circular field of view. The number of active PCUs varied between observing sessions and over the course of RXTE's mission two PCUs went out of order permanently<sup>4</sup>. The PCA is sensitive to photons in the energy range between 2 and 60 keV. Photon counts are processed independently by up to six Event Analyzers (EAs). Two EAs record data in the standard modes, namely Standard-1 ( $t_{\rm res} = 0.125 \, \rm s$ , one energy channel) and Standard-2 ( $t_{\rm res} = 16\,{\rm s},\,128$  energy channels). The rest of the EAs can be configured in a variety of modes, representing the trade-off between time and spectral resolution due to finite data transfer capacities while streaming the data from the satellite to Earth.

Incoming photons can be recorded in two data modes: either with all photon arrival times recorded separately ("Science Event" mode) or with arrival times binned in small time bins ("Science Array" mode). Typically, Science Event files have good spectral resolution, but suffer from data losses at high count rates. Those Science Array files, which have the bin size suitable for oscillation analysis, usually have little information about photon energies, but are less prone to data losses. Often, the data were recorded in both Scientific Event and Scien-

tific Array modes and sometimes different time resolutions and energy cuts are available for a single observation

Burst selection was based on the information available in the 2015 pre-release version of the MINBAR database, which contains the times of arrival, source associations and other properties of Type I bursts observed with different satellites. We selected all bursts observed with RXTE, excluding bursts which: (a) did not have high- $t_{\rm res}$  ( $t_{\rm res}$  < 1 ms) data during the burst and either immediately before or after the burst (b) did not pass the extended good time interval (GTI) criterion<sup>5</sup> (c) were missing spacecraft housekeeping data, or (d) had variable bin size in Scientific Array mode. The final sample contained 2118 bursts from 57 sources<sup>6</sup>. In this work we use the MINBAR catalogue burst entry number as a unique burst identifier.

For this paper we did not include Burst Catcher data, which can be also used for TBO searches (Zhang et al. 1998; Kaaret et al. 2002). This omission was not crucial as there were no bursts that were missing high time-resolution data on the burst rise, or throughout the burst, that would have been covered by the relevant Burst Catcher mode (the one with time resolution of  $500\,\mu s$  or less). Nevertheless, several bursts with severe data gaps may benefit from the use of burst catcher data (e.g. burst #2266 from Aql X-1, see also Zhang et al. 1998).

For each of the 2118 bursts, we downloaded the data for the observations<sup>7</sup> covering the MINBAR burst arrival time. We made a reference light curve, using the Standard-1 data re-binned to 0.5 s and searched for a LC peak within  $\pm 1$  min of the MINBAR burst arrival time. The peak time  $t_{\text{peak}}$  served as the absolute reference point within each burst. LCs were visually inspected and the baseline window was selected manually for each burst. For most of the bursts the baseline window lay within  $(t_{\text{peak}} - 150, t_{\text{peak}} - 30)$  s, but often it was placed in the burst tail (if no pre-burst data were available) or was shorter because of observation duration constraints or the presence of other bursts nearby. The on-burst window,  $(t_{\text{peak}} - dt_{\text{rise}}, t_{\text{peak}} + dt_{\text{decay}})$ , was confined to the region where photon count exceeded the baseline mean plus two of its standard deviations. The on-burst window was manually adjusted for bursts with peculiar shapes and faint bursts. Figure 3 shows an example of LCs, the baseline and on-burst windows for two bursts from 4U 1728-34, recorded in different data modes.

In the event that more than one high- $t_{\rm res}$  data mode was available for a single burst, we selected files with the largest number of photons per on-burst window, fewer gaps or with finer time resolution. We did not discard

 $<sup>^4</sup>$  https://heasarc.gsfc.nasa.gov/docs/xte/recipes/stdprod\_guide.html

<sup>&</sup>lt;sup>5</sup> https://heasarc.gsfc.nasa.gov/docs/xte/abc/data\_files.html

<sup>&</sup>lt;sup>6</sup> We omitted two known RXTE superbursts (in't Zand 2017).

<sup>7</sup> legacy.gsfc.nasa.gov

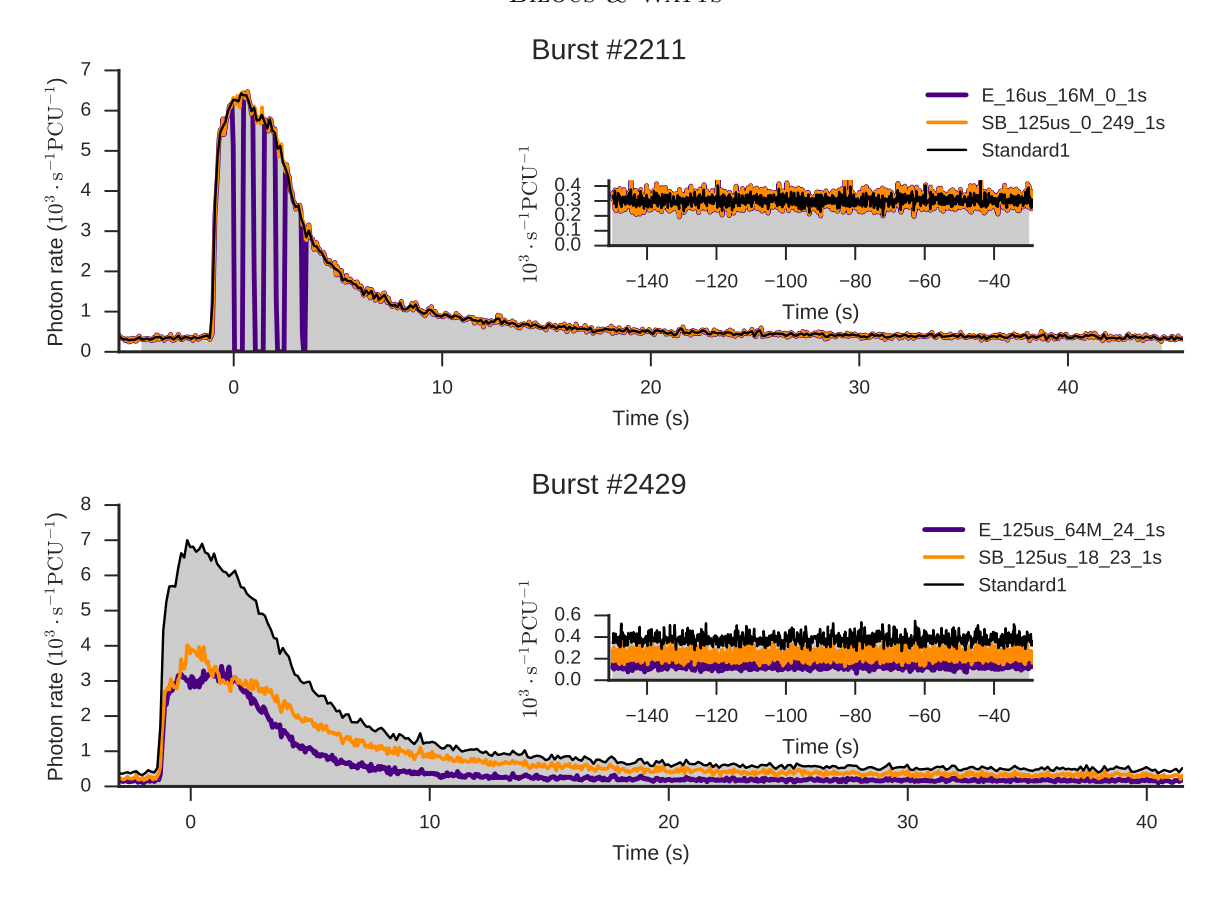


Figure 3. The light curves of two bursts from 4U 1728-34. The black line shows total count rate from the Standard-1 data, with the native 0.125-s resolution. The violet and orange lines show Science Event (data mode E\_125us\_64M\_24\_1s) and Science Array (SB\_125us\_18\_23\_1s) data files from the same observations, binned with 31.25-ms bins. Time is measured from the peak of the Standard-1 light curve, binned with 0.5-s bins. The grey area marks the on-burst or baseline (inset) windows. For the top subplot, the high-resolution data was recorded in whole energy band available to RXTE, and Science Event data suffer from gaps due to the high photon count rate. For the bottom subplot, only parts of the band were recorded with high time resolution, resulting in different LC shapes.

any photons based on their energy, and merged together data files which covered parts of the energy band (e.g. SB\_250\_us\_0\_13\_2s and SB\_250\_us\_14\_35\_2s). Sometimes files recorded in different data modes contained completely the same information; in this case the data mode was chosen arbitrarily. For uniformity, we converted Scientific Array files to the pseudo-Scientific Event format by recording the counts in each time bin as individual photons with time of arrival equal to the bin start time.

Photon arrival times were converted from the Mission Elapsed Time (MET) seconds to the UTC time system with the TIMEZERO value. This leads to timing accuracy of  $100\,\mu s$ , which is sufficient for searching for burst oscillations in small windows (up to 4s) if one is not trying to phase-connect oscillations between different bursts. Since the noise modeling relies on the

housekeeping data that provides information at regularly sampled time intervals in the MET, in this work we chose not to barycenter the data.

Appendix A provides more detailed information about the burst sample. Two overview figures show burst times of arrival, source-by-source (Fig. 17) and Standard-1 LCs (Fig. 18). Table 2 available in its entirety in machine-readable form lists entry # and burst arrival time from MINBAR,  $t_{\rm peak}$  in MET, rise, halfpeak and decay times, S/N of the burst peak, data mode and notes for each burst. Notes indicate manual windows for faint bursts and bursts with peculiar shapes, presence of data gaps, partial GTI coverage or incomplete burst coverage.

## 4. NOISE SIMULATION AND DATA ANALYSIS

In order to estimate the significance of oscillation candidates, for each burst we created a number of artificial oscillation-free bursts, which followed the properties of

<sup>&</sup>lt;sup>8</sup> https://heasarc.gsfc.nasa.gov/docs/xte/abc/time.html

real data as closely as possible. The same search analysis was then conducted on real and simulated data.

Originally, we simulated the bursts by scrambling the intervals between photon arrival times in  $\sim 0.1\,\mathrm{s}$  windows. The size of the window was chosen to be much larger than the presumed TBO period, but smaller than the timescales of most large-scale LC variations. A similar technique was used by Fox et al. (2001), however the authors scrambled the LC bins, not the time intervals between individual photons.

Such scrambling preserves deviations from the  $\chi^2$  noise distribution, but destroys any oscillation signal. However, it appeared that this method failed to produce enough statistically independent realizations of noise for some of the count rates. Statistical independence was assessed in the following way: we generated a sequence of 100 photons with constant rate and random arrival times, then reshuffled the time differences between them 1000 times, and computed the power spectra. For each harmonic, the Kolmogorov-Smirnov test was performed to test whether the 1000 realizations were consistent with being drawn from a  $\chi^2$  distribution. For about 45% of cases the p-value was smaller than 0.05, indicating large deviations from  $\chi^2$ . Acceptable p-values were obtained only for a number of photons larger than about 10000.

Thus, the scrambling method was abandoned. Instead, we performed random generation of photon time of arrivals (TOAs) using the approximated LC, with subsequent pruning according to known dead time.

# 4.1. Light curve modeling and simulation of photon TOA

RXTE records four types of events: "Good Xenon Events" (events which pass all of the discriminators and anti-coincidence vetoes, the desired astrophysical signal) and three types of events considered to be mostly due to instrumental background: "Coincidence Events", "Very Large Events", or "Propane Events" (Jahoda et al. 2006). "Good Xenon" events are recorded per PCU; for the rest the sum over all active PCUs is saved. All four types of events were simulated, since all of them cause dead time, influencing the number of recorded Good Xenon events.

In order to simulate the arrival times we used the information from the Standard-1 files, which contain events from the whole energy band, binned in  $0.125 \,\mathrm{s}$  bins. Sometimes, this binning is not sufficient for characterizing the burst rise properly. We therefore renormalized the Standard-1 LC<sup>9</sup> with the weights obtained from the higher- $t_{\rm res}$  data, binned to 1/8 of the Standard-1 resolution (15.625 ms), keeping the total

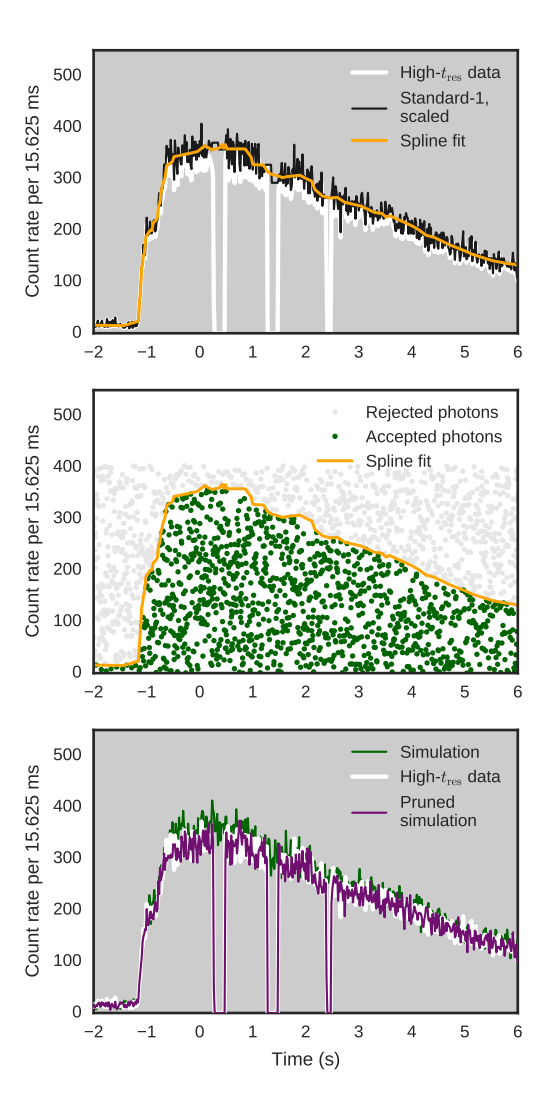


Figure 4. Top: the LCs of the high- $t_{\rm res}$  data, binned with 15.625 ms time bins (white), together with Standard-1 LC, scaled according to the fraction of dead time, and re-normalized to mimic the time resolution of the high- $t_{\rm res}$  LC outside the data gaps. The orange line shows a spline fit to the scaled and renormalized Standard-1 LC, smoothed with a 0.5-s median filter. *Middle:* Simulation of photon arrival time with the "acceptance-rejection" method. Only 1% of all simulated photons are plotted. *Bottom:* LC from the simulated photons before and after pruning by dead time and data gaps (green and purple, respectively).

number of Standard-1 events in  $0.125\,\mathrm{s}$  bins unchanged. If the higher- $t_{\mathrm{res}}$  data were unavailable due to data gaps, uniform weights were applied (Fig. 4, top). LC count rates were adjusted for the dead time (see more details in Sect. 4.2).

We followed two different procedures for simulating Good Xenon events and the instrumental background. For the Good Xenon events we used a method which was

<sup>&</sup>lt;sup>9</sup> Namely, Good Xenon and Propane + Coincidence LCs. The Very Large Event LC was not renormalized because its count rate is usually low and does not change much during the burst.

more expensive computationally, but which resulted in better reproduction of the stochastic variation of the count rate.

The method was as follows. First, the dead timecorrected LC was smoothed with a median filter with a typical length of 0.5s and a linear spline fit was performed to obtain the estimate of the count rate LC(t)in any arbitrary moment of time (Fig. 4, top). The tolerance of spline fit and the size of the median filter window were adjusted on a per-source basis, so that the fit was maximally smooth, yet preserved, by eye, the short-timescale variations in the LC shape. However, for frequencies below  $\sim 5\,\mathrm{Hz}$  it becomes complicated to distinguish between potential TBOs and non-TBO LC variation, so in this region spurious candidates may be present or the significance of TBO candidates may be underestimated (see discussion in Sect. 5). Light curves for each individual PCU were obtained by multiplying the spline fit by the total number of Standard-1 photons recorded by a given PCU, divided by the sum from all PCUs.

Then, the arrival times of the Good Xenon events were simulated for each PCU separately using the acceptance-rejection method (von Neumann 1951). We used the standard Python random number generator based on the Mersene Twister algorithm (Matsumoto & Nishimura 1998) to generate  $LC_{max} \times N_{bins}$  pairs of random variables (L, T). Here,  $LC_{max}$  is the maximum value of LC(t) and  $N_{\rm bins}$  is the number of 0.125-s time bins in the on-burst window (Fig. 4, middle). Both Land T were uniformly distributed within  $[0, LC_{max}]$  and the on-burst window, respectively. Then, the pairs with L < LC(T) were discarded. This way, a Poisson distribution of photon TOAs was created, with the instantaneous rate closely matching LC(t), but devoid of any oscillations with periods smaller than the characteristic time scale of the features of the modeled burst envelopes.

For the Propane, Coincidence and Very Large events we used a simpler procedure. The light curve counts were divided by the number of PCUs, and for each time bin with local count rate C we generated the following number of uniformly distributed TOAs:

$$N = \text{floor}(C) + \text{Binom}[N = 1, p = \text{frac}(C)],$$
 (9)

where floor denotes the floor function and Binom is a binomial random variable with number of trials N and success probability p. This way the number of simulated photons is very close to the real data value and thus the simulation does not emulate the Poisson noise which is present in the data.

## 4.2. Dead time pruning

Simulated events were subsequently pruned to account for the detector's dead time. Dead time calculation for RXTE is rather complex and thus deserves a detailed examination. According to Jahoda et al. (2006),

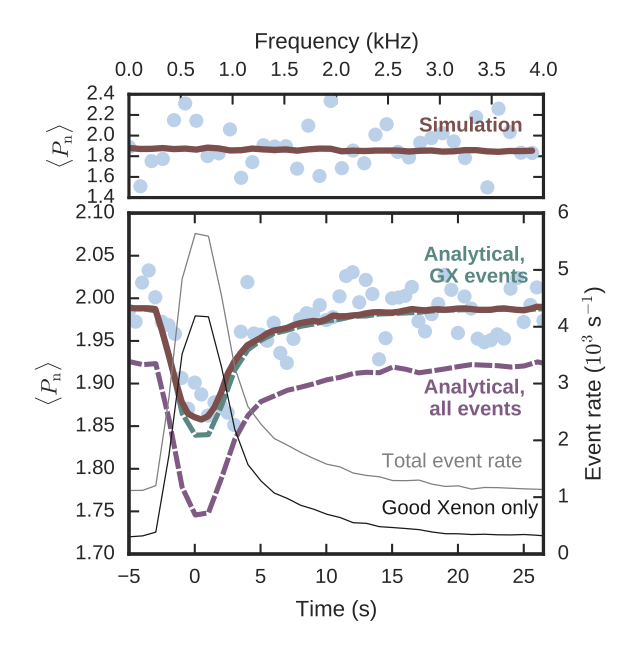


Figure 5. The average noise power  $\langle P_{\rm n} \rangle$  for one of the PCUs from burst #2980 from Aql X-1 for  $t_b=122\,\mu{\rm s}$  and 1-s FFT windows, overlapping by 0.5 s.  $Top\colon\langle P_{\rm n} \rangle$  for the window with the largest photon count rate versus FFT frequency, averaged by 108 harmonics. Light circles show the actual data, while the dark line shows the mean of 1000 simulations. Bottom: frequency-averaged  $\langle P_{\rm n} \rangle$  in each of the FFT windows for the actual data (light circles) and the simulation (dark solid lines). The dashed curves show the analytically calculated  $\langle P_{\rm n} \rangle$  from Eq. 10 for two event rates: GX only (upper curve) and total event rate (lower curve). Overlayed are the GX and total event count rates.

RXTE PCUs process events independently and the dead time is caused by all events recorded by the PCU. Any event recorded belongs to one and only to one of the four classes<sup>10</sup>: Good Xenon, Coincidence, Very Large, or Propane Events.

In general, there exist two types of dead time: paralyzable (cumulative), where events entering the detector during dead time themselves cause further dead time (even though they are not recorded); and non-paralyzable, where events entering detector during dead time are completely ignored. For RXTE, the actual dead time is a mixture of both types, depending also on event class and assigned energy. However, for most of cases  $t_d$  can be approximated as  $10 \,\mu s$  non-paralyzable dead time (set by the analog-to-digital converter, ADC) for all classes except VL events. For VL events, the dead time can vary between  $70 \,\mu s$  and  $500 \,\mu s$  and depends on

 $^{10}~~{\rm http://heasarc.nasa.gov/docs/xte/recipes/pca\_deadtime.}$  html

the instrumental setting, most of the time being approximately  $170 \,\mu s$  (Jahoda et al. 2006).

Zhang et al. (1995) developed an analytic formula for the Leahy-normalized noise PS in the presence of dead time. The mean value  $\langle P_{\rm n} \rangle$  is always less than 2 by some amount which depends on event rate, the type of dead time and its value, the LC bin size,  $t_b$ , and the FFT frequency. The analytic formula for paralyzable dead time has a much simpler form than that for the non-paralyzable dead time.

Jahoda et al. (2006) gives an example showing how to calculate the dead-time modifications to pure noise for a count rate below  $10^4$  cts  $PCU^{-1}$  s<sup>-1</sup>, applying the correction for the paralyzable dead time. Disregarding larger  $t_d$  for the VL events:

$$\langle P_{\rm n} \rangle = 2 - 4r_0 t_d \left( 1 - \frac{t_d}{2t_b} \right) - 2r_0 t_d \frac{N-1}{N} \left( \frac{t_d}{t_b} \right) \cos \left( \frac{\pi \nu}{\nu_{\rm Nyq}} \right).$$
 (10)

Here n indicates noise (as in Sect. 2),  $r_0$  is the output rate of all events (all four types combined),  $t_d$  is the dead time,  $t_b$  is the bin size,  $\nu$  is the FFT frequency, N is the number of frequencies in the PS,  $\nu_{\rm Nyq}$  is the Nyquist frequency. The authors also give an ad hoc correction for the larger  $t_{\rm d}$  of VL events, which is much smaller than the one introduced by Eq. 10 for our  $t_d$  and  $t_b$  and VL event rates.

Although technically RXTE dead time is a complex mixture of both paralyzable and non-paralyzable dead times, with the non-paralyzable dead time of ADC contributing the most at energies below  $\approx 20\,\mathrm{keV}$ , for the typical RXTE rates and  $t_b$  size used in this work, the formulas for paralyzable and non-paralyzable dead times yield essentially the same corrections. Thus, the more simple Eq. 10 can be used to estimate the dead time influence on the average noise power.

For our simulations, we treated dead time as purely non-paralyzable. Note that we do not model the absence of dead time caused by events which triggered only  $V_X$  or alpha chains. According to Jahoda et al. (2006), not doing this leads to a small overestimation of dead time fraction by  $\delta t_{\rm d}/t_{\rm b}\approx 0.0014$ , an amount nearly constant throughout the mission.

Fig. 5 shows the average signal power in Burst #2980 from Aql X-1 (in which no TBOs were detected). Photons from only one PCU were selected, and a bin size of  $1/8192\,\mathrm{s}\approx122\,\mu\mathrm{s}$  was used, together with an FFT window of 1 s. For this choice of binning and the rates of Good Xenon (GX) and other events the noise power has only a minuscule dependence on FFT frequency. We have summed all harmonics above 10 Hz (below 10 Hz the PS may be affected by red noise) and compared the noise power to the mean obtained from 1000 simulations, which appeared to match the data well (Fig. 5).

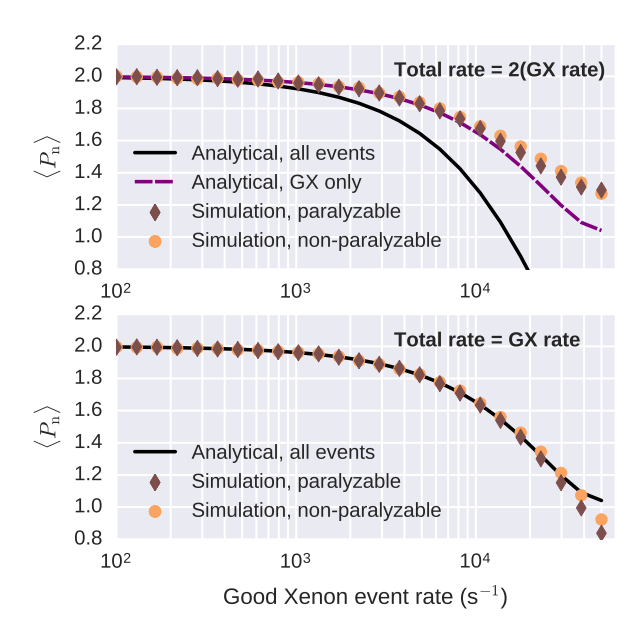


Figure 6. Simulation of Leahy-normalized  $P_{\rm n}$  for the 1-s Poisson event sequence with  $t_d=10\,\mu{\rm s},\,t_b=122\,\mu{\rm s},$  and various event rates.  $P_{\rm n}$  is averaged for 50 simulations and 4094 FFT harmonics (omitting two lowest harmonics). Diamonds and circles show paralyzable and non-paralyzable dead time, respectively. The analytic formula is Eq. 10 for the total event rate (solid line) and the GX event rate (dashed line). Top: only half of the simulated events were considered to be GX events, the rest were deleted before computing the PS. Bottom: all simulated events were considered to be GX events.

Attempting to apply Eq. 10 yielded interesting results: if the rate was taken to be the rate of all events (since all of them cause dead time), as stated in Jahoda et al. (2006), the dead time correction was considerably and consistently larger than that required to match both data and simulations. However the correction did match observations well if only the GX events were taken into account. It appears that for the given range of event rates and the bin/dead time windows, the operations of dead time pruning and selection of GX events are commutative, meaning that GX photons have the same noise power distribution as if they were not affected by the dead time from all other event types. As simulations have shown, this does not hold true for larger count rates (Fig. 6), however, such large count rates do not occur in our burst sample.

To summarize, dead time was accounted for in the following way: initially LC curves for all four event types were re-normalized using the fraction of dead time calculated with the observed rates<sup>11</sup>. Then the TOAs of the four types of events were simulated separately and combined to form a "mixed-bag" event sequence which mimicked the real data. Then events which arrived within  $10\,\mu\mathrm{s}$  after previous non-VL event and variable  $t_d$  after VL event were removed. Those events were assumed not to cause dead time themselves, so the dead time was by definition non-paralyzable. This procedure was performed for each PCU separately, and then the resulting photon lists were merged together.

# 4.3. Accounting for data gaps and occasional limited energy range

Data gaps are losses of data due to saturated telemetry occurring for bursts with high count rate. They typically last from a fraction of a second to several seconds and are not reflected in the Good Time Interval table of the data files. To search for data gaps, we selected all time intervals with gaps between two successive photons being larger than 0.02 s. In order to exclude "natural" gaps in bursts with intrinsically low count rate, we calculated the estimated number of photons inside the potential gap and selected only those gaps where this number was larger than two. The number of photons inside the gap was estimated from the mean photon count rate of Standard-1 data and adjusted for the overall difference in the energy band (multiplied by a sum of all Standard-1 counts divided by the sum of all high- $t_{res}$  counts for the time bins where the latter was larger than 0). All simulated photons inside the data gaps were deleted.

Finally, the photon sequences were adjusted for the difference in energy band between high- $t_{\rm res}$  data and the Standard-1 data (e.g. Fig. 3). For each 0.125-s bin, the ratio between Standard-1 LC and the high- $t_{\rm res}$  data LC was estimated and the simulated data were pruned by deleting the appropriate fraction of photons at random (Fig. 4, bottom).

Both real and simulated photon sequences were binned with sub-ms time bins. For observations in Good Xenon data mode, the bin size was  $t_b = 2^{-14} \, \mathrm{s} \approx 61 \, \mu \mathrm{s}$ , yielding about 8 phase bins in pulse profile at the highest frequency searched. For all other modes, the bin size was two times larger, corresponding to the typical  $t_{\rm res} = 122 \, \mu \mathrm{s}$ . Although 24 bursts had larger  $t_{\rm res}$ , they were still binned with the smaller bin size. Among those bursts, five had  $t_{\rm res} = 2^{-11} \approx 488 \, \mu \mathrm{s}$ , all of them from GRS 1747–312. For these bursts any candidates at frequencies above the Nyquist frequency of 1024 Hz were discarded.

## 4.4. Fourier transform

Fourier transforms were taken for the binned sequences in series of 0.5, 1, 2 and 4-s sliding windows,

each window starting  $0.5\,\mathrm{s}$  later than the previous one. The FFT coefficients R and I were recorded for harmonics between 2 and  $2002\,\mathrm{Hz}$ . The lower limit was set by the smallest non-zero harmonic for the PS in  $0.5\,\mathrm{s}$  windows. The upper limit reflects the largest possible NS spin frequency allowed by current reasonable models of the neutron star equation of state (Haensel et al. 2009).

In what follows, we will operate with FFT coefficients in a  $(\nu,t,T_{\rm win})$  cell, with  $\nu$  being the FFT frequency, t referring to the center of the time window and  $T_{\rm win}$  being the given window size. The 500 simulation runs were used to make distributions of  $R_{\rm n}$  and  $I_{\rm n}$  in each cell. The  $I_{\rm n}$  and  $R_{\rm n}$  had, most of the time, Gaussian distributions with the mean influenced by the baseline variation and the standard deviation influenced by the dead time (Fig. 7). We used the mean and unbiased estimate of standard deviation of the first  $N_{\rm smp}=400$  simulation runs to normalize  $R_{\rm m}$  and  $I_{\rm m}$  of the real data. Power spectra from the remaining 100 runs, normalized as the same way as the real data, were used to estimate detection significance.

The mean and standard deviation  $R_n$  and  $I_n$  used for re-normalizing are inevitably influenced by the limited number of simulation runs. For pure Poisson noise, the means are random variables with normal distribution, having  $\mu=0$  and  $\sigma^2=1/N_{\rm smp}=0.05$ . Since  $N_{\rm smp}\gg 1$ , the standard deviation is also distributed normally, with  $\mu = 1$  and  $\sigma^2 = 2/(N_{\rm smp} - 1)$ . Since the dead time influence has negligible dependence on Fourier frequency, for the normalization we averaged the standard deviation by  $800 \times T_{\text{win}}$  harmonics in order to reduce the stochastic error caused by the limited number of simulations. Simulation of 10<sup>9</sup> pairs of standard normal random variables showed that re-normalizing them by the mean and standard deviation drawn from the appropriate Gaussian distributions causes about 10% of detections above the threshold set by  $p_{\chi^2}=2\times 10^{-7}$  (adopted as the detection criterion, see Sect. 4.5) to be false positives. Another 10\% of un-normalized candidates had power below the threshold after normalization. It is hard to estimate the rate of false negatives or false positives for the real-data candidates, since it depends on the intrinsic distribution of TBO powers. However, we checked the normalization values for all candidates that were deemed interesting, for example occurring in an unusual place in the burst or being detected from a burst without previously reported TBOs.

In rare cases of a gap occupying most of the FFT window,  $I_{\rm n}$  and  $R_{\rm n}$  become covariant at the lowest Fourier frequencies. In such cases the subsequent analysis is not applicable, so we discarded candidates from those cells. The covariance threshold was estimated as follows: we simulated 500 independent normal random variables and the distribution of covariance was calculated. The threshold was set as 5 times the standard deviation of the covariances.

<sup>&</sup>lt;sup>11</sup> The RXTE Cook Book states that "the VLE rate is not affected by dead time", this was not reproduced in the simulations.

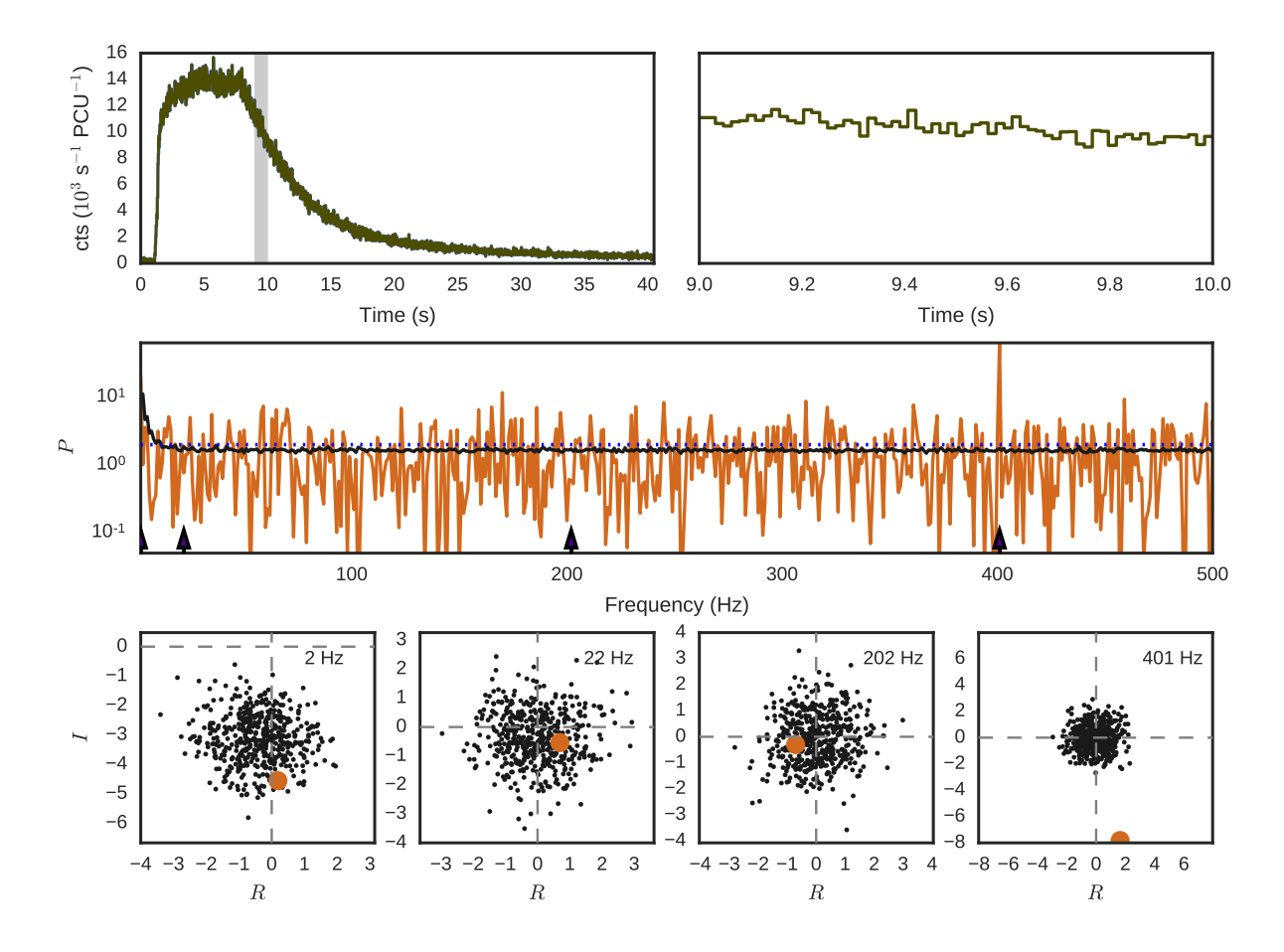


Figure 7. Upper row: LC of burst #3038 from SAX J1808.4–3658 detected on 2002-10-17 07:19:24 UT. On the left, grey shaded area marks the 1-s FFT window. The zoomed-in LC in the same window is shown on the right. Middle row: PS from the real data (orange) and the mean of 500 simulations (black). The arrows show four sample FFT frequencies (rightmost with TBOs) and the blue dotted line shows P=2. Bottom row: the distribution of Fourier coefficients for the four sample FFT frequencies (black dots – simulated data, orange circle – real data). I=0 and R=0 are marked with dashed lines.

We also checked for the covariance along the frequency axis. Such covariance stems from abrupt changes in photon count within the window, caused by data gaps or even on the burst rise if the latter is sharp. For each time window and simulation we calculated autocorrelation function (ACF) from the renormalized simulated  $P_{\rm n}(\nu)$ . ACFs from all 500 simulations were added together and the 50% half-width of the peak was measured, with the baseline levels subtracted from the peak. We discarded PS in the given time window (regardless of frequency) if the 50% half-width of the ACF peak was larger than 5 harmonics. Such bursts were marked with "freq cov" comment in the notes column of Table 2.

Finally, we removed the cells covering regions where the simulated LC deviated substantially from the real data due to narrow gaps or spikes. Substantial deviation was defined being larger than 10 standard deviations of the simulated photon count in given 0.125 s or 15.625 ms time bins. Such bursts were marked with "bad LC" comment in the notes column of Table 2.

# 4.5. Filtering potential oscillation candidates and computing fractional amplitudes

In order to filter potential TBO candidates, we selected all cells with renormalized  $P_{\rm m} > P_{\rm up}$ , where  $P_{\rm up}$  corresponded to a  $\chi^2$  probability of getting  $2 \times 10^{-4}$  chance candidates per single spectrum:

$$p_{\chi^2}(P_{\rm up}) = \frac{2 \times 10^{-4}}{2000 \times T_{\rm win}}.$$
 (11)

The choice of  $p_{\chi^2}(P_{\rm up})$  was arbitrary and motivated by the requirement to have a manageable number of candidates for the given data sample. For 0.5, 1, 2 and 4-s FFT windows  $P_{\rm up}$  was 30.85, 32.24, 33.62, and 35.01, respectively.  $P_{\rm up}$  was adopted as the upper limit in the event that no candidate detections were found.

Since the power values in adjacent cells are covariant both in time and (to a smaller extent) in frequency, the number of trials is not equal to the number of cells,  $N_{\rm cell}$ , and the simple significance formula  $p_{\chi^2}(P_{\rm m}) \times N_{\rm cell}$  is not

readily applicable. To assess the significance of detections, we performed the same candidate search for the simulated data and compared the number of oscillation candidates from the real data with the distribution of the same values from the simulated data.

For each potential candidate we computed fractional amplitude (FA) using Eq. 8 and the median value of  $P_{\rm s}|P_{\rm m}$  from Table 1,  $P_{\rm s}=P_{\rm m}+1$ . The uncertainties in fractional amplitudes were calculated by linear error propagation of the independent parameters in Eq. 8 (Ootes et al. 2017). For the uncertainty on  $P_{\rm s}$ , we took [0.159, 0.841] percentiles of the  $P_{\rm s}|P_{\rm m}$  distribution. The uncertainty on the number of photons in the FFT window was taken to be Poissonian and the uncertainty in the background level was taken to be the standard deviation of count rates in the baseline window, computed in the overlapping windows of the length equal to the current FFT window.

A few potential uncertainties are not included in the given FA errors. Firstly, we do not include the variation of background within the burst from Worpel et al. (2015), since it is not available for all bursts in our sample. We also do not correct for the possibility of the TBO frequency falling between FFT harmonics. Simulation showed that with our choice of FFT windows and oversampling in time, fractional amplitude can be underestimated by as much as a factor of 0.68. However only in 9% of cases (assuming no prior knowledge of TBO frequency) suppression of FAs is stronger than 0.85.

Finally, we did not account for bias caused by the limited number of trials. Simulated distribution of  $P_{\rm s}|P_{\rm m}$  for the normalized data had a mean and median consistent with the ones from Table 1. The standard deviation of  $P_{\rm s}|P_{\rm m}$  for the normalized data was larger by a small value of  $\lesssim 0.4\%$ .

#### 4.6. Organizing the results

Table 2 gives a general picture of the maximum power recorded for each individual burst, as well as the smallest FA of potential detection (defined by the threshold detection probability, Eq. 11). Besides renormalized power  $P_{\rm m}$ , it lists its frequency and  $T_{\rm win}$ , as well as smallest FA<sub>up</sub> for all four  $T_{\rm win}$ .

Table 3 contains basic properties for each source (number of bursts, total duration, median S/N of the burst peak, minimum and median upper limits on FAs in 1-s window at the burst peak), providing an overview of the amount and quality of observational material for each source as well as the extent of FA range that can be probed by our analysis. The properties of oscillation candidates are given per frequency group, with a group being defined as the candidates with  $|\delta\nu| \leq 2 \,\mathrm{Hz}$  (matching the lowest frequency resolution). For each frequency group we list the number of bursts with TBO candidates in this frequency range and the number of bursts with candidates in one of three non-overlapping

regions: "R", defined as the region between rise and peak of the burst; "B" starting at the peak and spanning three times half-peak width (more or less corresponding to the traditional on-burst windows); and "T" covering the rest of the burst tail. For each frequency group we list also the average  $P_{\rm m}$  of the candidates in each of the four Fourier windows. The remaining three columns give a handle on the number of spurious candidates in both real and simulated data, listing the total number of real-data non-TBO candidates (counting the ones from overlapping windows as independent and omitting low-frequency ones), the average number of candidates in the simulated data (averaged over 100 simulation runs) and the percentile of the real-data number with respect to a 100-run simulation sample, p.

Table 4 gives more detailed information about each group of candidates (except for the low-frequency ones) for each individual burst, listing MINBAR burst entry, MINBAR TOA, frequency range, location of candidates within the burst (R, B or T), number of independent time windows and the maximum FA for each size of Fourier window.

Finally, for each group of candidates we provide reference plots, aggregating information about frequency, time of arrival, power and FA of candidates, as well as upper limits on FAs. Fig. 8 gives an example of such a plot, with separate panels for the burst LC and the frequency, FA, and power of the candidates. To conserve space, the rest of the reference plots are made more condensed, without legends and with individual panels merged together.

#### 5. RESULTS

## 5.1. Low-frequency noise

The mean values of simulated Fourier coefficients,  $\langle R_{\rm n} \rangle$  and  $\langle I_{\rm n} \rangle$ , give us a handle on how much the power spectrum is affected by the change of photon count rate during Fourier window. Fig. 9 shows an example of the frequency-dependent distribution of the absolute values of Fourier coefficients for all  $(\nu, t, T_{\rm win} = 1\,{\rm s})$  cells in the bursts from 4U 1702–429, omitting the cells with large frequency covariance or large discrepancy between the simulated and real LCs (see Sect. 4.4). At higher Fourier frequencies the spread of  $\langle R_{\rm n} \rangle$  and  $\langle I_{\rm n} \rangle$  is mostly determined by the finite number of simulation runs, whereas at the lower frequencies we record an excess of large coefficient values. For the majority of the sources this excess continues to at least 100 Hz. In rare cases the frequencies as high as 1000 Hz can be still affected.

Re-normalization of Fourier coefficients allowed us to remove most of the described power excess. However, we still record a relatively large number of strong candidates at frequencies below  $\sim 15\,\mathrm{Hz}$ . Some of these candidates can be associated with obvious flaws in LC modeling, where our spline failed to reproduce short peaks or drops in the LC (Fig. 10, left, hereafter "type I" low-frequency candidates). Other low-frequency candi

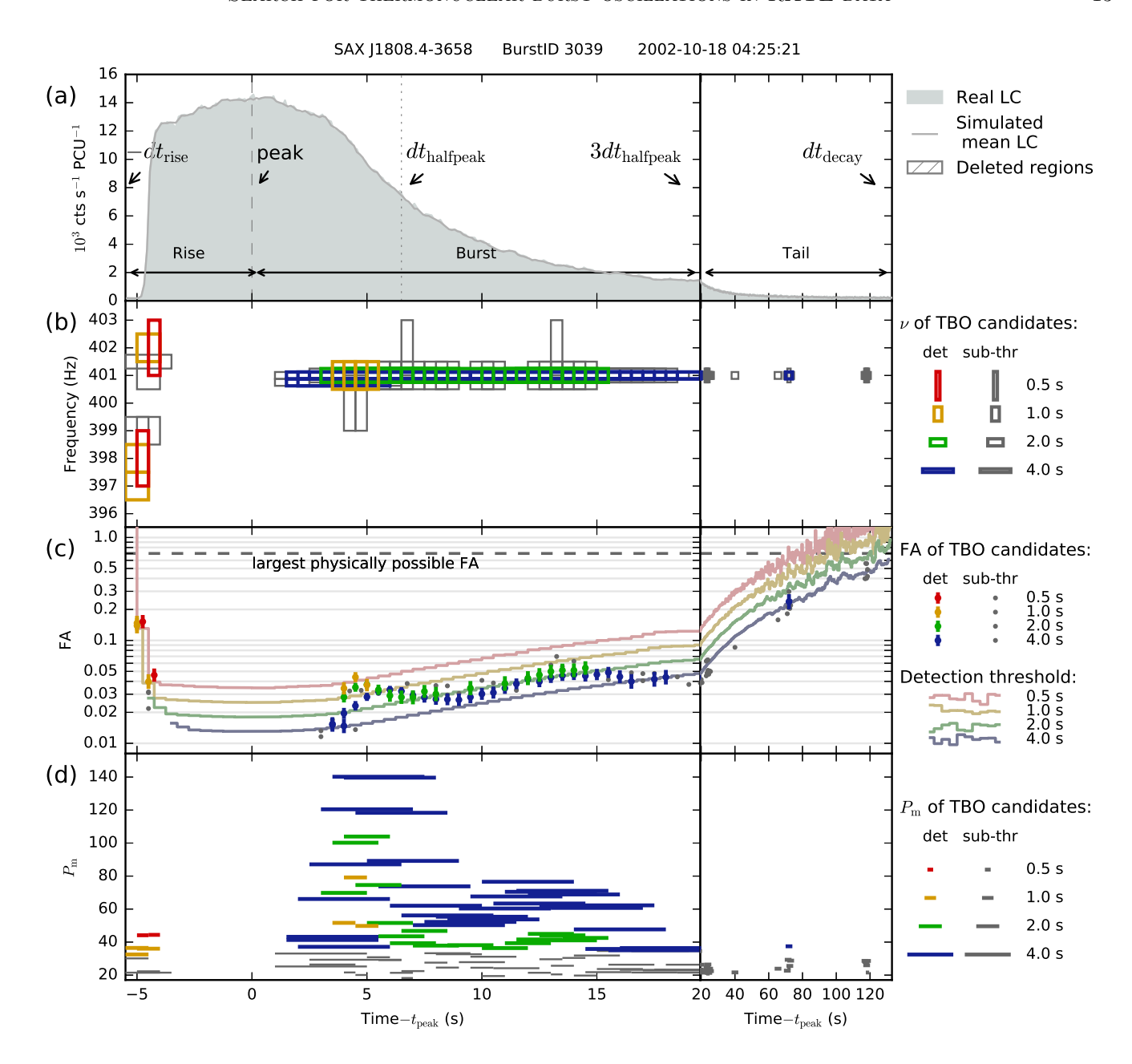


Figure 8. An example of a diagnostic plot for a cluster of TBO candidates belonging to the same frequency group. For each plot pair, the left panel corresponds to RB (Rise+Burst) regions, the right to T (Tail, note the different time scale). (a) LC, binned in 0.125-s time bins for the real (shaded) and mean of the simulated (line) data sets. Vertical lines mark  $t_{\rm peak}$  and  $dt_{\rm halfpeak}$ . The regions excluded from the analysis (outside GTI, with large frequency covariance in the power spectra, or bad LC modeling) are shown as dashed (absent in this particular plot). (b) Time and frequency of detected (det) TBO candidates, represented by boxcars with width equal to the width of the time window and the height to the Fourier spectral resolution. The color encodes the length of the window (red, yellow, green and blue for 0.5–4-s windows, respectively). Sub-threshold (sub-thr) candidates, with  $p_{\chi^2} < 10^{-1}/(2000 \times T_{\rm win})$  are plotted as grey. (c) FAs of TBO candidates vs time (color error bars, see Sect. 4.5 for details on the uncertainty calculation) and sub-threshold candidates (grey dots) The FAs are given at the center of each sliding time window and are not corrected for the lack of signal during data gaps. Adopted upper limits on FA are set by the power corresponding to the threshold probability (lines). The dashed horizontal line marks FA of 0.7, the maximum rms FA which is allowed physically. (d) Normalized  $P_{\rm m}$  of candidates vs. time, with the length and the color of the mark representing the length of the FFT window.

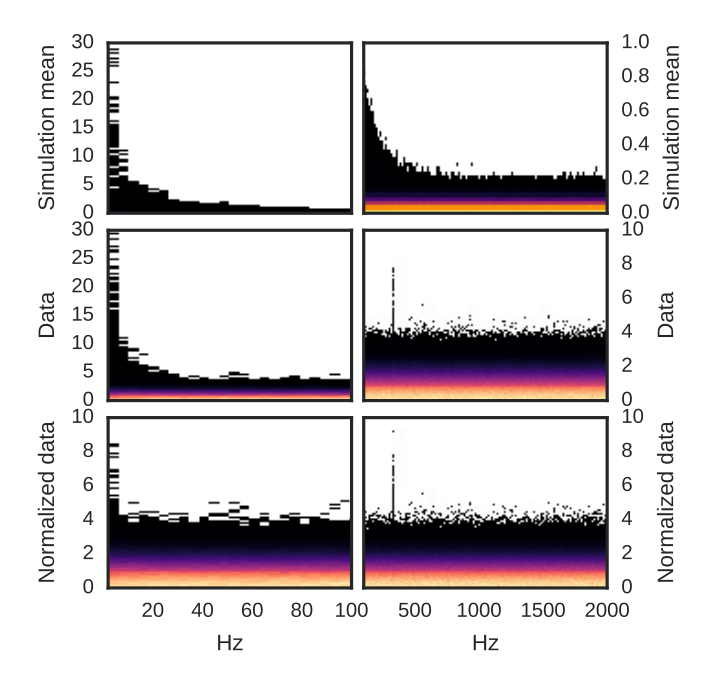


Figure 9. An example of the frequency-dependent distribution of both Fourier coefficients |I| and |R|. The distribution was computed in 1s windows using the data from 4U 1702-429. For plotting purposes, the harmonics from 2 to 2000 Hz were grouped in 4 Hz bins. Color marks histogram values in a given 2D (frequency/coefficient value) bin. White corresponds to zero counts in a given bin, black to one or a few. The color becomes progressively lighter as the number of counts increases. The left and right panels highlight different parts of the distribution, below and above 100 Hz, respectively. For both panels, the top subplot shows the average coefficients from the simulated photon sequences. Middle subplot shows the data and the lower subplot shows the normalized data, with the mean value of the simulated coefficients subtracted. Simulations removed most of the lowfrequency noise, but some of it is still present at the very low frequencies.

dates cannot be immediately connected to the imperfect LC modeling (hereafter "type II" low-frequency candidates). Several sources (e.g. Cyg X-2, EXO 0748-76, EXO 1745-248) exhibited such unexplained bursts of low-frequency candidates spanning multiple harmonics and sometimes showing at distinctly separate frequencies (Fig. 10, right). The origin of this type II low frequency noise remains unclear: it could well be astrophysical, associated with either the bursting surface or the accretion disk (see for example van der Klis 2006).

Although mostly recorded from fast-spinning neutron stars, TBOs can occur at frequencies as low as 11 Hz (IGR J17480-2446, Cavecchi et al. 2011). So far, only one such slow TBO source is known and finding another one (or the one spinning at even lower frequency) would be very interesting. In general, however, we found that

power spectra at the lowest frequencies of few Hz are difficult to interpret, since it is hard to distinguish between LC variation and oscillations here. An example of such a problematic spectrum is shown in Fig. 11. Oscillations with a frequency of about 3 Hz are clearly visible in the lightcurve. With the given choice of smoothing and spline fitting parameters, LC modeling removes some of the count rate variation and changes the shape of the peak in the power spectrum. More stringent LC models can reproduce the observed LC variations, removing the peak completely

We have inspected visually all diagnostic plots featuring type II low-frequency candidates looking for signals resembling the 11 Hz TBOs from IGR J17480—2446: with detections in multiple independent time windows and multiple bursts, at frequencies larger than the lowest recorded frequency of 2 Hz and without candidates of comparable strength at the nearby, but distinctly separate frequencies. No such candidates were found.

## 5.2. Dead time

In Section 4.2 we reviewed the methods of estimating the influence of the instrument's dead time on the observed noise statistic  $P_n$ . In this section we will examine the  $P_n$  from the whole set of observations in our sample.

In order to investigate the dead time influence, we recorded the mean non-normalized simulated power at frequencies above 1 kHz. At these frequencies the bias caused by LC variation is small for all of our sources (Sect. 5.1). We found that the simulated noise power did not have any discernible dependence on the number of PCUs that were on, and varied between 1.5 and 2, depending on the total photon count rate recorded by the PCUs (obtained from Standard-1 data files). This count rate is always equal to or larger than the count rate derived from the high- $t_{\rm res}$  data.

Fig. 12 (left) provides the reference for average simulated noise power versus count rate per PCU in high- $t_{\rm res}$  and Standard-1 files. For count rates larger than  $8\times 10^3\,{\rm cts\,s^{-1}\,PCU^{-1}},\,P_{\rm n}$  is smaller than about 1.7, differing dramatically from the value of 2 prescribed by the ideal  $\chi^2$  noise model. Thus, neglecting dead time influence for bright bursts can lead to an underestimation of the potential signal significance by orders of magnitude. The average power is considerably smaller than 1.7 at the peaks of at least one burst from 4U 0614+09, 4U 1608-552, Aql X-1, HETE J1900.1-2455, and SAX J1808.4-3658.

Comparison of noise powers between real and simulated data is not straightforward because of the large intrinsic noise variance: for  $P_{\rm n}$  obeying  $\chi^2$  distribution with two degrees of freedom, the standard deviation of noise powers is 2, the same as the mean value. Averaging all harmonics above 1 kHz reduces the standard deviation to  $\approx 0.045$  for  $T_{\rm win}=1\,{\rm s}$  and allows us to pinpoint the influence of dead time. For simulated data, additional averaging by 100 simulation runs further reduces

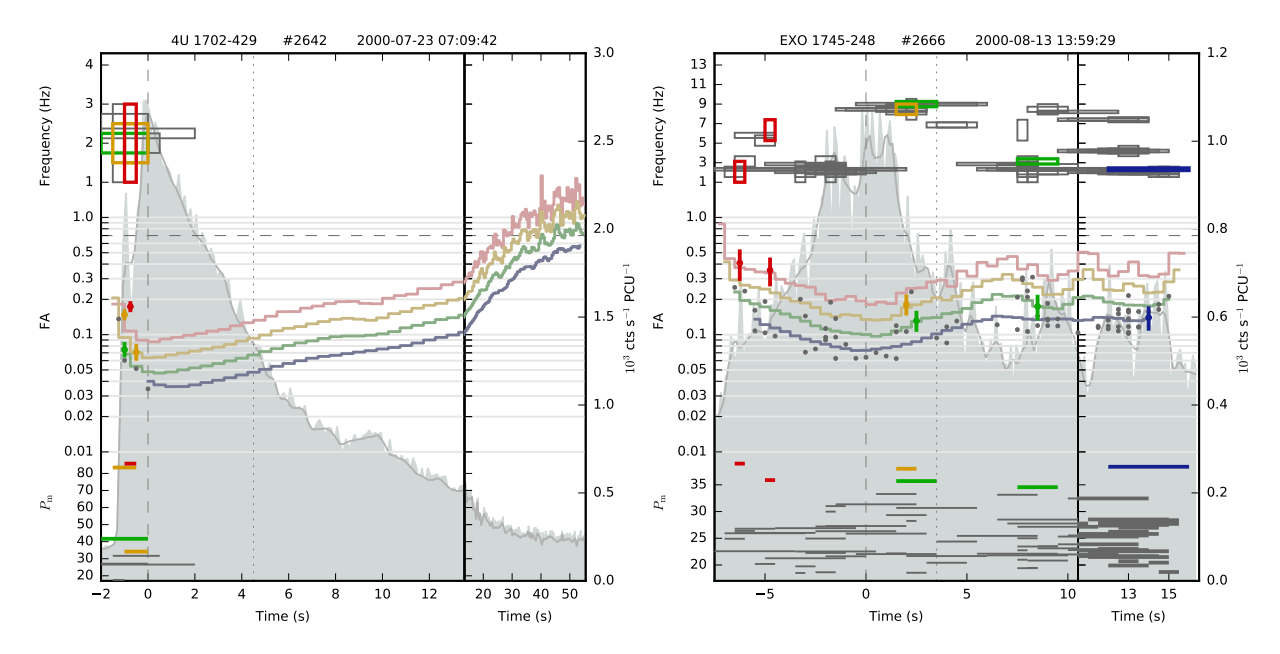


Figure 10. Left: a group of low-frequency oscillation candidates appearing due to imperfect modeling of burst LC, which did not reproduce a short spike around t = -1 s (type I low-frequency candidates). Right: clusters of low-frequency candidates not immediately connected to flaws in LC modeling (type II).

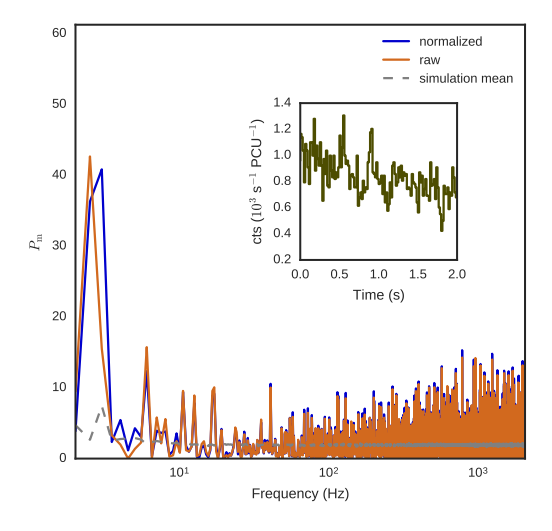


Figure 11. An example of 1D power spectrum in 2-s window right after the peak of a faint burst (#3306) from Cyg X-2. Blue/brown line shows normalized and un-normalized spectra, respectively, with the mean of the simulated spectra shown with a dashed line. The inset features the LC in the same window, with  $\sim$  3-Hz oscillations readily visible.

the standard deviation by a factor of 10. Fig. 12 (right) shows the 2D distribution of such average noise powers in real and simulated data. For most values of simulated power, the noise powers for the real data appeared to be statistically slightly larger than the corresponding simulated power, most probably stemming from the simplifications we made during dead time pruning. The dis-

crepancy can reach as much as 0.15 for  $\langle P_{\rm n} \rangle \lesssim 1.6$ , but is not larger than 0.02 for the more common  $\langle P_{\rm n} \rangle \gtrsim 1.8$ . This leads to an overestimation of the real data candidate significance by a factor that can be as large as few (for the largest count rates), but more commonly of about a few percent.

It is worth mentioning that dead time also biases the measured fractional amplitudes of TBO candidates, since the fraction of dead time is different during the crests and troughs of the oscillation trains. Using non-normalized  $P_{\rm m}$  in Eq. 8 may bias FAs by as much as a factor of  $(1.5/2)^{0.5} \approx 0.87$ .

## 5.3. Overall simulation quality and glimmer candidates

In order to assess whether our simulations are adequately reproducing the data, we compared the distributions of normalized powers  $P_{\rm m}$  for the real and simulated data sets. For each source and  $T_{\text{win}}$  we combined powers in two frequency regions: between 15 and 1000 Hz (thus, excluding any low-frequency noise), and between 1000 and 2000 Hz (see Fig. 13, left, for an example). The distributions for real data and the mean distribution of 100 simulation runs match reasonably well. Moreover the distribution of normalized  $P_{\rm m}$  is well described by  $\chi^2$  statistics, assuming a conservative number of trials (i.e. treating all time windows as independent, Fig. 13, right). The same is true for the candidates from all four  $T_{\rm win}$  combined – the estimates of the average number of candidates using Eq. 5 and assuming all windows and harmonics to be independent are not dramatically different from the average number of candidates from the simulation runs (see also Table 3).

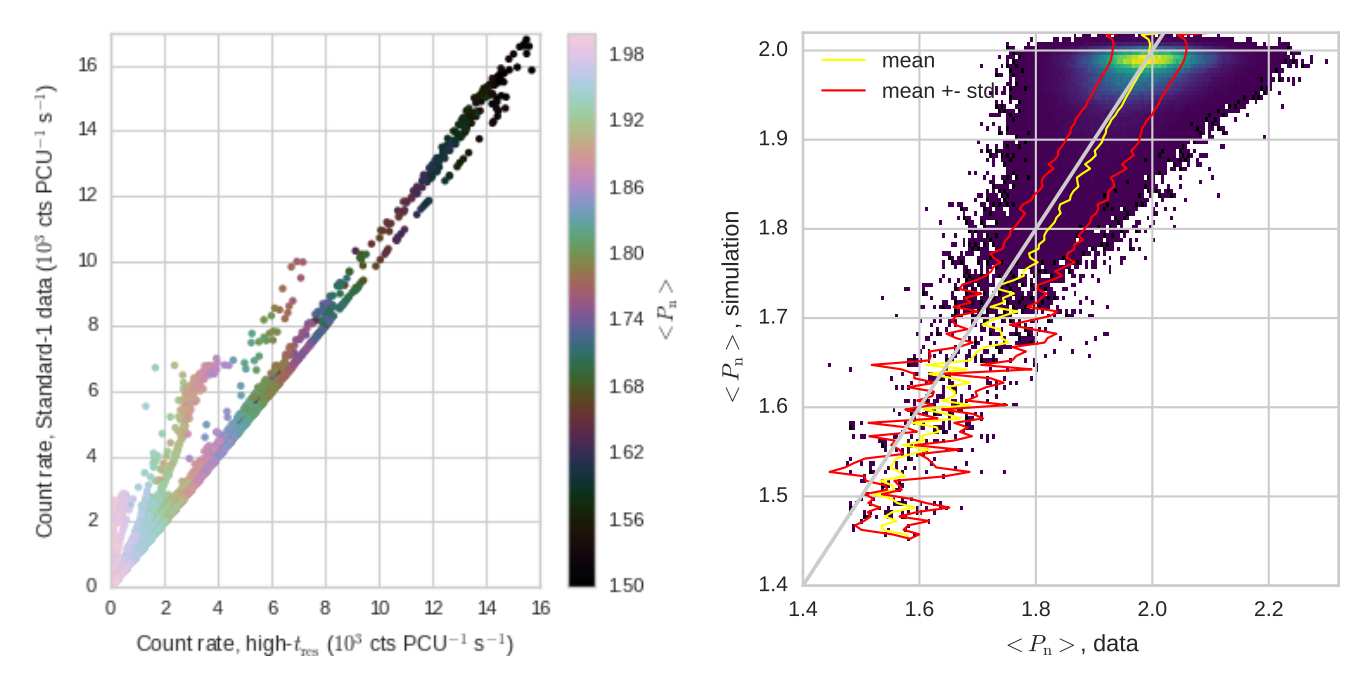


Figure 12. Left: simulated noise power vs. count rate in Standard-1 and high- $t_{\rm res}$  files for 1-s Fourier windows for all sources. Right: 2D histogram of the mean simulated vs. real data noise power averaged over frequencies above 1 Hz. Yellow/red lines show mean and  $\pm$ std of real data noise power for a given value of simulated power. The color represents the number of counts in each cell of the histogram, with the darkest one being the smallest (1 count). On both plots the simulated power is averaged over 100 simulation runs and all harmonics above 1 kHz.

However, for some of the sources the match is not perfect. After normalizing the real-data distribution by the corresponding mean and standard deviation of 100 simulated-data distributions, one can see that there is a systematic discrepancy between the two for  $P_{\rm m}\lesssim 20$ . The amount of discrepancy is usually larger for frequencies below 1000 Hz and varies considerably from source to source. It may stem from imperfect dead time or LC modeling, or any weak broadband astrophysical signal.

For some of the sources, we found a small excess of higher-power candidates (e.g. with  $P_{\rm m}>35$  on Fig. 13). This excess can be present in either of the two frequency groups and is equivalent to 5–10 standard deviations in a given power bin. The examination of the cumulative versions of the normalized power distributions for all  $T_{\rm win}$  combined showed that for several sources, e.g. 4U 1608–522, EXO 0748–676, Cyg X-2, and others, the number of candidates above the detection threshold on the real data (excluding frequency ranges of known TBO) is larger than the corresponding number in  $\geq 99\%$  of the simulation runs ( $p \leq 0.01$ , see Table 3). On the other hand, the prolific TBO source 4U 1636–536 yielded fewer real-data noise candidates than any of 100 simulations. The origin of this discrepancy is unclear.

Such marginally significant noise candidates (dubbed "glimmer candidates", reflecting potential attractiveness) are detected in a single independent time window,

at seemingly random, never repeating frequencies<sup>12</sup> and throughout all on-burst windows. Some of the candidates occur at lower frequencies in time windows with substantial count rate variation and their significance is very sensitive to LC modeling. Glimmer candidates can be present in the bursts with TBOs, sometimes even in the same time bins as TBOs. Folded glimmer candidates produce sinusoidal profiles and some of them are stronger than weak TBOs (e.g. Fig. 14).

It must be noted that whether the source has glimmer candidates depends on the detection threshold. For example SAX J1808.4–3658 has p=0.22 at standard detection threshold, however the power of some of the noise candidates is much larger than any of the simulated powers. On the other hand, for MXB 1658–298 p drops from 0.06 to 0.01 if the threshold probability is multiplied by 3.7 (Sect. B.1.4).

One must be very careful in interpreting glimmer candidates. By definition, the source has glimmer candidates if the number of detections outside TBO frequencies and not immediately connected to low-frequency noise is larger than the number of candidates in 99% of simulation runs. This means that assuming a sufficiently large number of bursts per source, 1% of all sources will

 $<sup>^{12}</sup>$  Except for two 1108-Hz candidates from EXO 0748-676, see Table 3.

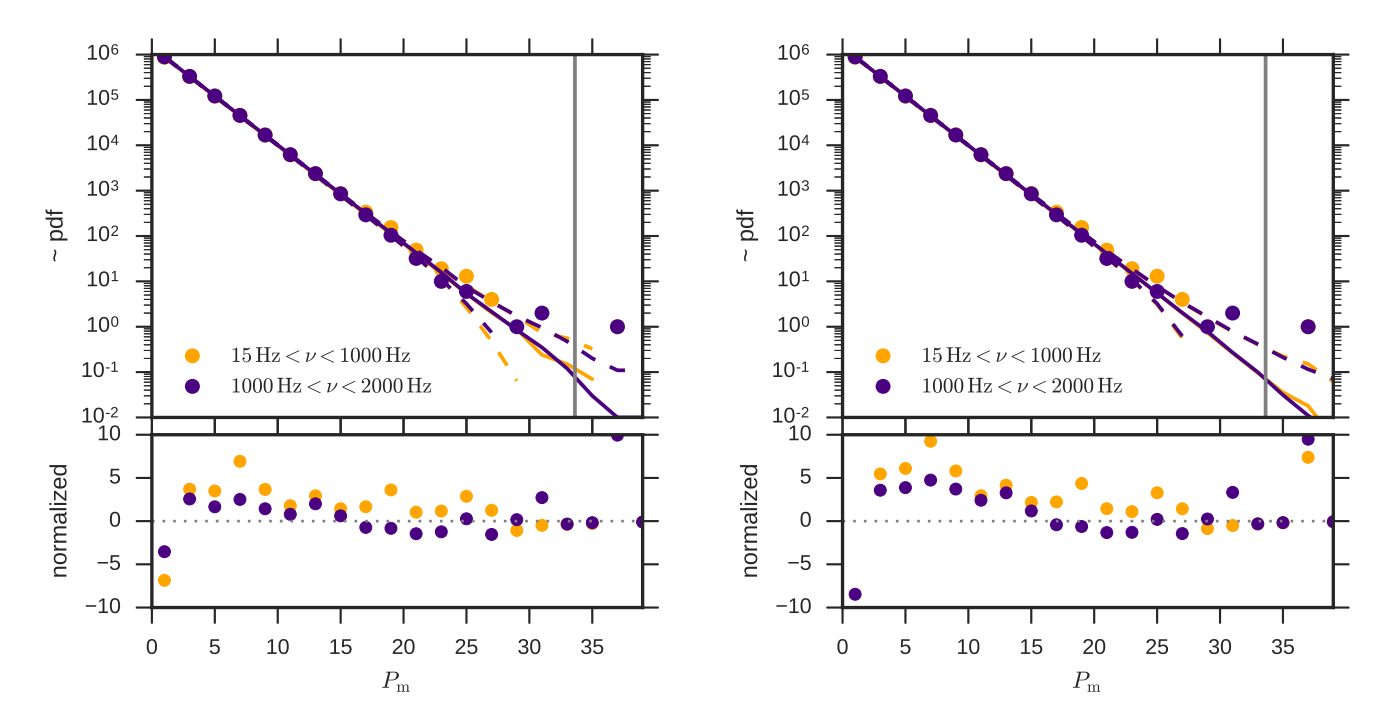
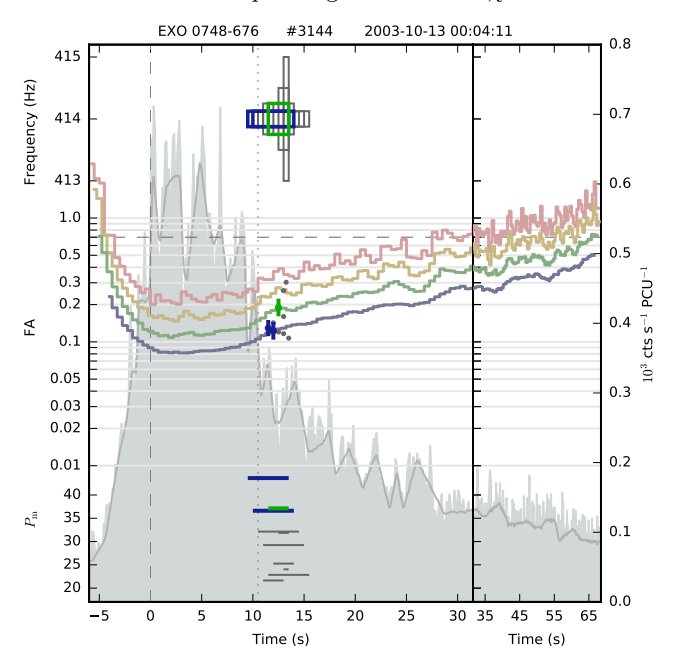


Figure 13. Histogram of power values for 2-s time windows for all bursts from Cyg X-2 in two frequency groups (dots) compared to the mean (solid line) of 100 simulations (left panels) and 4000  $\chi^2$ -distributed random values (right panels, for conservative number of trials). Dashed lines show one standard deviation offset from the simulation mean. Vertical grey lines show the candidate selection threshold. Bottom panels show histogram counts for the real data, normalized by the mean and standard deviation of the corresponding simulated or  $\chi^2$  distributions.



**Figure 14.** An example of a glimmer candidate, one of the marginally significant noise candidates from EXO 0748-676. This source has TBOs at  $\approx 553\,\mathrm{Hz}$  (see Sect. B.1.1).

have glimmer candidates purely due to chance. At our detection threshold, five sources, or 8.8% had  $p \leq 0.01$ ,

which is larger than the expected 1%, suggesting that at least some of the glimmer candidates may have an astrophysical origin. Some may for example be connected to type II low-frequency candidates which happen to occur at somewhat higher frequency and more than 2 Hz apart from other candidates, thus being placed in a separate frequency group by our grouping procedure.

## 5.4. TBOs from known oscillation sources

Seventeen TBO sources were known prior to our analvsis. These are the sources with TBOs detected at similar frequencies, in several independent time bins, several bursts or at frequencies close to the frequency of APPs. All of these sources yielded candidates at the frequencies close to those reported previously and all but one had more candidates than any of the simulation runs (p = 0)in a purely blind search. We note that the TBO candidates from the accreting MSP HETE J1900.1-2455 would not have been significant in our blind search which neglected closeness to the known APP frequency for this source, since the TBOs come from one independent time window and have moderate power. For the other sources, sometimes we did not have any candidates (including sub-threshold, see Sect. 5.8 for our definition of sub-threshold candidates) where they have been reported previously. This may be explained by differences in data processing.

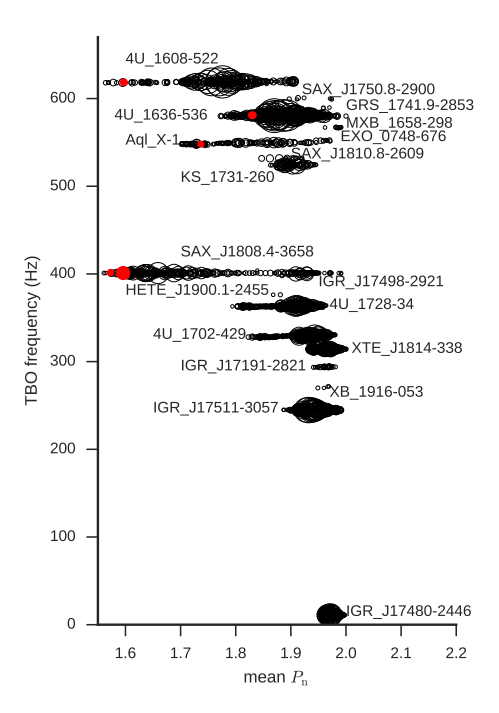


Figure 15. Frequency against mean simulated noise power for candidates in the groups covering the frequencies of known TBO sources. The size of the marker is set by  $P_{\rm m}$  of a candidate. Red markers show candidates, for which at least one of the absolute values of the mean simulated Fourier coefficients was likely to be influenced by the variation of count rate within the Fourier window.

In general, we find that the measured power of TBO candidates depends strongly on the size of the Fourier window and its location. Because we searched in several windows of different length, we were able to give a more complete picture of the fractional amplitudes, which may be important for bursts with more than one oscillation train, i.e. bursts with photospheric radius expansion (PRE), with a short train of TBOs in the rise and a longer train after the burst peak). We have compiled an extensive dataset of fractional amplitudes (Table 4) as well as upper limits for each of the four window lengths (Table 2), to support future studies of TBO physics (see Sect. 6).

For many of the TBO sources a considerable fraction of TBO candidates came from the data regions with large influence from dead time (Fig. 15). Low-frequency noise does not have much of an influence – only in a few cases the absolute mean values of the simulated Fourier coefficients were larger than  $6 \times 0.05$  (see Sect. 4.4, 5.1 and Fig. 9). More information about each TBO source is given in Section B.1.

## 5.5. Tentative TBO detections from the literature

Eight sources in our sample had tentative TBO detections prior to our analysis (see Table 2 in Watts 2012).

Here we summarize the results of our analysis of these sources, more detailed information about each of them is given in Section B.2.

No TBO candidates were detected in the only burst from 4U 0614+09, observed by RXTE. Previously, the 415-Hz oscillations were reported from one burst observed with Swift. The FA limits from the RXTE burst are more stringent than the detection reported from the Swift, but as we know from other sources, TBOs are not consistently detectable in all bursts from a given source.

The previously reported 529-Hz TBO candidate from 1A 1744-361 was also detected in our analysis, however it was too faint to be significant given the number of trials. The presence of sub-threshold candidates tracing out a small frequency drift argues in favour of this candidate being a genuine TBO, but a new detection is needed to confirm this.

TBO candidates from 4U 1254–69 (95 Hz), XTE J1739–285 (1122 Hz), and SAX J1748.9–2021 (410 Hz), discovered in time windows with sizes similar to the range of  $T_{\rm win}$  used in this work were in our analysis not significant enough to pass the detection threshold. The sources did not have any clusters of sub-threshold candidates close to the reported frequencies. TBO from another two sources, MXB 1730–335 (306 Hz) and GS 1826–24 (611 Hz) were claimed based on stacked power spectra. None of our candidates for these sources were close to the frequencies reported in the previous papers.

XB 1916-053, with its pair of TBO candidates at frequencies 2 Hz apart remained controversial in our analysis. In addition to these two candidates, we detect four other strong candidates, all of them potentially due to type II low-frequency noise. None of the simulated data sets had as many candidates as the real data, whether or not one counted the 270-Hz candidates as a TBO. A more precise estimate of the significance of this signal should take into account frequency separation between the candidates; however this is outside the scope of this current work.

## 5.6. New TBO discoveries

One more TBO source has been discovered, SAX J1810.8–2609, yielding strong ( $P_{\rm m}=79$ ) 531-Hz oscillations in one independent time window (see Sect. B.3.4). The candidate power so strong that it has small  $p(\chi^2)$  probability assuming the most conservative number of trials (counting all harmonics and all time bins from the whole 57-source sample as independent). Full details of this discovery are reported in Bilous et al. (2018).

Besides that, we recorded an interesting pair of  $\sim$  600-Hz candidates from IGR J17473–2721 (see also Sect. B.3.3). These candidates were faint (p>0.5), but came within 3 Hz from each other and framed the burst peak during a burst with PRE, showing typical features of TBOs from established TBO sources (e.g. SAX J1750.8–2900).

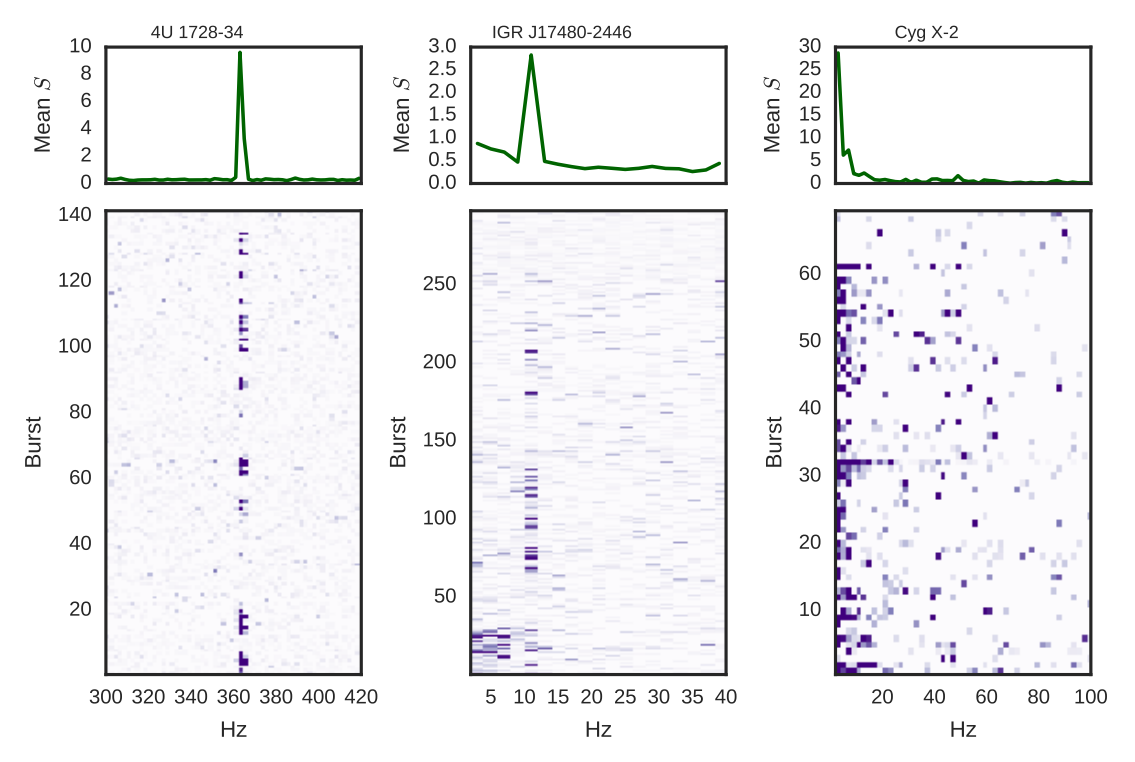


Figure 16. Total power of candidates with  $p_{\rm sb}(\chi^2)$  from Eq. 12, normalized by the size of the on-burst window for three sources. For all three panels the color map has been saturated at the Leahy-normalized power of 15. Left: Known TBO source 4U 1728-34. Bursts without regular candidates do not, in general, have sub-threshold candidates. Center: IGR J17480-2446 has only two 11-Hz candidates above the standard detection threshold (Eq. 11), but many more sub-threshold candidates. Right: Cyg X-2, exhibiting many sub-threshold candidates at random frequencies.

#### 5.7. Other sources

Out of the remaining thirty sources in our sample that had no published record of TBOs prior to our study twenty-three were unremarkable, with the number of noise candidates reproduced well by simulations. Some of these sources also had low-frequency noise of type I or II. Seven more sources had a marginally significant number of candidates (albeit occurring at random frequencies), or stronger and more broadband low-frequency noise. More details can be found in Sect. B.3.

#### 5.8. Subthreshold candidates

Even if an individual candidate has moderate power that is below our nominal threshold, a cluster of subthreshold candidates in a relatively narrow frequency range may indicate the presence of TBOs. We performed a simple search for such a clustering of sub-threshold candidates by summing the powers of all candidates with:

$$p_{\rm sb}(\chi^2) < \frac{10^{-1}}{2000 \times T_{\rm win}},$$
 (12)

which corresponds to  $P_{\rm m}$  of 17.03, 18.42, 19.81, and 21.19 for  $T_{\rm win}$  of 0.5–2 s. The sums,  $S(\nu)$ , were additionally added in 2-, 4- or 8-Hz frequency bins and normalized by burst duration. The stacks of  $S(\nu)$  were

then inspected visually for traces of power excess correlated in frequency.

Interestingly, for known TBO sources the bursts without TBO candidates did not necessarily yield subthreshold candidates, with  $S(\nu)$  in the TBO frequency range being similar to  $S(\nu)$  at other frequencies (e.g. Fig. 16, left). Nevertheless, some of the known TBO sources did have sub-threshold TBO candidates, with the most prominent example being IGR J17480–2445. Only two bursts from this source have candidates at 10–11 Hz in Table 3, but many more bursts have relatively large  $S(\nu)$  (Fig. 16, middle).

About half of sources in our sample exhibited low-frequency noise on  $S(\nu)$  stacks, sometimes extending to  $\sim 20\,\mathrm{Hz}$ . For Cyg X-2, this frequency region was particularly noisy with multiple sub-threshold candidates at random frequencies (Fig. 16, right).

None of the sources showed any obvious clustering of candidates at frequencies different from the frequencies of known TBOs. This was something of a surprise: we had anticipated that there would be sub-threshold candidates emerging from such a large data set. It also must be noted that, similarly to most TBO searches, our analysis does not include the effects of any potential smearing due to intrinsic TBO frequency drift and Doppler shifts due to the motion of the Earth and the binary orbit, all of which would reduce detectability.

#### 6. SUMMARY

In this work, we conducted a large-scale blind search for thermonuclear burst oscillations for the majority of type-I X-ray bursts observed by RXTE. In comparison to previous work, our analysis encompassed more sources, and probed potential signals on a range of time scales and further into burst tails, treating all sources in a uniform fashion.

In order to estimate the significance of selected oscillation candidates, we developed a more realistic noise model by simulating photon sequences with variable count rate which mimicked the real light curves and was affected by dead time. Fourier spectra from simulated sequences were used to renormalize the corresponding Fourier spectra from the real data and thus to remove the low-frequency noise due to variable count rate, and to restore the dead-time-affected average power.

Our noise model showed that abrupt LC variations, for example during the burst rise or data gaps, can bias the noise statistics in a frequency-dependent manner at frequencies up to approximately 100 Hz, or, in several cases, even up to 1 kHz (thus, not being confined to low frequencies any more). LC modeling allowed us to remove most of this bias. However, in some cases we still detect strong candidates below 16 Hz. These low-frequency candidates did not immediately resemble known low-frequency TBOs from IGR J17480-2446: with detections in multiple independent time windows and multiple bursts, at frequencies larger than the lowest recorded frequency of 2 Hz and without candidates of comparable strength at the nearby, but distinctly separate frequencies. Some of the detected low-frequency candidates are clearly generated by single, poorly modeled sharp peaks or dips in LCs, these we refer to as "type I" low-frequency candidates.

Several more sources yielded candidates not immediately connected to flaws in LC modeling (e.g. Cyg X-2, 4U 1729-34, EXO 0748-676, EXO 1745-248, and others). Such candidates, dubbed "type II" low frequency candidates, frequently appeared to be grouped in time and/or frequency, sometimes appearing at distinct frequencies simultaneously. It is possible that these type II low frequency candidates may have an astrophysical origin: perhaps a non-TBO process on the burning surface, or varying emission due to the effect of the burst on the accretion flow (see for example Worpel et al. 2013, 2015). Generally, the signal at the lowest frequencies in our spectra (below approximately 5 Hz) is quite hard to interpret, since its strength depends substantially on how closely the model LC follows the real one.

The instrumental dead time had, somewhat surprisingly, a rather large influence on the power spectra statistics, with the average noise power dropping below 1.7 for the burst peaks of five sources, some of them with TBOs. Neglecting the influence of dead time can

lead to underestimation of candidate TBO significance by as much as two orders of magnitude.

Overall, our noise models provide an important insight into the statistics of RXTE power spectra, but they do not give a perfect description of the data, most probably because of the set of assumptions regarding the dead time influence and what constitutes a "real" LC. Also, some bias is caused by the limited number of simulations run to derive the statistical properties of noise. From the computational point of view, it is much easier to estimate the average noise power using harmonics past  $\gtrsim 1\,\mathrm{kHz}$ , renormalize the power spectra and use  $\chi^2$  probability distribution with conservative number of trials (treating all time windows as independent, regardless of overlap) to estimate the candidate significance. However, this approach would not work at lower Fourier frequencies during the burst rise or during data gaps.

We have also found that abrupt changes in the LC rate (sharp rise or a data gap) can lead to covariance between adjacent Fourier harmonics and can manifest as a fast change of TBO frequency. A quantitative investigation of this phenomenon will be presented in subsequent work. Overall, data gaps obliterate part of the signal and bias the fractional amplitude evolution: using data with gaps should be avoided if at all possible. Future X-ray telescopes aiming to study this phenomenon should aim for high throughput.

For our study, we have selected all candidates with renormalized  $\chi^2$  probabilities less than  $2\times 10^{-4}$  per spectrum. This resulted in the power thresholds varying with time window size. Our choice of detection threshold was to some degree arbitrary, but was motivated by a wish to analyze a manageable number of candidates. The significance of these candidate detections was then estimated by comparing the number of candidates in the real data to a pool of an additional 100 of simulated spectra, renormalized in the same way as the real data.

Our candidates included all previously known TBOs. For one of the sources, the accreting MSP HETE J1900.1–2455, the detection in a single time window was not significant because of the large number of trials in our analysis. The study that reported this finding originally searched a narrower frequency range around the known pulsar frequency (Watts et al. 2009). We find that the power of candidates depends dramatically on the specific window sizes and degrees of overlap used.

Overall, we have compiled an extensive data set containing information on the frequency and fractional amplitudes of all selected candidates, as well as upper limits on fractional amplitudes derived from the threshold powers. We anticipate that this information will be a valuable resource for future studies of TBO properties, particularly when used in conjunction with the burst property database MINBAR. The conditions under which TBOs are excited and detectable are impor-

tant factors in assessing the viability of physical models for the TBO mechanism (Watts 2012).

Eight sources in our dataset had prior claims of TBOs where the claimed detections were either weak and came from one independent time window (or, in the case of XB 1916–053, two close but separated frequencies) in a single burst or several stacked bursts. We were unable to confirm TBOs from any of those sources. Some of the previously claimed detections had smaller powers in our analysis (which can be sensitive to the choice of the time windows) and were not significant when compared to noise simulations. For 4U 0614+09 we had different bursts than the ones with potential TBOs (which came from a different telescope); the burst in the RXTE sample showed no TBO candidates. Other claimed detections were based on analysis of stacked spectra and yielded no candidates in our time windows.

One of the sources without previously reported TBOs, SAX J1810.8-269 yielded a strong, brief 531-Hz pulsation in one of the bursts. The signal was detected in one independent time window, however its strength ( $P_{\rm m} > 70$ ) speaks in favour of it being a TBO (for more in-depth significance analysis, see Bilous et al. 2018). The other sources did not provide any compelling TBO candidates, despite our removing most of the low-frequency noise and making better significance estimates for bright bursts. In addition, we found no groups of sub-threshold candidates, probing probabilities up to 100 higher than our adopted detection threshold. This was somewhat surprising: we had anticipated finding at least some clusters of sub-threshold candidates in such a large burst sample.

An interesting (albeit not formally significant in our analysis) pair of  $\sim 600\text{-Hz}$  TBO candidates was recorded from IGR J17473-2721. The candidates were rather faint, but came close in frequency (within 3 Hz) and framed the burst peak during a burst with PRE. More than half of the simulation runs had as many or more candidates (at arbitrary frequencies) with at least the same significance.

Another source with previously-reported potential TBOs with similar characteristics, XB 1916–053 had much more significant candidates, with as few as 2% of the simulations runs having the candidates at least as strong as the strongest one on the real data. Overall, IGR J17473–2721 and XB 1916–053 would be interesting sources for subsequent follow-up.

Our estimate of candidate significance treated all frequencies as independent and did not include important TBO features such as frequency drift coupled with signal disappearance during PRE. In the case of weaker signals, it is currently unclear how small a gap in frequency should be for the signals to be attributed to a single TBO.

We have found that some of the sources exhibited a marginally significant number of noise candidates, meaning that 99% or more simulations runs had a

smaller number of candidates. These candidates appeared at random frequencies both below and above 1 kHz in single independent time windows and were often stronger than some of the TBO detections in individual bursts, reaching  $P_{\rm m} \gtrsim 40$ . We dub them *glimmer candidates*. It is possible that some of the glimmer candidates are of astrophysical origin (especially the ones at lower frequencies).

## 7. CONCLUSIONS

TBOs are transient phenomena with rapidly changing properties. The measured power of potential TBO candidates depends greatly on the specific choices regarding data selection, such as energy filters, time windows, degree of overlap, summing harmonics or adjacent time windows and stacking spectra from different bursts. Thus, considering the researcher's natural desire to find TBOs, one must be very careful with estimating the number of trials resulting from tweaking the search parameters and exploring multiple sources.

While searching for high-power narrowband signals using Fourier transform in overlapping time windows, it is generally reasonable to use a  $\chi^2$  model of the distribution of the noise powers with the conservative number of trials, after correcting for dead time influence, LC variation and making sure that the harmonics in Fourier spectra are not covariant. However, it is strongly advisable to verify that a  $\chi^2$  distribution actually describes well the noise powers of a given dataset.

Our search for TBOs resulted in several short (each detected in one independent time window) candidates with powers comparable to those of the fainter TBOs  $(P_{\rm m} \sim 30-40)$ . These candidates, dubbed "glimmer" are marginally significant, meaning that 99% or more simulations runs had a smaller number of candidates. They produce sinusoidal oscillation profiles and are in all aspects resembling fainter TBOs. However, they occur at random frequencies within a single source and sometimes are coincident in time with real TBOs. Partly, glimmer candidates may stem from selection bias, however an astrophysical origin is not excluded. Regardless of their nature, the phenomenon of glimmer candidates may explain the large number of unconfirmed singlewindow detections, e.g Kaaret et al. (2002), especially considering the tendency of underestimating the number of trials.

For the potential detections with the smaller power, the best corroboration of TBO nature is detecting the signal at the same frequency in independent time windows; however with the intrinsic frequency drift and Doppler modulations complicate it. It is therefore important to develop a procedure for estimating significance of signals with drifting or jumping signal. This would help refining the significance of frequency jump in MXB 1658–298 (Wijnands et al. 2001), drifting candidate in 1A 1744–361 (Bhattacharyya et al. 2006), a pair of 270-Hz candidates XB 1916–053 (Galloway et al.

2001) and potential pair of 600-Hz candidates from IGR 17473-2721 (this work).

Despite our efforts, we did not find TBOs below 200 Hz and during high count rates. Several measures can be undertaken in order to obtain a better, more complete picture of TBOs. Obtaining new data using better instrumentation with higher throughput leads to better sensitivity and the absence of data gaps allows a better characterization of the frequency evolution. Continuing searching is also an option, since TBOs may appear from the sources without promising candidates, although having some theoretical guidance would be better, something the data could be used for. Further improvement of TBO searches can also be made by selecting only that part of energy spectrum where there are most burst

photons, in order to minimize the relative contribution of background. Having ephemerides would also help to correct for the Doppler change in frequency: this would be especially helpful for the ultra-compact binaries such as  $4U\ 1820-303$  or the potential ultra-compact binary  $2S\ 0918-549$ .

A.V.B. and A.L.W. acknowledge support from ERC Starting grant No. 639217 CSINEUTRON- STAR (PI: A.L. Watts). We would like to thank Duncan Galloway and the MINBAR team for sharing a pre-release version of the MINBAR database with us. A.V.B. thanks Hauke Worpel for sharing the data on background variation during type I bursts.

#### **APPENDIX**

A. TIMES OF ARRIVAL, LIGHT CURVES, AND TABLES

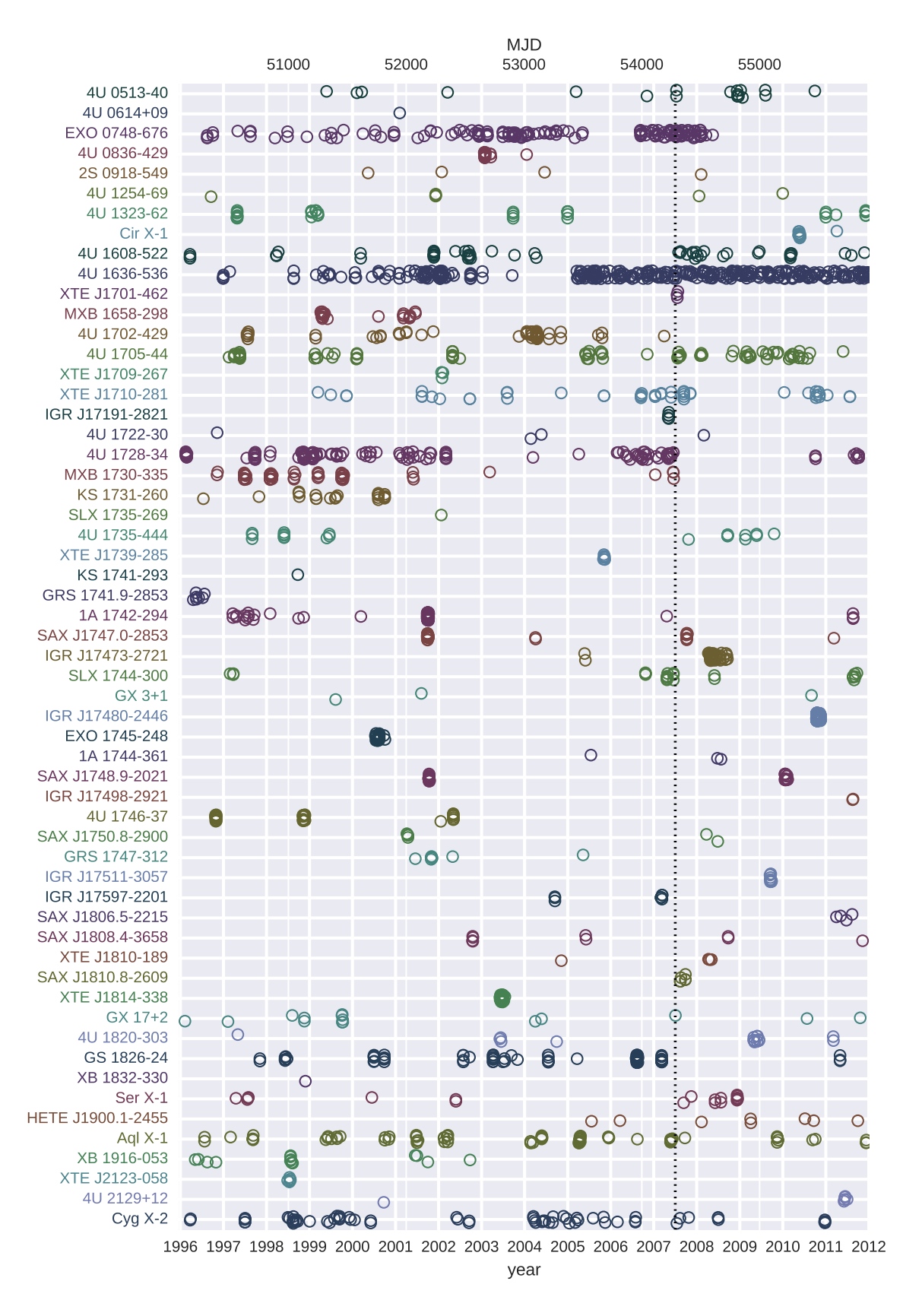


Figure 17. Times of arrival of 2118 bursts from MINBAR catalogue, for which high  $t_{\rm res}$  data were available. The sources are ordered by their coordinates (right ascension first). Dotted vertical line marks the end of the time cut for the sample of Galloway et al. (2008), however not all of the sources before that date have been examined in Galloway et al. (2008). Some of the bursts are so close to each other that the markers overlap completely.

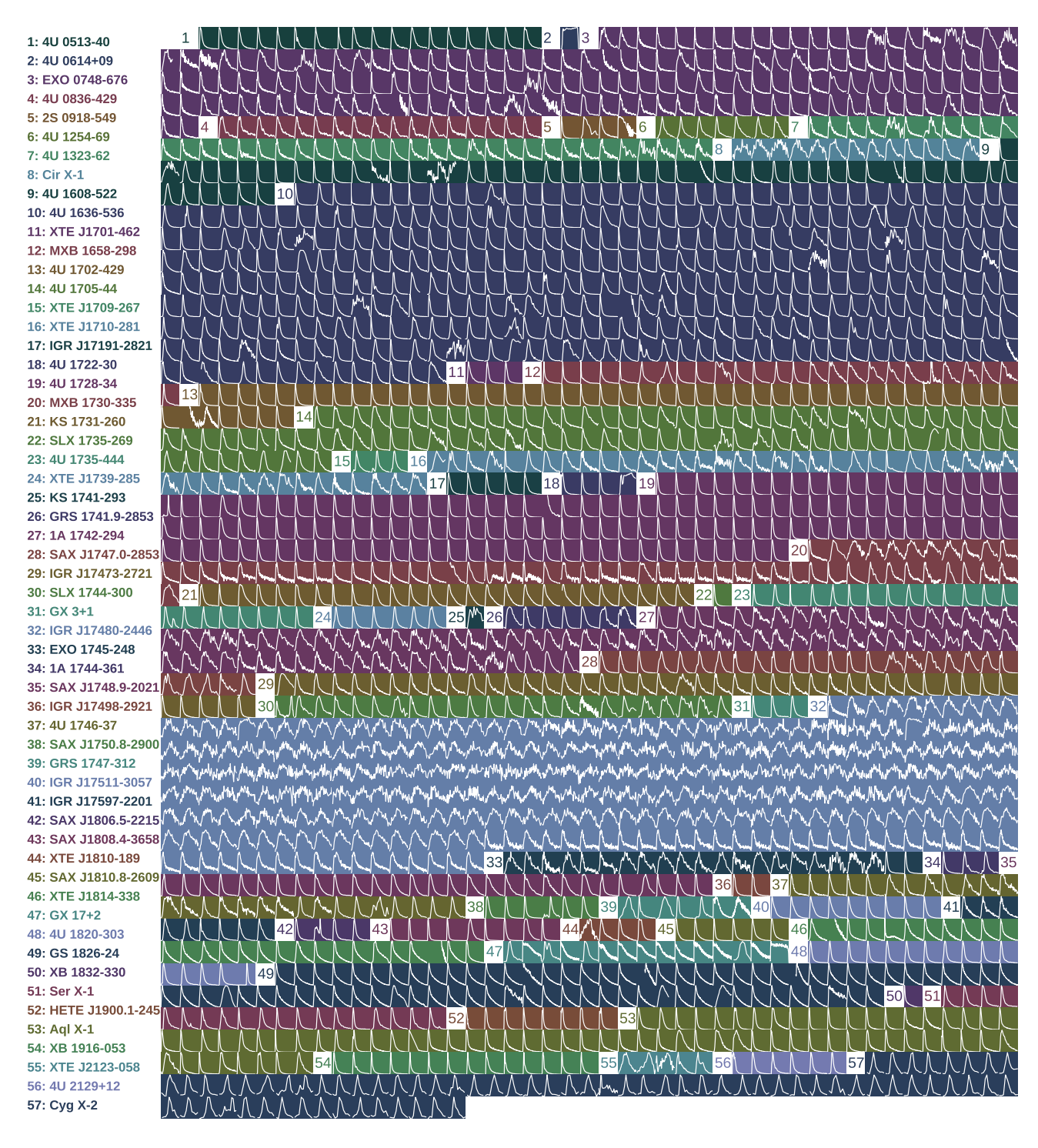


Figure 18. Light curves from Standard-1 data for 2118 bursts from MINBAR catalogue for which high  $t_{res}$  data were available. of bursts from the previous figure. The sources are ordered by their coordinates (right ascension first). Time span matches the adopted on-burst window for each burst, the y-axis scale is different for each burst.

Table 2. Data and FA<sub>up</sub> for one of the sources. This table is available in its entirety in machine-readable form.

1	2	3		4	5	6	7	8	9	10	11	12	13		14b in F <i>A</i>		
Source	Entr	y MINBAF	R TOA	$T_{ m peak} \  m (MET)$	Rise (s)	Half- max (s)	Tail (s)	Peak S/N	Data mode	Notes	$P_{ m m}$	x ν	$T_{ m win}$	0.5			4.0 (s)
HETE J1900.1-2455	3301	2005-07-21	23:00:32	364604449.9	14.5	30.5	413.5	1607.7	E_125us_64M_0_1	sgaps,	34.8	383.50	4.0	4.6	4.5	3.3	2.4
										bad LC,							
										freq cov							
	3362	2006-03-20	11:34:06	385472056.4	7.5	9.5	118.0	510.1	SB_125us_8_249_1	ls	29.2	228.00	4.0	4.6	3.3	$^{2.4}$	1.7
	3667	2008-02-10	20:32:51	445293182.9	9.0	5.5	86.0	435.8	E_125us_64M_0_1	s	35.2	12.00	0.5	7.2	5.2	3.8	2.7
	3818	2009-04-02	08:57:54	481280277.9	2.0	5.5	76.0	729.4	SB_125us_8_249_1	ls	43.5	376.25	4.0	6.1	4.5	3.3	2.5
	3820	2009-04-04	19:06:51	481489619.9	6.0	3.5	97.0	777.7	E_125us_64M_0_1	s	28.5	1471.00	2.0	6.6	4.8	3.5	2.6
	3944	2010-07-07	21:04:32	521154292.9	12.0	6.5	118.5	672.8	E_125us_64M_0_1	s	32.6	674.50	2.0	7.1	5.2	3.8	2.7
	3960	2010-09-20	05:29:04	527578164.4	7.5	8.5	92.0	427.1	SB_125us_8_249_1	ls	27.6	1313.50	4.0	6.0	4.3	3.1	2.3
	8257	2011-09-29	23:43:46	559957439.4	7.5	5.0	74.5	554.3	E_125us_64M_0_1	s	30.3	776.00	4.0	7.0	5.1	3.7	2.8

Note—Table 2 columns: (1) source name; (2) burst entry # in MINBAR database; (3) burst TOA in MINBAR database; (4) time of the burst peak; (5)  $dt_{\text{rise}}$ , the size of the rise window; (6)  $dt_{\text{halfpeak}}$ , the time span between peak and the half-peak on the trailing side; (7)  $dt_{\text{decay}}$ , time span between the the peak and burst decay; (8) peak S/N; (9) observing modes used for TBO search; (10) notes, including: manual RBT windows faint bursts or bursts with peculiar shapes, presence of data gaps, partial GTI coverage, missing data for at the edges of on-burst window, covariance between Fourier harmonics, local failures in LC modeling; (11) maximum measured power  $P_{\text{m}}$ , low-frequency noise excluded; (12) frequency of maximum  $P_{\text{m}}$ ; (13)  $T_{\text{win}}$  of the maximum  $T_{\text{m}}$ ; (14) best upper limit on FA in four window sizes (14a-d).

Table 3. Overview of bursts and TBO candidates

1	2	3	4	5a	5b	6a	6b	6c	7	8		9b			10a	10b	10c	10d
		m . 1		1-s I	$\mathrm{A_{up}}$	# of 1	noise car	$_{ m ididates}$	_		$N_{\rm b}$	rst V	vith	$\det$	Mean	$P_{ m m}$ in	ı FFT	windov
Source	$N_{ m brst}$ total	Total duration (s)	$\begin{array}{c} {\rm Median} \\ {\rm SN_{peak}} \end{array}$	min	med	$\chi^2$	mean simul	real data	p	$^{\nu}_{\rm (Hz)}$	Ang	y R	В	Т	$0.5\mathrm{s}$	$1.0\mathrm{s}$	$2.0\mathrm{s}$	$4.0\mathrm{s}$
4U 0513-40	18	896.5	135.3	8	13	1.43	1.10	2	0.28	2.00 - 3.25	1	0	1	0	39.3	52.0	56.6	51.9
										1378.75	1	0	0	1				37.4
4U 0614+09	1	34.5	1406.4	2	2	0.06	0.02	0	1.00									
EXO 0748-676	159	15560.0	100.7	5	14	24.90	22.05	39	0.01	2.00-14.50	67	47	55	9	38.5	42.9	47.2	50.6
										86.00	1	0	0	1	31.2			
										113.00	1	0	0	1			34.4	
										147.50	1	0	0	1			38.7	
										288.00	1	0	0	1			34.2	
										327.50	1	0	0	1			39.9	
										333.75	1	0	0	1				36.1
										339.00	1	0	0	1			36.7	
										361.00	1	0	0	1				38.5
										390.00	1	0	0	1				35.3
										399.50	1	0	1	0			34.4	
										414.00	1	0	1	0			37.1	40.1
										470.00	1	1	0	0	31.8			
										539.00	1	0	0	1				40.6
										551.50 - 552.50	<b>2</b>	<b>2</b>	0	0	34.5	45.5		
										599.00	1	0	0	1			40.4	
										700.50	1	0	0	1			36.0	
										812.50	1	0	0	1			35.3	
										831.50	1	0	1	0				35.6
										867.00	1	0	0	1				35.7
										873.00-874.00	2	0	1	1		32.7		
										948.00	1	0	0	1		32.4		
										1005.00	1	0	0	1		35.6		
										1027.25	1	0	0	1				35.3
										1108.00	2	0	0	2			35.6	
										1181.00	1	0	0	1		35.3		
										1234.00	1	0	1	0		38.3		
										1376.50	1	0	0	1				35.9
										1390.00	1	0	0	1	31.5			
										1585.00	1	0	0	1		33.5		
										1598.00	1	0	1	0	31.1			
										1865.00	1	0	0	1		34.2		
										1890.00	1	0	0	1	31.2			
										1978.00	1	0	0	1			34.4	

Table 3 (continued)

Name	1	2	3	4	5a	5b	6a	6b	6c	7	8	9a			9d	10a	10b	10c	10d
Solution   Solution		N <sub>1</sub>	Total	Median						_	u								
1	Source	total			min	med	$\chi^2$			p	(Hz)	Any	R	В	Т	$0.5\mathrm{s}$	$1.0\mathrm{s}$	$2.0\mathrm{s}$	$4.0\mathrm{s}$
25015-59   4	4U 0836-429	17	1082.0	33.8	9	11	1.73	1.62	1	0.82						37.5		36.2	41.1
Mathematical Mat	2S 0918-549	4	514.0	82.9	4	10	0.82	0.72	1	0.51	2.00 - 7.00	1	0	1	0	43.0		45.4	
1																			
Column	4U 1323-62	40	2814.5	53.5	12	21	4.50	4.11	5	0.38						35.5		43.0	48.0
City   1																32.2		34 3	
Circumo											1458.00	1	0	0	1	01.0	32.8	01.0	
1	Cir X-1	13	372.5	13.6	21		0.60	0.71	0	1.00	1598.00	1	0	U	1	31.3			
1	4U 1608-522	52	5998.5	418.3	4	5	9.60	8.72	15	0.00							78.4	82.1	60.8
1											94.00	1	0	0	1			38.9	
1   1   1   1   1   1   1   1   1   1																31.6		35.0	
1																30.9		24.6	
1																	34.4	34.0	
1																	55.4	66.5	81.1
Mathematical Registration											996.50	1	0	0	1	55.4			35.9
Mathematical Registration																35.9	34.2		
Mathematical   Math											1818.75	1	0	0	1			05.4	35.7
1																		35.4	35.5
1	4U 1636-536	368	20954.0	162.6	3	8	33.53	32.26	18	1.00	4.00 - 6.25							36.6	
																	33.7	33.7	
																30 Q	35.1		
Record   R											576.00 - 582.00	<b>75</b>	<b>32</b>	64	1			59.1	65.5
The color of the																			
State   Stat											708.00	1	0	0	1				
The color of the																31.9			35.4
No.   No.																			
Name											1537.00	1	0	1	0	51.5		33.7	
MKB 1658-298																	32.8	35.6	
MXB 1658-298	WED 14504 400		05.0	101 =	_		0.1.1	0.14		0.10	1990.00	1	0	0	1			00.0	
$ \begin{array}{c ccccccccccccccccccccccccccccccccccc$																			
4U 1702-429											566.75 - 567.25		1	1		26.4	37.2		40.6
1																			
$ \begin{array}{c ccccccccccccccccccccccccccccccccccc$	4U 1702-429	50	3231.5	332.2	4	5	5.17	5.40	7	0.32				1		56.3	53.1		
$ \begin{array}{c ccccccccccccccccccccccccccccccccccc$											326.00 - 330.50	32	6	32	0	40.6	51.3	61.8	63.3
$\begin{array}{c ccccccccccccccccccccccccccccccccccc$																	32.9	36.9	
$\begin{array}{c ccccccccccccccccccccccccccccccccccc$											873.75	1	0	1	0		-	22.0	38.4
4U 1705-44 91 4239.5 77.2 5 11 6.78 6.24 5 0.67 2.50-3.00 2 0 1 1 37.7 37.0 37.0 421705-44 91 4239.5 77.2 5 11 6.78 6.24 5 0.67 2.50-3.00 2 0 1 1 1 37.7 37.0 37.0 37.2 4239.5 1 1 1 1 1 1 1 1 1 1 1 1 1 1 1 1 1 1 1											1528.00								
$\begin{array}{c ccccccccccccccccccccccccccccccccccc$	AII 1705 AA	01	4990 F	77.9	E	11	6 70	6.24	5	0.67	1833.50						37 7		
$ \begin{array}{c ccccccccccccccccccccccccccccccccccc$	10 1100-44	JI	±209.0	11.2	J	11	0.10	0.24	J	0.07	16.00	1	0	1	0			01.0	
XTE J1709-267   3   68.0   59.3   10   12   0.11   0.09   0   1.00   1																		37.3	37.2
$ \begin{array}{c ccccccccccccccccccccccccccccccccccc$											1120.00	1	0	0	1	00:	32.4	00	
$ \begin{array}{c ccccccccccccccccccccccccccccccccccc$	XTE J1709-267	3	68.0	59.3	10	12	0.11	0.09	0	1.00	1674.00	1	U	0	1	36.4			
$\begin{array}{cccccccccccccccccccccccccccccccccccc$																	24.4		35.2
1335.00   1   0   1   0   34.8											589.00		0	0	1		34.4		36.8
																33.4	34 8		
	IGR J17191-2821	5	176.0	132.6	8	10	0.28	0.23	0	1.00									

 $Table \ 3 \ continued$ 

Table 3 (continued)

1	2	3	4	5a	5b	6a	6b noise car	6c	7	8	9a		9c	9d	10a	10b	10c	10d
Source	$N_{ m brst}$ total		$\begin{array}{c} {\rm Median} \\ {\rm SN_{peak}} \end{array}$		$_{ m med}^{ m FA_{up}}$	$\chi^2$	mean simul	real data	p	$_{ m (Hz)}^{ u}$	Any		vith B	Т		1.0 s		window 4.0 s
		(s)								293.50-294.25	2	0	2	0		40.5	42.1	47.4
4U 1722-30 4U 1728-34	$\begin{array}{c} 4 \\ 141 \end{array}$	356.5 $6643.5$	252.4 $292.7$	$\frac{4}{3}$	5 5	0.57 $10.63$	$0.45 \\ 9.28$	1 11	$0.27 \\ 0.36$	22.00 $2.00-5.00$	1 11	0 4	1 3	0 6	$\frac{36.5}{42.1}$	40.0	36.4	37.4
										8.00	1	0	1	0	31.1			
										22.00 $108.50$	1 1	0	$\frac{1}{0}$	0 $1$	33.5		33.7	
										362.00-364.00	34	14	30	1	42.8	48.2	58.7	64.1
										381.00 419.00	1 1	0	0 1	$\frac{1}{0}$		36.4		35.6
										822.00 $1550.50$	1 1	0	1	0 1		33.0		35.8
										1574.00	1	0	0	1	33.3			33.8
										1678.00 $1829.00$	1 1	0	0	1 1		$34.5 \\ 32.8$		
										1965.00	1	1	0	0		32.2		
MXB 1730-335	57	5223.5	18.8	7	18	8.36	6.99	10	0.16	2.00-6.00 $18.25$	15 1	2 0	3 1	13 0	38.0	37.7	38.4	$38.4 \\ 46.4$
										33.50	1	0	1	0				35.2
										396.00 406.00	1 1	0 1	0	1 0	$32.0 \\ 34.2$			
										468.00	1	0	0	1	31.0			
										592.00 732.50	1 1	0	$\frac{1}{0}$	0 $1$		33.5		36.4
										1051.50	1	0	0	1			36.4	
										1464.00 $1643.50$	1 1	0	0 $1$	$\frac{1}{0}$		32.7		35.3
KS 1731-260	26	1881.5	136.7	4	6	3.01	2.77	3	0.43	44.00	1	0	1	0	32.9		0.4.0	
										173.50 <b>523.50–524.50</b>	1 <b>3</b>	0 <b>0</b>	1 <b>3</b>	0 <b>0</b>	49.0	62.9	34.9 <b>62.6</b>	74.2
AT TT 1 = 0 = 0 = 0				_	_					1840.00	1	0	1	0		32.3		
SLX 1735-269 4U 1735-444	$\frac{1}{22}$	$104.5 \\ 524.0$	578.1 137.6	5 5	5 8	$0.17 \\ 0.84$	$0.19 \\ 0.86$	$0 \\ 2$	$\frac{1.00}{0.23}$	378.00	1	0	0	1	33.6			
VTE 11720 205	c	200 5	102 5	0	10	0.22	0.26	0	1.00	888.50	1	0	0	1			37.3	
XTE J1739-285 KS 1741-293	$\frac{6}{1}$	208.5 10.0	123.5 7.6	8 81	10 81	$0.33 \\ 0.02$	$0.26 \\ 0.02$	0	1.00 $1.00$									
GRS 1741.9-2853	7	365.5	93.7	6	9	0.58	0.44	1	0.31	2.00-4.00 <b>589.00-589.75</b>	3 <b>2</b>	0 <b>0</b>	3 <b>2</b>	1 <b>0</b>	39.7	41.9	44.7 <b>34.1</b>	45.1
										1829.25	1	0	1	0			34.1	<b>38.3</b> 36.6
1A 1742-294	86	2516.0	14.4	7	42	4.03	3.54	2	0.83	702.00 $1340.00$	1 1	0	1 1	0	$31.2 \\ 31.3$			
SAX J1747.0-2853	27	841.0	94.9	6	12	1.35	1.09	0	1.00									
IGR J17473-2721	44	2933.5	46.3	5	8	4.69	4.97	4	0.67	2.00-6.25 $10.00$	16 1	10 0	12 0	12 1	39.0 <b>32.5</b>	41.7	38.8	42.8
										240.00	1	0	0	1	33.7			
										602.00 605.00	1 1	$\frac{1}{0}$	0 $1$	0	31.3		36.9	
SLX 1744-300	24	620.5	24.7	9	23	0.99	0.88	4	0.01	2.00	1	1	0	0			46.6	
										96.00 $928.25$	1 1	0	0 $1$	$\frac{1}{0}$		32.3		37.0
										1278.00	1	0	0	1				35.2
GX 3+1	3	112.0	149.5	5	7	0.18	0.16	0	1.00	1978.00 2.00	1 1	0 1	0	1	32.8 30.9	41.3	36.9	
IGR J17480-2446	297	11272.5	6.4	22		18.04		24	0.14	2.00 - 2.50	1	1	1	0	34.3		42.6	36.5
										6.00 <b>10.00–11.00</b>	1 <b>2</b>	$\frac{1}{2}$	0 <b>1</b>	0 <b>1</b>	31.2 <b>38.1</b>	45.1	64.6	96.0
										115.00-116.00	2	2	0	0	31.7		34.1	
										$380.00 \\ 459.00$	1 1	$\frac{1}{0}$	0	0 1	31.5			37.3
										689.50 $751.00$	1 1	1 1	0	0		36.4	35.5	
										771.50	1	0	1	0			34.0	
										830.00 994.00	1 1	0	0 1	$\frac{1}{0}$	38.2	34.2		
										997.00	1	0	1	0	JU.2		37.6	
										1003.50 $1050.00$	1 1	0 $1$	1	0	31.2		35.3	
										1168.00	1	0	0	1	31.2			
										1396.00 $1436.00$	1 1	0	0 $1$	$\frac{1}{0}$		$32.4 \\ 32.4$		
										1630.00	1	1	0	0		32.3	10 =	
										$1662.50 \\ 1782.00$	1 1	1 1	0	0			$40.7 \\ 37.2$	
										200	-						~	

Table 3 (continued)

1	2	3	4	5a	5b FA <sub>up</sub>	6a	6b	6c ndidates	7	8	$9a$ 9 $N_{\rm brs}$	9b	9c	9d	10a Mean	10b	10c	10d window
Source	$N_{ m brst}$	Total duration	$\frac{\text{Median}}{\text{SN}_{\text{peak}}}$		med	$\chi^2$	mean simul	real	p	u  (Hz)	Any			Т		1.0 s		4.0 s
	total	(s)	peak				Silliui	data		1793.00	1	1	0	0		33.9		
										1833.50	1	0	1	0		33.9		37.4
										1837.00		1	0	0		32.7		
EXO 1745-248	22	895.5	14.3	5	13	1.43	1.50	1	0.73	2.00-11.25 $14.50$		15 0	12 <b>0</b>	9	37.9	42.6	42.6 $38.7$	43.3
1A 1744-361	3	76.0	56.4	9	20	0.12	0.12	1	0.10	529.00		1	0	0		35.4	36.7	
SAX J1748.9-2021	29	1197.5	117.5	5	8	1.92	1.92	2	0.51	2.00-2.50	1	1	0	0		36.0	42.0	39.1
										372.00	1	0	0	1		33.3	0= 0	
IGR J17498-2921	2	109.5	286.2	7	8	0.18	0.25	0	1.00	549.00 2.00	1 1	0	0	1			37.6	35.5
1010 317490-2921	2	103.5	200.2	'	0	0.10	0.25	U	1.00	401.00		o	$\mathbf{\hat{2}}$	o			35.3	40.7
4U 1746-37	28	1082.0	42.9	12	21	1.73	1.41	2	0.39	966.00		0	0	1	31.4			
CAN 11770 0 0000		200 5	222 7	_	0	0.00	0.00	0	1.00	1887.75		0	1	0	05.0	0 F =	40.	37.8
SAX J1750.8-2900 GRS 1747-312	6 7	203.5 $461.5$	$220.7 \\ 50.3$	5 9	8 21	$0.33 \\ 0.74$	$0.33 \\ 0.61$	0	1.00	599.00-600.75	1	1	1	0	35.8	35.7	43.7	45.3
IGR J17511-3057	9	421.5	241.5	5	10	0.67	0.63	0	1.00	244.00-245.00	9	4	9	2	37.7	47.9	53.3	75.5
IGR J17597-2201	9	374.5	85.1	10	15	0.60	0.59	2	0.16	2.00	2	2	0	0	34.5			
										390.00		0	1	0		32.5	20.0	
SAX J1806.5-2215	4	160.0	147.4	10	11	0.26	0.23	0	1.00	1529.00 2.00	1 1	0	0	1	31.2		36.8	
SAX J1808.4-3658	9	1000.0	987.1	2	3	1.60	1.64	3	0.22	2.00-2.50	1	1	0	0	47.5	37.6	34.4	
										8.00	1	0	1	0	57.5	64.8	36.5	
										397.00-404.00	7	5	7	2	57.7	59.7	64.7	64.0
XTE J1810-189 SAX J1810.8-2609	$\frac{4}{6}$	486.0 $496.5$	45.9 $424.5$	8	10 6	$0.78 \\ 0.79$	$0.24 \\ 0.70$	0	1.00 $1.00$	531.75-532.00	1	0	1	0			45.5	58.0
XTE J1814-338	28	3198.0	100.8	9	12	5.12	4.93	2		314.00-314.50		23	26	11	35.0	38.7	49.9	59.0
										1601.00		0	0	1		32.4		
										1858.00	1	0	1	0	33.7			
GX 17+2	15	4076.5	25.8	13	24	6.52	7.14	6	0.69	457.00	$\frac{1}{1}$	0	1 1	0		34.4	35.2	
										714.00 860.00	1	0	1	0		33.6	33.2	
										1320.00		0	1	Ö	33.5	00.0		
										1862.75	1	0	1	0				37.4
4II 1990 202	16	E 49.0	100.4	4	c	0.07	0.72	9	0.10	1918.00	1	0	1	0	31.4	20.7		
4U 1820-303	16	542.0	182.4	4	6	0.87	0.72	2	0.18	280.00 $1687.00$		0 1	$\frac{1}{0}$	0		$39.7 \\ 34.6$		
GS 1826-24	77	10171.5	105.7	5	7	16.27	15.86	15	0.63	2.00-2.25	3	0	0	3		36.2	38.7	38.4
										34.50		0	1	0			38.5	
										110.00	1	0	0	1		24.1	33.9	
										133.00 $220.00$	1 1	0	0	1 1	32.8	34.1		
										410.00	1	0	0	1	33.1			
										471.50	1	0	0	1			34.2	
										790.00		0	1	0	31.3			20.0
										1099.25 $1105.50$	$\frac{1}{1}$	1	0	0 $1$			37.2	38.0
										1142.50		0	1	0			· · · · <u>· · · · · · · · · · · · · · · </u>	37.2
										1506.00		0	0	1	33.3			
										1805.00	1	0	0	1 0	20.1		34.2	
										1844.00 1863.00		0	1	1	32.1	33.5		
XB 1832-330	1	155.5	369.0	6	6	0.25	0.22	0	1.00	1000.00	-			-		00.0		
Ser X-1	19	395.0	78.4	6	9	0.63	0.74	1	0.51	2.00-5.00	1	1	1	0	54.8	54.8	45.4	38.8
HETTE 11000 1 0455	0	1141 5	C10 F	9	-	1.00	1.50	4	0.00	279.00	1	0	0	1	50.7	F1 F	35.2	
HETE J1900.1-2455	8	1141.5	613.5	3	5	1.83	1.50	4	0.08	2.00 5.75–6.00		0 1	1 1	0	52.7	$51.5 \\ 37.5$		37.5
										12.00		1	0	o	35.2	01.0		01.0
										376.25	1	0	1	0				40.6
Aql X-1	73	7364.0	208.2	4	5	11.78	11.04	13	0.33	2.00-6.00	8	1	3	5	37.7	39.2	40.7	40.2
										$156.25 \\ 252.25$	$\frac{1}{1}$	0	$\frac{1}{0}$	0 1				$35.9 \\ 35.1$
										271.50		0	0	1				39.4
										547.50 - 550.00	8	2	8	0	41.0	38.9	46.8	54.2
										590.00	1	0	1	0	91.0			36.7
										908.00 $1212.00$		0	0	1 1	$31.0 \\ 33.7$			
										1212.00	1	0	1	0	55.7			35.8
										1305.00		1	0	0		34.8		20.0
										1331.00	1	1	0	0		39.2		
										1388.00		0	0	1	20.7	32.7		
										$1418.00 \\ 1462.25$		0	0 $1$	1 0	32.7			36.2
										1402.20	1	U	1	U				50.2

Table 3 (continued)

1	2	3	4	5a	5b	6a	6b	6c	7	8	9a	9b	9c	9d	10a	10b	10c	10d
				1-s I	$A_{\mathrm{up}}$	# of r	oise car	didates			$N_{\rm b}$	rst V	vith	$\det$	Mean	$P_{ m m}$ in	ı FFT	window
Source	$N_{ m brst}$ total	Total duration (s)	$\begin{array}{c} {\rm Median} \\ {\rm SN_{peak}} \end{array}$	min	med	$\chi^2$	mean simul	real data	p	$^{\nu}_{\rm (Hz)}$	An	y R	В	Т	0.5 s	1.0 s	$2.0\mathrm{s}$	4.0 s
		•								1670.00	1	0	0	1	31.2			
XB 1916-053	14	711.5	381.0	5	6	1.14	1.18	7	0.00	2.00 - 3.00	4	2	3	0	44.5	35.7	36.0	35.1
										6.50	1	0	1	0			36.1	
										11.50	1	1	1	0			37.4	
										21.00	1	1	0	0		35.7	37.3	
										270.00 - 271.75	1	0	1	0		41.4	36.4	36.1
										1588.00	1	0	1	0	31.4			
XTE J2123-058	5	202.5	14.3	12	23	0.32	0.22	1	0.19	122.50	1	1	0	0			33.8	
4U 2129+12	6	353.0	146.1	6	13	0.56	0.56	0	1.00									
Cyg X-2	69	444.0	20.7	10	18	0.71	0.51	4	0.01	2.00 - 12.00	14	3	13	1	37.1	40.7	39.7	45.4
*0										16.00	1	0	1	0	31.8			
										48.00	1	0	1	0		33.3	37.4	
										1713.00	1	1	0	0			36.4	

Note—Table 3 columns: (1) source name; (2) number of bursts suitable for TBO search; (3) total burst duration; (4) median S/N ratio of the burst peak on the sample of all bursts from the given source; (5) upper limits on FA in 1-s Fourier windows on a burst peak, (a) minimum (b) median; (6) number of noise candidates above selected detection threshold (excluding low-frequency candidates and candidates in the known TBO frequency range), (6a) predicted by Eq. 4, treating all time windows as independent, (6b) mean number per simulation run, averaged over 100 simulation runs, (6c) number of noise candidates from the real data; (7) percentile of the real-data number of noise candidates with respect to a 100-run simulation sample; (8) boundaries of the frequency groups (groups of candidates with frequency separation  $|\delta \nu| \le 2$  Hz), with known TBO frequencies in bold and low-frequency groups in grey; (9) number of bursts with candidates in a given frequency group, in any region (9a) and in the Rise, Burst, or Tail regions (9b-9d); (10) average  $P_{\rm m}$  of the candidates in each of the four Fourier windows sizes (10a–10d).

Table 4. Fractional amplitudes of candidates per burst

1	2	3	4	5	6a	6b	6c	6d	6e	7a	7b	7c	$7\mathrm{d}$
					Inde	epene	nt tin	ne win	dows		Max FA	1 (%)	
Source	Entry	MINBAR TOA, UT	$^{\nu}_{\rm (Hz)}$	Where	any	$0.5  {\rm s}$	1.0	s 2.0 s	$4.0\mathrm{s}$	$0.5\mathrm{s}$	$1.0\mathrm{s}$	$2.0\mathrm{s}$	$4.0  \mathrm{s}$
4U 0513-40	3797	2009-01-08 12:23:21	1378.75	-T	1	0	0	0	1	-	-	-	$30_{25}^{35}$
EXO 0748-676	2396	1998-06-28 15:28:19	86.00	-T	1	1	0	0	0	$78_{60}^{98}$	-	-	_
	3415	2006-09-08 21:57:59	113.00	-T	1	0	0	1	0	-	-	$34_{29}^{41}$	_
	3564	2007-07-15 23:32:38	147.50	-T	1	0	0	1	0	-	_	$45^{53}_{38}$	_
	3132	2003-09-21 23:14:21	288.00	-T	1	0	0	1	0	-	-	$19_{16}^{22}$	_
	2237	1996-08-15 21:47:35	327.50	-T	1	0	0	1	0	_	-	$22_{19}^{25}$	_
	3144	2003-10-13 00:04:11	333.75	-T	1	0	0	0	1	-	-	-	$28^{33}_{23}$
	3497	2007-03-31 07:49:15	339.00	-T	1	0	0	1	0	_	-	$52_{43}^{62}$	_
	3146	2003-10-13 07:19:21	361.00	-T	1	0	0	0	1	_	_	-	$34_{28}^{40}$
	3069	2003-02-19 06:09:11	390.00	-T	1	0	0	0	1	_	_	_	$37_{30}^{45}$
	2983	2002-04-20 12:34:20	399.50	-P-	1	0	0	1	0	_	_	$22_{18}^{26}$	-
	3144	2003-10-13 00:04:11	414.00	-P-	1	0	0	1	1	_	_	$19_{16}^{22}$	$13_{11}^{15}$
	2983	2002-04-20 12:34:20	470.00	R	1	1	0	0	0	$22_{19}^{26}$	-	_	_
	3175	2004-03-17 17:17:31	539.00	-T	1	0	0	0	1	_	_	_	$20^{23}_{17}$
	3462	2007-01-14 14:08:45	551.50 - 552.00	R	1	1	1	1	0	$17^{20}_{14}$	$14_{12}^{16}$	$15^{18}_{13}$	_
	3642	2007-12-13 13:29:20	552.50	R	1	0	0	1	0	-	_	$15_{13}^{17}$	_
	2396	1998-06-28 15:28:19	599.00	-T	1	0	0	1	0	_	_	$67_{51}^{85}$	_
	3048	2002-12-12 15:35:50	700.50	-T	1	0	0	1	0	_	_	$21_{18}^{25}$	_
	3158	2004-01-24 17:35:31	812.50	-T	1	0	0	1	0	_	_	$38_{31}^{45}$	_
	3043	2002-12-05 00:48:22	831.50	-P-	1	0	0	0	1	_	_	-	$11_{10}^{13}$
	2335	1997-08-17 15:08:28	867.00	-T	1	0	0	0	1	_	_	_	$36_{30}^{43}$
	3069	2003-02-19 06:09:11	873.00	-P-	1	0	1	0	0	_	$26^{31}_{22}$	_	-
	3131	2003-09-19 23:03:23	874.00	-T	1	0	1	0	0	_	$90_{67}^{114}$	_	_
	3046	2002-12-07 22:14:14	948.00	-T	1	0	1	0	0	_	$35_{29}^{41}$	_	_
	2698	2000-12-18 15:11:16	1005.00	-T	1	0	1	0	0	_	$82_{62}^{102}$	_	_
	3152	2004-01-13 01:29:38	1027.25	-T	1	0	0	0	1	_	_	_	$30^{36}_{25}$
	2672	2000-08-29 09:51:42	1108.00	-T	1	0	0	1	0	_	_	$99_{74}^{126}$	_
	3131	2003-09-19 23:03:23	1108.00	-T	1	0	0	1	0	_	_	$31_{26}^{37}$	_
	2592	1999-10-17 04:10:58	1181.00	-T	1	0	1	0	0	_	$99_{72}^{127}$	_	_

 ${\bf Table~4~} (continued)$ 

1	2	3	4	5	6a Inde	6b epener	6c nt tim	6d ne win	6e dows	7a	7b Max F	7c A (%)	7d
Source	Entry	MINBAR TOA, UT	$^{\nu}_{\rm (Hz)}$	Where	any	$0.5\mathrm{s}$	$1.0\mathrm{s}$	$2.0\mathrm{s}$	$4.0\mathrm{s}$	$0.5\mathrm{s}$	$1.0\mathrm{s}$	$2.0\mathrm{s}$	$4.0\mathrm{s}$
	3622	2007-10-16 17:15:18	1234.00	-P-	1	0	1	0	0	_	$27_{23}^{32}$	_	_
	3175	2004-03-17 17:17:31	1376.50	-T	1	0	0	0	1	-	-	_	$18_{16}^{22}$
	2334	1997-08-13 23:05:04	1390.00	-T	1	1	0	0	0	$102_{74}^{132}$	-	-	-
	3066	2003-02-18 06:01:41	1585.00	-T	1	0	1	0	0	_	$54_{44}^{65}$	_	_
	3069	2003-02-19 06:09:11	1598.00	-P-	1	1	0	0	0	$38_{32}^{46}$	_	_	_
	3221	2004-08-03 01:34:11	1865.00	-T	1	0	1	0	0	_	$68_{54}^{83}$	_	_
	2698	2000-12-18 15:11:16	1890.00	-T	1	1	0	0	0	$173_{93}^{254}$	-	_	_
	3065	2003-02-18 01:14:51	1978.00	-T	1	0	0	1	0	_	_	$39_{33}^{47}$	_
4U 0836-429	3058	2003-01-28 16:02:35	1112.00	-P-	1	0	1	0	0	_	$13_{11}^{16}$	-	_
2S 0918-549	2619	2000-05-12 19:50:17	1725.75	—Т	1	0	0	0	1	_		_	$52_{43}^{63}$
4U 1323-62	2283	1997-04-27 01:34:26	415.00	R—	1	0	1	0	0	_	84 <sup>107</sup> <sub>63</sub>	_	- 43
10 1020 02	2469	1999-01-18 07:18:56	656.00	—Т	1	1	0	0	0	$82_{64}^{101}$	- 63	_	_
	3245	2004-12-31 08:00:43	676.50	R—	1	0	0	1	0	-64	_	$17^{20}_{14}$	_
	2469	1999-01-18 07:18:56	1458.00	—Т	1	0	1	0	0	_	$88_{67}^{111}$	- 14	_
	2286	1997-04-27 07:40:51	1598.00	—Т	1	1	0	0	0	$87_{67}^{109}$	-	_	_
4U 1608-522	2882	2001-11-21 00:06:55	10.00	-P-	1	1	0	0	0	$7.0_{5.9}^{8.3}$	_	_	
TO 1000-044	2886	2001-11-21 00:00:55 2001-11-22 05:31:17	94.00	-г- —Т	1	0	0	1	0	7.0 <sub>5.9</sub>	_	$39_{32}^{46}$	_
	2882	2001-11-22 03:31:17	128.00	—T	1	1	0	0	0	$26_{22}^{32}$	_	- -	_
	3141			—1 —T	1	0	0		0	$20_{22}$			_
		2003-10-07 21:04:46	350.00					1		$10_{8}^{12}$	_	$12_{10}^{14}$	_
	3837	2009-06-15 16:18:16	464.00	-P- T	1	1	0	0	0		_	- 	_
	3141	2003-10-07 21:04:46	506.50		1	0	0	1	0	_	- 30	$74^{93}_{56}$	_
	2609	2000-03-09 00:44:25	592.00	—Т	1	0	1	0	0	_	$25^{30}_{21}$	4 25.0	2.74.2
	2380	1998-03-27 14:05:19	619.50	-P-	1	0	0	1	1	- 47.4	- - 08.0	$4.3_{3.7}^{5.0}$	$3.7^{4.2}_{3.3}$
	3018	2002-09-09 03:50:29	617.50-619.50	-P-	3	1	1	1	3	$6.4_{5.6}^{7.4}$	$7.0^{8.0}_{6.2}$	$5.6_{4.9}^{6.3}$	$3.4^{3.9}_{3.0}$
	3019	2002-09-12 04:18:15	618.00-620.00	-P-	7	4	7	4	3	$8.9_{7.6}^{10.5}$	$9.7^{10.6}_{8.9}$	$9.1^{9.8}_{8.5}$	$7.9^{8.3}_{7.5}$
	3637	2007-11-28 11:38:31	616.00-620.00	RP-	7	6	7	5	3	$9.8^{11.4}_{8.3}$	$8.3_{7.4}^{9.3}$	$6.1_{5.5}^{6.8}$	$6.7_{6.2}^{7.2}$
	3639	2007-11-30 23:21:36	618.00	-P-	1	1	1	1	0	$8.0_{6.7}^{9.5}$	$7.5^{8.6}_{6.6}$	$4.6^{5.4}_{3.9}$	10.1
	3913	2010-03-06 22:49:52	619.25–620.00	-P-	2	0	1	2	2	- 7.4	$10_{9}^{12}$	$12^{13}_{11}$	$9.2^{10.1}_{8.3}$
	8227	2011-06-13 03:43:12	618.00-619.50	-P-	7	2	6	4	4	$6.3_{5.5}^{7.4}$	$7.3_{6.3}^{8.4}$	$6.3_{5.6}^{6.9}$	$6.5_{5.9}^{7.0}$
	2883	2001-11-21 04:47:09	896.00	—Т	1	1	0	0	0	$47^{57}_{38}$	_	_	-
	2217	1996-03-22 16:38:24	996.50	-T	1	0	0	0	1	_	-	_	$43_{36}^{51}$
	3074	2003-03-29 04:26:46	1176.00	-T	1	0	1	0	0	-	$33_{27}^{39}$	-	_
	3833	2009-06-06 11:45:04	1416.00	-T	1	1	0	0	0	$34_{28}^{40}$	-	-	
	2882	2001-11-21 00:06:55	1818.75	-T	1	0	0	0	1	-	-	_	$39_{32}^{47}$
	8227	2011-06-13 03:43:12	1888.00	-T	1	0	0	1	0	-	_	$14_{12}^{17}$	-
	2887	2001-11-22 13:01:21	1977.50	—Т	1	0	0	0	1	-	-	_	$26^{31}_{22}$
4U 1636-536	2542	1999-06-18 23:43:04	5.50	-P-	1	0	0	1	0	-	-	$3.7^{4.3}_{3.1}$	-
	3033	2002-09-29 06:24:16	6.25	-T	1	0	0	0	1	-	-	_	$29^{34}_{24}$
	3304	2005-07-31 04:57:15	4.00	R—	1	0	1	0	0	_	$13_{11}^{15}$	_	_
	3318	2005-08-30 05:01:41	33.00	—Т	1	0	1	0	0	_	$23_{19}^{27}$	_	_
	3903	2010-02-01 08:41:30	41.00	-T	1	0	0	1	0	_	_	$42_{35}^{51}$	_
	3314	2005-08-29 16:53:00	255.00	-T	1	0	1	0	0	_	$68_{54}^{83}$	_	_
	3478	2007-03-07 03:32:52	402.00	-P-	1	1	0	0	0	$26^{31}_{22}$	_	_	_
	2257	1996-12-28 22:39:25	579.00 – 581.00	RP-	2	1	1	1	1	$19_{16}^{\overline{22}}$	$20^{23}_{17}$	$3.8_{3.2}^{4.4}$	$2.5_{2.1}^{2.9}$
	2258	1996-12-28 23:54:04	580.00 – 582.00	RP-	1	1	1	1	1	$13_{12}^{15}$	$11_9^{\overset{1}{12}}$	$10_9^{12}$	$8.8^{10.1}_{7.7}$
	2259	1996-12-29 23:26:47	581.00 – 582.00	-P-	3	2	2	3	2	$10_9^{12}$	$7.4_{6.5}^{8.4}$	$7.3_{6.6}^{8.2}$	$6.1_{5.5}^{6.7}$
	2260	1996-12-31 17:36:53	580.75	-P-	1	0	0	0	1	-	-	-	$3.1_{2.7}^{3.5}$
	2418	1998-08-19 11:44:39	578.00-582.00	RP-	4	4	3	3	1	$26^{30}_{23}$	$31_{27}^{35}$	$6.0_{5.3}^{6.8}$	$4.0_{3.5}^{4.6}$
	2419	1998-08-20 03:40:09	579.50-581.50	RP-	3	2	3	2	2	$12_{10}^{14}$	$12_{11}^{14}$	$7.3_{6.6}^{8.0}$	$5.8_{\underline{5.3}}^{6.3}$
	2420	1998-08-20 05:14:12	580.00-582.00	RP-	4	3	3	3	1	$25_{22}^{27}$	$28^{31}_{25}$	$14_{13}^{16}$	$7.0_{6.4}^{7.8}$
	2496	1999-02-27 08:47:29	580.00-582.00	RP-	2	2	2	2	1	$10_{9}^{12}$	$13_{11}^{14}$	$6.1_{5.2}^{7.0}$	$3.4_{3.0}^{3.9}$
	2540	1999-06-10 05:55:30	580.00-581.00	-P-	4	3	2	3	2	$12_{11}^{14}$	$12_{11}^{14}$	$12_{11}^{13}$	$9.8^{10.4}_{9.1}$
	2542	1999-06-18 23:43:04	580.00-581.00	RP-	1	1	1	1	1	$20_{18}^{23}$	$22_{20}^{25}$	$5.8_{5.1}^{6.7}$	$3.0^{3.5}_{2.6}$
	2544	1999-06-19 17:30:58	580.00-581.00	-P-	3	3	2	2	2	$12_{11}^{13}$	$9.3_{8.4}^{10.2}$	$8.5^{9.2}_{7.9}$	$5.0_{2.6}^{2.6}$ $5.9_{5.4}^{6.4}$
	2546	1999-06-21 19:05:53	581.00-581.25	-P-	1	0	1	1	1	-	$6.1_{5.2}^{7.1}$	$4.5_{3.9}^{5.2}$	$3.3_{2.9}^{3.9}$
	2576	1999-09-25 20:40:49	580.00-581.00	-r - R	1	1	1	0	0	$32_{27}^{38}$	$11_9^{12}$	4.5 <sub>3.9</sub>	3.3 <sub>2.9</sub>
	2010	1000-00-20 20.40.49	550.00-561.00	1.—	1	1	1	U	U	$15_{13}^{17}$	$11_{9}^{12}$ $11_{10}^{12}$	$13_{12}^{14}$	$8.9_{8.4}^{9.4}$

 $Table\ 4\ continued$ 

Table 4 (continued)

1	2	3	4	5	6a Inde	6b	6c	6d ie win	6e	7a	7b Max FA	7c	$7\mathrm{d}$
Source	Entry	MINBAR TOA, UT	u  (Hz)	Where	any			2.0 s	4.0 s	0.5 s	1.0 s	2.0 s	4.0 s
	2658	2000-08-09 01:18:40	579.75-581.50	-P-	5	1	4	4	3	$6.9_{6.0}^{8.0}$	$9.4_{8.4}^{10.5}$	$6.5_{5.6}^{7.6}$	$5.8_{5.3}^{6.4}$
	2659	2000-08-09 08:56:53	581.00-581.75	-P-	3	0	2	3	2	-	$6.7^{7.7}_{5.9}$	$8.4^{9.3}_{7.6}$	$6.2_{5.6}^{6.8}$
	2660	2000-08-12 23:32:21	581.00-581.50	-P-	2	0	2	1	1	_	$8.3_{7.5}^{9.2}$	$6.6_{5.9}^{7.2}$	$5.4_{4.9}^{5.0}$
	2693	2000-11-05 04:21:59	580.00-581.00	RP-	2	1	2	2	1	$15_{13}^{17}$	$16_{14}^{18}$	$4.6_{\underline{4.1}}^{5.3}$	$4.2_{3.8}^{4.7}$
	2695	2000-11-12 18:02:28	580.50 - 581.25	-P-	3	0	3	3	3	-	$7.3_{6.2}^{8.6}$	$6.5^{7.4}_{5.6}$	$6.4_{5.5}^{7.4}$
	2699	2001-01-28 02:47:13	581.00 - 581.50	-P-	2	0	2	2	1	_	$6.8_{6.0}^{7.8}$	$4.7_{4.1}^{5.4}$	$5.7_{5.3}^{6.2}$
	2701	2001-02-01 21:00:50	581.00 - 581.50	-P-	3	0	1	3	2	-	$6.3_{5.5}^{7.2}$	$7.0_{6.0}^{8.2}$	$5.1_{4.3}^{6.0}$
	2702	2001-02-02 02:24:20	581.50	-P-	1	0	0	0	1	_	_	_	$3.2^{3.7}_{2.7}$
	2723	2001-04-30 05:28:34	581.00 – 581.50	-P-	1	0	1	1	0	_	$5.3_{4.5}^{6.2}$	$3.6^{4.3}_{3.1}$	-
	4177	2001-06-15 03:14:04	580.75 - 581.50	-P-	3	0	3	3	2	-	$13_{11}^{14}$	$12_{11}^{13}$	$8.3_{7.5}^{9.2}$
	2756	2001-08-28 06:41:20	581.00 – 581.50	-P-	3	0	3	2	2	-	$5.5_{4.8}^{6.4}$	$5.3_{4.8}^{6.0}$	$4.6^{5.1}_{4.2}$
	2808	2001-09-30 14:47:17	580.00 - 580.50	RP-	2	0	1	1	0	-	$10_9^{12}$	$3.4_{2.9}^{4.1}$	-
	2876	2001-11-01 07:38:19	580.75 - 581.25	-P-	3	0	2	3	2	-	$8.3_{7.1}^{9.6}$	$6.8_{6.0}^{7.8}$	$6.5^{7.3}_{5.8}$
	2906	2002-01-09 00:26:38	580.25 - 581.50	-P-	3	0	1	3	2	_	$5.5_{4.6}^{6.5}$	$7.7_{6.6}^{9.1}$	$6.7_{5.7}^{7.8}$
	2907	2002-01-09 12:48:24	580.00 - 581.25	-P-	2	1	2	2	2	$7.2^{8.4}_{6.1}$	$7.9_{7.0}^{9.0}$	$5.1_{4.5}^{5.9}$	$3.2^{3.8}_{2.7}$
	2917	2002-01-12 01:53:57	581.00 - 581.50	RP-	1	0	1	1	1	-	$14_{12}^{16}$	$12_{11}^{14}$	$8.6^{9.9}_{7.4}$
	2921	2002-01-12 21:35:34	579.00 - 581.50	RP-	4	2	3	2	1	$15_{13}^{17}$	$28^{33}_{24}$	$16^{18}_{14}$	$7.8_{7.0}^{8.7}$
	2923	2002-01-13 01:29:03	580.00 - 581.25	RP-	3	2	2	2	1	$23_{20}^{26}$	$27^{30}_{24}$	$21_{19}^{22}$	$6.2_{5.5}^{6.9}$
	2926	2002-01-13 12:47:26	581.00	R—	1	0	0	1	0	_	-	$19_{16}^{22}$	-
	2930	2002-01-14 01:22:36	580.00 - 582.00	RP-	4	3	2	3	2	$52_{44}^{61}$	$19_{16}^{23}$	$17^{19}_{15}$	$8.9_{8.0}^{9.7}$
	2932	2002-01-14 12:20:36	581.25 - 582.00	-P-	3	1	0	2	2	$14_{12}^{17}$	-	$6.3_{5.5}^{7.2}$	$7.5_{6.5}^{8.7}$
	2949	2002-01-22 07:07:20	579.00 – 581.00	R	3	2	1	2	0	$21_{18}^{24}$	$23_{20}^{26}$	$16^{18}_{14}$	-
	2960	2002-01-30 23:06:55	580.00 - 582.00	RP-	3	1	1	2	2	$13_{10}^{15}$	$14_{11}^{16}$	$5.1_{4.3}^{6.1}$	$4.8^{5.5}_{4.2}$
	2961	2002-02-05 22:21:51	579.00 – 582.00	RP-	4	1	2	3	2	$22_{19}^{25}$	$25_{21}^{29}$	$6.8_{5.9}^{7.9}$	$6.2^{7.0}_{5.4}$
	2963	2002-02-11 17:35:07	579.00 – 581.00	RP-	2	1	2	1	1	$14_{12}^{16}$	$13_{11}^{15}$	$5.1_{4.6}^{5.8}$	$4.0_{3.5}^{4.5}$
	2984	2002-04-26 05:07:18	576.00 - 581.50	RP-	6	2	5	5	3	$10_9^{12}$	$9.4_{7.9}^{11.0}$	$8.0_{7.0}^{9.1}$	$6.6_{5.8}^{7.6}$
	3035	2002-10-04 06:01:44	580.00	R—	1	0	1	0	0	_	$8.4_{7.1}^{10.0}$	-	-
	3255	2005-03-23 05:27:59	580.50	R—	1	0	0	1	0	_	-	$10_{9}^{12}$	-
	3284	2005-05-26 07:30:53	580.50-581.00	-P-	2	0	0	1	2	- 10	-	$7.4_{6.4}^{8.4}$	$6.6_{5.7}^{7.7}$
	3308	2005-08-10 05:36:36	578.00-581.25	RP-	2	2	2	1	1	$16^{18}_{14}$	$17^{20}_{15}$	$4.5_{3.9}^{5.2}$	$3.7_{3.3}^{4.2}$
	3309	2005-08-14 02:06:27	580.00-581.00	-P-	1	1	1	1	0	$8.8_{7.4}^{10.5}$	$6.7^{7.9}_{5.6}$	$5.2^{6.1}_{4.5}$	-
	3310	2005-08-16 01:45:37	580.00-581.00	RP-	2	1	1	1	1	$42^{48}_{36}$	$52^{61}_{43}$	$5.2_{4.6}^{6.0}$	$4.0^{4.6}_{3.5}$
	3368	2006-04-15 13:14:39	581.00-581.50	R—	1	0	1	1	0	-	$27^{31}_{23}$	$8.2^{9.4}_{7.0}$	-
	3378	2006-07-03 01:46:32	580.00-581.50	RP-	2	1	1	1	1	$43_{34}^{52}$	$5.7_{4.8}^{6.7}$	$5.2_{4.5}^{6.0}$	$4.7_{4.2}^{5.4}$
	3379	2006-07-24 11:49:14	580.50-581.00	-P-	1	0	1	1	0	_	$5.6_{4.8}^{6.6}$	$4.4_{3.8}^{5.1}$	- 7 5
	3429	2006-09-26 11:48:28	581.00-581.25	-P-	1	0	0	0	1	- 40	- 47	- 27	$6.4_{5.4}^{7.5}$
	3447	2006-11-09 22:35:52	580.00-581.00	R—	2	1	2	1	0	$42^{49}_{36}$	$40^{47}_{34}$	$24_{21}^{27}$	- 5.6
	3448	2006-11-11 21:38:56	580.50-581.50	-P-	3	0	2	3	2	_	$8.4^{9.5}_{7.5}$	$6.4_{5.5}^{7.4}$	$5.1_{4.5}^{5.6}$
	3450	2006-11-15 05:58:35	580.00-581.50	-P-	3	0	1	3	2	- 1.16	$5.7_{4.9}^{6.7}$	$6.3_{5.4}^{7.4}$	$5.5_{4.7}^{6.4}$
	3512	2007-05-02 10:04:35	580.00-581.00	R—	1	1	1	0	0	$14_{11}^{16}$	$15^{18}_{13}$	- 28.3	7
	3548	2007-06-20 01:03:05	581.00-581.50	-P-	2	0	1	1	2	1018	$6.3_{5.3}^{7.5}$	$7.2^{8.3}_{6.2}$	$5.0_{4.4}^{5.7}$
	3549	2007-06-21 02:12:11	579.00-580.00	R—	1	1	1	0	0	$16^{18}_{13}$	$18_{15}^{21}$	- 46.9	- 4 45 0
	3606	2007-09-28 17:15:19	581.00-581.50	-P-	1	0	1	1	1	_	$7.9^{9.0}_{7.0}$	$6.1_{5.4}^{6.9}$	$4.4_{3.9}^{5.0}$
	3615	2007-10-11 11:03:39	581.00	-P-	1	0	1	0	0	_	$6.5_{5.5}^{7.6}$	- - 09.0	- c =7.2
	3634	2007-11-12 07:37:31	581.50	-P-	2	0	0	2	1	- 0 410.0	- - 18.3	$7.8^{9.0}_{6.8}$	$6.5^{7.2}_{5.9}$
	3676	2008-03-05 19:07:58	580.00-581.50	-P-	2	1	1	2	2	$8.4_{7.1}^{10.0}$	$7.1_{6.2}^{8.3}$	$8.8^{10.1}_{7.7}$	$7.0^{8.0}_{6.1}$
	3707	2008-05-02 03:56:52	580.50-581.00	-P-	2	0	2	2	1	_	$7.3_{6.3}^{8.5}$	$6.0_{5.4}^{6.7}$	$5.1_{4.6}^{5.7}$
	3722	2008-05-28 19:34:00	581.00	–P–	1	0	0	1	0	_	_	$4.9_{4.2}^{5.8}$	0 19.3
	3750	2008-07-31 06:25:40	580.50-581.25	–PT	3	0	0	3	3	_	_	$8.2^{9.6}_{7.1}$	$8.1_{7.1}^{9.3}$
	3771	2008-10-07 01:21:08	579.00	R—	1	0	0	1	0	1015	- 11 <sup>12</sup>	$7.5^{8.7}_{6.4}$	1011
	3813	2009-03-14 19:59:22	580.00-582.00	–P–	5	3	2	5	4	$12_{10}^{15}$	$11_9^{12}$	$11_{10}^{13}$	$10_{9}^{11}$
	3839	2009-06-22 06:29:52	580.50-581.50	RP-	3	0	2	3	2	_	$12_{10}^{13}$	$11_{10}^{12}$ $7.28.3$	$9.0^{9.8}_{8.2}$
	3851	2009-09-05 05:16:18	580.00-581.00	-P-	2	0	2	1	1	_	$8.6^{10.2}_{7.3}$	$7.2^{8.3}_{6.1}$	$6.1_{5.4}^{7.0}$
	3884	2009-12-01 00:38:47	581.25-581.50	-P-	2	0	0	2	1	_	- 0.210.5	$6.1_{5.3}^{6.9}$	$4.6_{4.1}^{5.3}$
	3885	2009-12-03 07:43:50	580.75-581.00	-P-	2	0	2	1	1	_	$9.3_{8.3}^{10.5}$	$7.6_{6.8}^{8.5}$	$4.6^{5.4}_{4.0}$
	3891	2010-01-16 01:59:57	581.50	-P-	1	0	0	1	1	_	- 7 c9.0	$7.9_{6.8}^{9.3}$	$7.5^{8.6}_{6.6}$
	8080	2010-06-09 23:45:39	581.00	-P-	1	0	1	1	1	_	$7.6^{9.0}_{6.5}$	$6.1_{5.2}^{7.1}$	$4.7_{4.1}^{5.4}$

 $Table\ 4\ continued$ 

Table 4 (continued)

1	2	3	4	5	6a Inde	6b epener	6c nt tim	6d ie wind	6e dows	7a	7b Max F	7c A (%)	$7\mathrm{d}$
Source	Entry	MINBAR TOA, UT	$ \frac{\nu}{(\mathrm{Hz})} $	Where	any			2.0 s	$4.0\mathrm{s}$	0.5 s	1.0 s	2.0 s	4.0 s
	3943	2010-06-27 16:26:40	580.50	-P-	1	0	0	1	0	_	_	$4.4_{3.8}^{5.3}$	_
	3955	2010-08-28 03:38:57	579.00	R	1	0	1	0	0	_	$19_{16}^{23}$	3.8	_
	8211	2011-04-01 15:22:59	580.75-581.00	-P-	2	0	1	2	2	_	$12_{11}^{14}$	$12^{13}_{10}$	$9.1_{8.0}^{10.3}$
	8267	2011-10-22 23:59:39	580.00-581.25	-P-	2	1	2	1	1	$9.2_{7.7}^{10.9}$	$8.8_{7.8}^{10.0}$	$5.9_{5.2}^{6.8}$	$5.3_{4.6}^{6.1}$
	3628	2007-10-27 08:29:43	636.00	—Т	1	0	1	0	0	9.2 <sub>7.7</sub>	$80_{61}^{100}$	-	-
	3581	2007-08-14 11:05:17	681.00	-P-	1	0	1	0	0	_	$13_{11}^{16}$	_	_
	2260	1996-12-31 17:36:53	708.00	—Т	1	1	0	0	0	$26^{31}_{21}$	-	_	_
	3277	2005-04-26 10:16:59	798.00	-P-	1	1	0	0	0	$14_{12}^{16}$	_	_	_
	3670	2008-02-22 19:28:28	803.25	—Т	1	0	0	0	1	12	_	_	$39_{33}^{46}$
	8076	2010-05-20 04:47:23	1262.00	-T	1	1	0	0	0	$60_{49}^{73}$	_	_	-
	2951	2002-01-24 21:05:32	1520.00	-T	1	1	0	0	0	20104	_	_	_
	3353	2006-02-06 16:21:20	1537.00	-P-	1	0	0	1	0	62 <sub>62</sub>	_	$20_{16}^{23}$	_
	3498	2007-04-04 19:50:41	1667.00	-P-	1	0	1	0	0	_	$21_{17}^{25}$	16	_
	2940	2002-01-15 23:26:47	1864.00	—Т	1	0	0	1	0	_	-	$14_{12}^{17}$	_
	2984	2002-04-26 05:07:18	1990.00	—Т	1	1	0	0	0	$97_{70}^{126}$	_	- 12	_
XTE J1701-462	3567	2007-07-17 12:24:26	80.00	-P-	1	1	0	0	0	$18_{15}^{22}$	_	_	_
MXB 1658-298	4178	2001-03-07 12:24:34	108.00	-P-	1	1	0	0	0	$108_{77}^{142}$	_	_	
WAD 1056-296		1999-04-09 14:47:34				0		0	0	10077	$14_{11}^{16}$	_	_
	2517 $2518$		567.00	R— —T	1 1	0	1	0	1	_	14 <sub>11</sub>	_	$8.0_{6.9}^{9.3}$
		1999-04-10 09:49:37	566.75	—1 —T						_	_	_	0.0 <sub>6.9</sub>
	2519	1999-04-14 11:48:56	566.75-567.25		1	0	0	0	1	_	_	_	$11_{9}^{13}$
	2524	1999-04-21 11:45:57	567.25	-P-	1	0	0	0	1	- 0=108	_	_	$11_9^{12}$
	2724	2001-04-30 17:41:33	728.00	—Т	1	1	0	0	0	$87_{67}^{108}$	_	_	_
4TT 4 BOO 400	2525	1999-04-24 14:43:11	786.00	-P-	1	1	0	0	0	$58_{44}^{74}$	_		
4U 1702-429	2671	2000-08-25 14:46:46	273.00	—T	1	0	0	1	0	- 12	- 7 5	$7.8^{9.2}_{6.6}$	7 7
	2323	1997-07-19 18:40:58	329.00-330.00	-P-	3	1	1	3	2	$10_{9}^{12}$	$6.5^{7.5}_{5.6}$	$8.6^{9.7}_{7.7}$	$7.0^{7.7}_{6.4}$
	2326	1997-07-26 09:03:23	328.50-330.00	-P-	2	1	2	2	2	$9.2_{7.8}^{10.8}$	$11_{10}^{12}$	$8.4^{9.1}_{7.6}$	$5.8_{5.2}^{6.4}$
	2327	1997-07-26 14:04:18	326.00-330.00	RP-	5	4	4	3	2	$9.0^{10.6}_{7.7}$	$12^{13}_{11}$	$9.4^{10.1}_{8.7}$	$6.2^{6.8}_{5.7}$
	2330	1997-07-30 07:22:37	327.50-330.00	-P-	3	2	3	3	1	$8.8_{7.5}^{10.3}$	$7.5^{8.7}_{6.6}$	$6.8_{6.0}^{7.6}$	$5.6^{6.3}_{5.1}$
	2331	1997-07-30 12:11:56	329.00-330.50	-P-	8	5	6	5	3	$14_{12}^{17}$	$13_{12}^{15}$	$11_{10}^{12}$	$10^{11}_{10}$
	2489	1999-02-21 23:48:32	328.00-330.00	-P-	3	1	2	2	2	$8.9_{7.4}^{10.6}$	$6.5_{5.6}^{7.5}$	$5.0_{4.2}^{5.9}$	$4.3_{3.8}^{4.9}$
	2490	1999-02-22 04:56:05	327.00-328.50	RP-	2	0	1	1	0	_	$6.4_{5.5}^{7.5}$	$3.8_{3.2}^{4.4}$	-
	2642	2000-07-23 07:09:42	329.00 – 329.75	-P-	2	0	2	2	2	-	$10_{9}^{12}$	$9.4_{8.5}^{10.5}$	$7.2^{8.1}_{6.4}$
	2704	2001-02-04 03:50:29	327.50-330.00	-P-	3	1	1	3	1	$7.5_{6.5}^{8.7}$	$5.1_{4.4}^{6.0}$	$6.4_{5.4}^{7.5}$	$5.3_{4.7}^{6.1}$
	2711	2001-04-01 15:47:17	328.00 – 328.50	RP-	1	0	1	1	0	-	$5.6_{4.8}^{6.6}$	$4.0_{3.4}^{4.7}$	-
	2712	2001-04-01 21:55:53	328.50 – 330.00	-P-	5	3	4	3	3	$11_9^{13}$	$12_{11}^{13}$	$10_9^{11}$	$10_9^{11}$
	2880	2001-11-16 17:02:11	329.00	-P-	1	0	1	1	0	-	$5.8_{4.9}^{6.8}$	$4.7_{4.0}^{5.5}$	-
	3156	2004-01-18 21:12:37	329.25 – 329.50	-P-	1	0	0	1	1	_	-	$6.8_{5.9}^{7.9}$	$4.2_{3.6}^{5.0}$
	3157	2004-01-20 00:30:01	327.50 – 328.00	-P-	1	0	1	1	1	-	$5.8_{5.0}^{6.8}$	$4.6_{4.0}^{5.3}$	$3.2_{2.8}^{3.7}$
	3166	2004-02-29 01:59:38	329.00 – 330.25	-P-	4	1	3	3	3	$14_{12}^{17}$	$13_{11}^{15}$	$12_{11}^{13}$	$11_{10}^{13}$
	3167	2004-02-29 06:32:16	329.50 – 330.00	-P-	1	0	1	1	1	_	$7.3_{6.2}^{8.7}$	$6.4_{5.5}^{7.3}$	$5.3_{4.7}^{6.1}$
	3169	2004-03-01 23:26:40	327.50 – 328.50	RP-	1	0	0	1	0	_	-	$8.3_{7.0}^{9.7}$	_
	3170	2004-03-02 07:27:52	328.00	-P-	1	0	0	1	1	_	_	$3.9_{3.3}^{4.6}$	$3.4^{4.0}_{2.9}$
	3182	2004-04-08 22:12:46	329.00 - 329.50	-P-	1	0	1	1	1	_	$6.4_{5.5}^{7.5}$	$5.5_{4.9}^{6.3}$	$3.4_{2.9}^{4.0}$ $4.0_{3.4}^{4.7}$
	3183	2004-04-09 06:18:07	329.00-330.00	-P-	4	1	4	3	2	$15_{13}^{17}$	$13_{11}^{14}$	$10_9^{11}$	$9.7^{10.5}_{8.9}$
	3185	2004-04-09 21:32:20	329.00-329.75	-P-	2	0	0	2	1	-	-	$7.5_{6.7}^{8.3}$	$4.6_{4.0}^{5.3}$
	3190	2004-04-13 05:40:02	327.00-329.75	-P-	2	0	2	2	1	_	$11_9^{13}$	$9.9_{8.7}^{11.3}$	$7.8_{6.8}^{8.9}$
	3191	2004-04-13 12:11:53	329.50 – 329.75	-P-	1	0	0	1	1	_	-	$9.9_{8.7}^{11.2}$	$8.5^{9.7}_{7.5}$
	3192	2004-04-13 18:17:23	328.00	RP-	1	0	1	1	1	_	$6.0_{5.1}^{7.0}$	$5.0_{4.4}^{5.8}$	$3.5^{4.1}_{3.0}$
	3193	2004-04-14 18:32:01	329.00-329.75	-P-	1	0	1	1	1	_	$7.6_{6.4}^{9.0}$	$8.0_{7.0}^{9.1}$	$3.5_{3.0}^{4.1}$ $6.7_{5.9}^{7.6}$
	3194	2004-04-15 00:43:14	327.50-329.75	-P-	2	0	0	1	1	_	-	$4.9_{4.2}^{5.8}$	$3.9_{3.3}^{4.6}$
	3195	2004-04-16 02:08:57	329.50	-P-	1	0	0	1	0	_	_	$7.3_{6.3}^{8.5}$	- 3.3
	3196	2004-04-16 20:29:36	327.00-330.25	-P-	5	3	5	2	2	$10_9^{12}$	$9.6_{8.4}^{10.9}$	$8.7^{9.6}_{7.9}$	$5.9_{5.2}^{6.7}$
	3197	2004-04-17 02:45:18	328.00-329.75	RP-	4	1	1	4	2	$10_{9}^{11}$	$7.8^{8.8}_{7.0}$	$10_9^{11}$	$8.3^{9.3}_{7.4}$
	3323	2005-09-17 10:26:25	328.00-328.50	-P-	1	0	1	1	0	- -	$5.7_{4.9}^{6.7}$	$4.1_{3.5}^{4.9}$	- -
	3328	2005-10-19 01:58:44	329.00-330.00	-r - -P-	3	1	3	3	2	$16_{14}^{19}$	$13_{11}^{15}$	$13_{12}^{15}$	$12_{11}^{13}$
											$8.6_{7.4}^{10.2}$	$6.7_{5.7}^{7.9}$	
	3496	2007-03-30 22:16:48	329.50-330.00	-P-	1	0	1	1	0	_		6 71.9	_

 $Table \ \textit{4} \ continued$ 

Table 4 (continued)

1	2	3	4	5	6a Inde	6b epener	6c nt tim	6d ne win	6e dows	7a	7b Max F	7c A (%)	7d
Source	Entry	MINBAR TOA, UT	$^{\nu}_{\rm (Hz)}$	Where	any	$0.5\mathrm{s}$	$1.0\mathrm{s}$	$2.0\mathrm{s}$	$4.0\mathrm{s}$	$0.5\mathrm{s}$	$1.0\mathrm{s}$	$2.0\mathrm{s}$	$4.0\mathrm{s}$
	3197	2004-04-17 02:45:18	577.00	—Т	1	0	1	0	0	_	$27_{23}^{32}$	_	_
	2670	2000-08-25 07:58:34	873.75	-P-	1	0	0	0	1	_	-	-	$2.5^{3.0}_{2.2}$
	3234	2004-11-03 03:28:32	1006.50	-T	1	0	0	1	0	-	_	$20_{17}^{24}$	_
	2712	2001-04-01 21:55:53	1528.00	R	1	0	0	1	0	_	-	$5.7_{4.9}^{6.8}$	_
	3220	2004-07-26 19:02:46	1833.50	—Т	1	0	0	1	0	_	_	$63_{50}^{77}$	_
4U 1705-44	2554	1999-07-14 15:14:24	3.00	-T	1	0	1	0	0	-	$34_{28}^{40}$	-	-
	3576	2007-08-07 23:42:22	2.50	-P-	1	0	0	1	0	_	_	$15^{18}_{13}$	_
	2988	2002-04-29 01:55:28	16.00	-P-	1	0	1	0	0	-	$36^{43}_{30}$	_	_
	3658	2008-02-05 01:59:00	90.25	-P-	1	0	0	0	1	_	-	_	$34_{29}^{40}$
	3909	2010-03-03 19:50:51	647.50	-T	1	0	0	1	0	_	-	$94_{72}^{117}$	_
	3847	2009-08-19 05:17:38	1120.00	-T	1	0	1	0	0	_	$26^{31}_{21}$	_	_
	3296	2005-07-01 03:07:42	1674.00	—Т	1	1	0	0	0	$51_{40}^{63}$	_	_	_
XTE J1710-281	3122	2003-08-03 19:14:42	3.00	R—	1	0	0	0	1	-	-	-	$18_{16}^{22}$
	3123	2003-08-07 02:08:00	20.00	-P-	1	0	1	0	0	-	$65_{52}^{79}$	_	_
	3476	2007-03-05 18:22:02	589.00	-T	1	0	0	0	1	_	_	_	$23_{19}^{27}$
	2594	1999-11-10 23:54:06	1044.00	-P-	1	1	0	0	0	$42^{50}_{35}$	-	_	-
	3235	2004-11-07 05:08:54	1335.00	-P-	1	0	1	0	0	-	$44_{36}^{52}$	-	-
IGR J17191-2821	3513	2007-05-04 02:32:06	293.50-294.00	-P-	1	0	1	1	1	_	$17_{15}^{20}$	$12_{10}^{14}$	$11_{10}^{13}$
	3518	2007-05-08 17:08:52	293.50-294.25	-P-	3	0	1	2	2	_	$12_{11}^{15}$	$13_{11}^{15}$	$12_{10}^{13}$
4U 1722-30	3199	2004-05-22 05:14:19	22.00	-P-	1	1	0	0	0	$7.1_{6.1}^{8.4}$	-	-	-
4U 1728-34	3463	2007-01-20 06:12:46	8.00	-P-	1	1	0	0	0	$5.1_{4.3}^{6.1}$	_	_	_
	2575	1999-09-22 05:14:11	22.00	-P-	1	1	0	0	0	$7.1_{6.0}^{4.3}$	_	_	_
	2640	2000-07-21 05:53:24	108.50	—Т	1	0	0	1	0	-	_	$48_{34}^{63}$	_
	2205	1996-02-15 21:10:21	363.00	-P-	1	0	0	1	0	_	_	$3.2^{3.7}_{2.7}$	_
	2207	1996-02-16 06:51:10	362.00-364.00	RP-	3	1	1	2	2	$6.8_{5.7}^{8.0}$	$5.4_{4.6}^{6.3}$	$5.0_{4.4}^{2.7}$	$5.0_{4.3}^{5.8}$
	2208	1996-02-16 10:00:47	362.00-364.00	-PT	5	2	4	5	3	$10_9^{12}$	$9.6^{10.9}_{8.5}$	$8.1_{6.9}^{9.4}$	$7.7^{8.7}_{6.8}$
	2209	1996-02-16 19:27:13	363.50	-P-	1	0	0	1	0	9	- 8.5	$4.4_{3.8}^{5.1}$	-
	2210	1996-02-18 17:31:52	363.00-363.50	-P-	2	0	1	2	0	_	$4.2_{3.6}^{5.0}$	$4.8_{4.1}^{5.6}$	_
	2346	1997-09-19 12:32:58	362.00-363.00	RP-	1	1	1	1	1	$9.2_{7.9}^{10.8}$	$9.2_{7.9}^{10.9}$	$5.9_{5.0}^{6.9}$	$3.5_{3.0}^{4.0}$
	2347	1997-09-20 10:08:53	362.50-364.00	RP-	5	4	3	3	2	$10_9^{12}$	$8.9_{8.0}^{10.0}$	$11_{10}^{11}$	$6.4_{5.9}^{7.0}$
	2348	1997-09-21 15:45:31	362.50	-P-	1	0	0	1	0	-	-	$4.2_{3.5}^{4.9}$	-
	2349	1997-09-21 18:11:07	362.00-363.50	RP-	2	1	1	2	2	$12_{10}^{13}$	$13_{12}^{15}$	$6.5_{5.6}^{7.5}$	$3.9_{3.4}^{4.5}$
	2350	1997-09-22 06:42:53	362.00-364.00	RP-	6	3	4	4	2	$13_{12}^{15}$	$9.3^{10.5}_{8.3}$	$11_{10}^{12}$	$8.1_{7.5}^{8.7}$
	2481	1999-01-31 22:02:00	362.00-363.00	-P-	1	1	1	1	1	$7.1_{6.2}^{8.1}$	$8.1_{7.2}^{9.0}$	$5.5_{4.9}^{6.1}$	$3.5_{3.1}^{4.0}$
	2485	1999-02-04 22:31:25	363.00-363.75	-P-	1	0	1	1	1	-	$6.9_{6.0}^{7.9}$	$5.1_{4.5}^{5.8}$	$3.0_{2.6}^{3.5}$
	2561	1999-08-19 09:33:48	363.00	RP-	1	0	0	1	1	_	-	$5.1_{4.4}^{6.0}$	$6.2_{5.3}^{7.2}$
	2562	1999-08-19 12:09:22	362.50-364.00	RP-	4	3	4	3	2	$12_{10}^{14}$	$11_{10}^{12}$	$9.0_{8.2}^{9.8}$	$7.2_{6.5}^{7.9}$
	2564	1999-08-19 15:46:58	362.00-364.00	-P-	3	1	2	3	2	$17_{14}^{10}$	$14_{12}^{16}$	$11_{10}^{12}$	$12_{11}^{13}$
	2565	1999-08-20 05:54:45	362.00-364.00	RP-	6	1	6	3	2	$9.8_{8.3}^{11.6}$	$9.2_{8.0}^{10.7}$	$8.8_{8.0}^{9.7}$	$6.8_{6.1}^{7.4}$
	2764	2001-09-17 22:15:24	362.50	-P-	1	0	0	1	0	9.08.3	9.28.0	$4.9_{4.2}^{5.7}$	0.06.1
	2869	2001-09-17 22:13:24 2001-10-18 03:33:29	362.00-363.75	-P-	3	0	2	3	2	_	$6.4_{5.6}^{7.5}$	$5.5_{4.6}^{6.5}$	$4.9_{4.3}^{5.5}$
	2873	2001-10-18 03:53:29 2001-10-27 23:53:44	362.00–363.00	-r - R	1	1	1	1	0	$15_{13}^{17}$	$15_{13}^{18}$	$10_{9}^{12}$	4.94.3
	3172			-P-		1	2	3	2	$13_{13}^{13}$ $13_{11}^{15}$	$13_{13} \\ 12_{11}^{14}$	$10_{9}^{10}$	$7.5_{6.7}^{8.4}$
	3369	2004-03-12 01:41:13 2006-04-17 12:25:42	363.50–364.00 363.00–364.00	RP-	3 6	5	6	4	2	$16_{13}^{11}$	$12_{11}^{14}$ $12_{11}^{14}$	$11_{10}^{12}$	0.010.7
					2			2	2		211 c = 7.5	7 18.0	$9.8^{10.7}_{8.9}$
	3375	2006-06-14 17:57:35	362.75–364.00	-P-		0	1			1014	$6.5_{5.6}^{7.5}$	$7.1_{6.2}^{8.0}$	$4.5_{3.8}^{5.2}$
	3384	2006-08-01 16:46:49	362.00-363.00	R—	1	1	1	0	0	$12_{10}^{14}$	$13_{11}^{15}$	0.010.1	- 6.5
	3398	2006-08-15 07:41:11	363.00–364.00	–P–	2	1	1	2	1	$12_{10}^{14}$	$8.9_{7.7}^{10.2}$	$9.2^{10.1}_{8.3}$	$5.7_{5.1}^{6.5}$
	3411	2006-08-23 08:59:34	362.00	R—	1	1	1	0	0	$13_{11}^{15}$	$13_{11}^{15}$	- 0.09.4	- - 48.4
	3412	2006-09-08 03:38:35	363.00–363.75	-P-	1	0	1	1	1	_	$9.6^{11.1}_{8.3}$	$8.2_{7.3}^{9.4}$	$7.4_{6.5}^{8.4}$
	3432	2006-10-04 09:56:23	363.75	-P-	1	0	0	0	1	- 0.411.1	- c c7.8	- - <del></del> 6.6	$4.7_{4.0}^{5.5}$
	3434	2006-10-16 04:54:24	362.00-362.50	-P-	1	1	1	1	1	$9.4_{7.9}^{11.1}$	$6.6^{7.8}_{5.7}$	$5.7^{6.6}_{5.0}$	$3.6^{4.3}_{3.1}$
	3505	2007-04-22 21:35:01	363.00	-P-	1	0	1	1	1	_	$8.1_{6.9}^{9.6}$	$6.6_{5.7}^{7.7}$	$5.2_{4.5}^{6.0}$
	3508	2007-04-24 23:57:46	362.50	-P-	1	0	0	1	0	- 1015	- 13	$5.1_{4.3}^{6.0}$	- 0.210.0
	3534	2007-05-28 10:31:30	363.00-364.00	-P-	4	1	4	3	2	$13_{11}^{15}$	$12_{10}^{13}$	$12^{13}_{11}$	$9.2_{8.4}^{10.0}$
	3538	2007-06-03 20:22:46	362.00	R—	1	0	0	1	0	-	- 7 9	$5.4_{4.5}^{6.3}$	7 °
	3966	2010-10-05 04:12:48	362.00-363.50	-P-	3	0	1	2	2	-	$6.7^{7.9}_{5.7}$	$8.9_{7.9}^{10.0}$	$7.0_{6.3}^{7.8}$
	8249	2011-08-28 17:40:52	363.00-364.00	RP-	2	0	2	1	1	-	$11_{10}^{13}$	$11_{10}^{12}$	$8.5^{9.6}_{7.6}$

 ${\bf Table~4~} (continued)$ 

1	2	3	4	5	6a Inde	6b epener	6c nt tim	6d ne win	6e dows	7a	7b Max F	7c A (%)	7d
Source	Entry	MINBAR TOA, UT	$^{\nu}_{\rm (Hz)}$	Where	any	$0.5\mathrm{s}$	$1.0\mathrm{s}$	$2.0\mathrm{s}$	$4.0\mathrm{s}$	$0.5\mathrm{s}$	$1.0\mathrm{s}$	$2.0\mathrm{s}$	$4.0\mathrm{s}$
	2476	1999-01-26 00:01:40	381.00	—Т	1	0	1	0	0	_	$41_{34}^{50}$	_	_
	3172	2004-03-12 01:41:13	419.00	-P-	1	0	0	0	1	_	-	_	$5.7_{4.8}^{6.7}$
	2515	1999-03-31 15:14:29	822.00	-P-	1	0	1	0	0	_	$5.5_{4.6}^{6.5}$	_	-
	8254	2011-09-17 12:24:55	1550.50	-T	1	0	0	0	1	_	_	_	$17^{20}_{15}$
	2476	1999-01-26 00:01:40	1574.00	-T	1	1	0	0	0	$44_{36}^{53}$	_	_	_
	3505	2007-04-22 21:35:01	1678.00	-T	1	0	1	0	0	-	$74^{94}_{57}$	_	_
	3372	2006-05-11 00:39:21	1829.00	-T	1	0	1	0	0	_	$67^{83}_{51}$	_	_
	2873	2001-10-27 23:53:44	1965.00	R	1	0	1	0	0	_		_	_
MXB 1730-335	2373	1998-02-07 20:04:55	18.25	-P-	1	0	0	0	1	_	-	_	$6.1_{5.2}^{7.0}$
	2372	1998-02-07 19:00:34	33.50	-P-	1	0	0	0	1	_	_	$\begin{array}{cccccccccccccccccccccccccccccccccccc$	$9.6^{11.4}_{8.2}$
	2365	1998-01-31 23:25:27	396.00	-T	1	1	0	0	0	$65^{84}_{47}$	_		-
	2423	1998-08-22 10:15:46	406.00	R—	1	1	0	0	0	$37_{30}^{44}$	$\begin{array}{cccccccccccccccccccccccccccccccccccc$	_	_
	2371	1998-02-04 20:21:48	468.00	—Т	1	1	0	0	0	$58_{46}^{72}$	_	$\begin{array}{cccccccccccccccccccccccccccccccccccc$	_
	2371	1998-02-04 20:21:48	592.00	-P-	1	0	1	0	0	-	$27_{22}^{32}$	_	_
	2363	1998-01-30 20:28:11	732.50	—Т	1	0	0	0	1	_	-	_	$42_{34}^{51}$
	4182	1999-10-02 09:28:24	1051.50	—Т	1	0	0	1	0	_	_	$38^{46}_{21}$	34
	4189	1997-07-07 13:29:07	1464.00	—Т	1	0	1	0	0	_	$151_{00}^{210}$	-	_
	2373	1998-02-07 20:04:55	1643.50	-P-	1	0	0	0	1	_		$\begin{array}{c} -\\ -\\ -\\ -\\ -\\ -\\ -\\ -\\ -\\ -\\ -\\ -\\ -\\ $	$10_9^{12}$
KS 1731-260	2430	1998-10-02 07:36:57	44.00	-P-	1	1	0	0	0	$13_{11}^{15}$		_	
NS 1751-200	2655	2000-08-07 20:23:26	173.50	-P-	1	0	0	1	0	-			_
	2231	1996-07-14 04:16:13	524.00-524.25	-P-	2	0	2	1	1	_		$5.3^{6.1}$	$4.3_{3.8}^{4.8}$
	2495	1999-02-26 17:13:09	523.50-524.00	-P-	1	1	0	1	0	$7.1_{6.1}^{8.4}$	0.05.1	3.04.7	4.03.8
	2497	1999-02-27 17:25:09	523.50-524.50	-P-	4	4	3	3	2	$13_{11}^{14}$	$9.6^{10.6}$	8 2 <sup>8.9</sup>	$7.2_{6.7}^{7.7}$
	2684	2000-09-29 14:08:35	1840.00	-P-	1	0	1	0	0	10 <sub>11</sub>	7 48.8	$2.0  \mathrm{s}$	1.26.7
4U 1735-444	3872		378.00	—r — —T	1	1	0	0	0	$125_{89}^{164}$	1.46.2		
40 1750-444	2339	2009-10-19 07:45:24		—1 —T	1	0	0		0	120 <sub>89</sub>	_	- 6176	_
CDC 1741 0 0059		1997-09-02 12:59:45	888.50	-P-	2			1					- c 47.5
GRS 1741.9-2853	2226	1996-05-15 19:32:24	589.00-589.75			0	0	1	1	_			$6.4_{5.4}^{7.5}$
	2228	1996-06-04 14:41:08	589.25	-P-	1	0	0	0	1	_		_	$5.3_{4.5}^{6.1}$
	2226	1996-05-15 19:32:24	1829.25	-P-	1	0	0	0	1	- 137		_	$15_{13}^{17}$
1A 1742-294	2781	2001-09-27 14:36:26	702.00	-P-	1	1	0	0	0	105 <sup>137</sup>		_	_
	2267	1997-03-20 17:07:16	1340.00	-P-	1	1	0	0	0	34 <sup>41</sup>			
IGR J17473-2721	3695	2008-04-26 00:50:50	10.00	-T	1	1	0	0	0	$34^{44}_{24}$	_	_	_
	3684	2008-04-08 13:36:27	240.00	-T	1	1	0	0	0	$48^{58}_{39}$	_	_	_
	3742	2008-07-17 08:25:41	602.00	R—	1	1	0	0	0	$13_{11}^{15}$	-	-	_
	3742	2008-07-17 08:25:41	605.00	-P-	1	0	0	1	0	_		$4.1_{3.5}^{4.8}$	
SLX 1744-300	3437	2006-10-23 10:54:20	96.00	-T	1	0	1	0	0	-	$68_{54}^{83}$	$2.0\mathrm{s}$	_
	3437	2006-10-23 10:54:20	928.25	-P-	1	0	0	0	1	-	$ \begin{array}{cccccccccccccccccccccccccccccccccccc$	_	$9.7_{8.3}^{11.4} \\ 25_{21}^{29}$
	3506	2007-04-23 17:34:12	1278.00	-T	1	0	0	0	1	-	-	$2.0  \mathrm{s}$	$25_{21}^{29}$
	3723	2008-05-30 05:48:51	1978.00	—Т	1	1	0	0	0	$221_{114}^{331}$	_	_	_
IGR J17480-2446	3983	2010-10-14 17:28:30	6.00	R—	1	1	0	0	0	$189_{98}^{281}$	-	-	-
	4192	2010-10-13 00:37:12	10.00 - 11.00	RPT	33	3	30	26	17	$77^{93}_{63}$	$88_{66}^{111}$	$69_{57}^{83}$	$57^{66}_{48}$
	4159	2010-10-25 07:42:54	11.00	R—	1	0	0	0	1	-	_	$\begin{array}{c ccccccccccccccccccccccccccccccccccc$	$99_{71}^{128}$
	4030	2010-10-15 20:28:31	115.00	R—	1	0	0	1	0	-	_	$88_{66}^{112}$	_
	4103	2010-10-21 14:05:06	116.00	R	1	1	0	0	0	$680^{1884}_{-523}$	-		_
	4057	2010-10-16 12:22:18	380.00	R—	1	1	0	0	0	$115_{76}^{156}$	_	_	_
	8144	2010-11-06 06:26:08	459.00	-T	1	0	0	0	1	_	_	_	$83_{61}^{107}$
	8123	2010-11-02 09:43:14	689.50	R—	1	0	0	1	0	_	_	$35_{29}^{42}$	_
	8183	2010-11-17 01:23:34	751.00	R—	1	0	1	0	0	_	$39^{47}_{33}$		_
	8152	2010-11-08 05:57:21	771.50	-P-	1	0	0	1	0	_		$56^{69}_{45}$	_
	8173	2010-11-14 06:06:23	830.00	-T	1	0	1	0	0	_	$83_{62}^{105}$	-	_
	8105	2010-10-29 14:01:01	994.00	-P-	1	1	0	0	0	$160_{100}^{222}$		_	_
	8135	2010-11-04 04:35:07	997.00	-P-	1	0	0	1	0	-			_
	8183	2010-11-17 01:23:34	1003.50	-P-	1	0	0	1	0	_		$38^{46}_{22}$	_
	4059	2010-11-17 01:23:54	1050.00	R—	1	1	0	0	0	$304_{74}^{536}$		-	_
	4050	2010-10-16 11:43:33	1168.00	—T	1	1	0	0	0	$247_{79}^{418}$	_	_	_
	4116	2010-10-10 11:45:55 2010-10-21 15:56:13	1396.00	—1 —T	1	0	1	0	0	241 <sub>79</sub>	$252_{74}^{431}$	_	_

 $Table\ 4\ continued$ 

Table 4 (continued)

1	2	3	4	5	6a Inde	6b epener	6c nt tim	6d ne win	6e dows	7a	7b Max FA	7c (%)	7d
Source	Entry	MINBAR TOA, UT	$_{ m (Hz)}^{ u}$	Where	any	$0.5\mathrm{s}$	$1.0\mathrm{s}$	$2.0\mathrm{s}$	$4.0\mathrm{s}$	$0.5\mathrm{s}$	$1.0\mathrm{s}$	$2.0\mathrm{s}$	$4.0\mathrm{s}$
	4152	2010-10-24 07:45:57	1630.00	R—	1	0	1	0	0	_	$318^{816}_{-180}$	_	_
	4111	2010-10-21 15:29:11	1662.50	R—	1	0	0	1	0	_	-	$123_{84}^{164}$	_
	8083	2010-10-27 09:49:25	1782.00	R—	1	0	0	1	0	_	_	$54_{44}^{65}$	_
	8169	2010-11-12 05:03:17	1793.00	R—	1	0	1	0	0	_	$141_{30}^{253}$	_	_
	3991	2010-10-14 19:32:14	1833.50	-P-	1	0	0	0	1	_	_	_	$37^{44}_{31}$
	8086	2010-10-27 10:18:54	1837.00	R—	1	0	1	0	0	_	$146_{89}^{204}$	_	_
EXO 1745-248	2666	2000-08-13 13:59:29	14.50	—Т	1	0	0	1	0	_	_	$20_{15}^{25}$	_
1A 1744-361	3298	2005-07-16 22:39:57	529.00	R—	1	0	1	0	0	_	$11_{9}^{13}$	-	_
SAX J1748.9-2021	2866	2001-10-14 05:37:34	372.00	—Т	1	0	1	0	0	_	8361	_	_
	2862	2001-10-13 07:43:35	549.00	-T	1	0	0	1	0	_	_	$81_{59}^{105}$	_
IGR J17498-2921	8239	2011-08-16 15:21:42	401.00	-P-	1	0	0	1	1	_	_		$9.7^{11.2}_{8.3}$
	8244	2011-08-20 14:10:05	401.00	-P-	2	0	0	1	2	_	_	$7.6_{6.4}^{9.0}$	$12_{11}^{14}$
4U 1746-37	2444	1998-11-08 02:23:41	966.00	—Т	1	1	0	0	0	$100_{72}^{129}$	_	$\begin{array}{c} A \ (\%) \\ \hline 2.0 \ s \\ \hline \\ - \\ 123_{84}^{164} \\ 54_{44}^{65} \\ \hline \\ - \\ - \\ 20_{15}^{25} \\ \hline \\ - \\ - \\ - \\ 81_{105}^{59} \\ \hline \\ 11_{13}^{105} \\ 7.6_{6.4}^{9.0} \\ \hline \\ - \\ - \\ 6.4_{5.5}^{7.5} \\ \hline \\ 12_{14}^{11} \\ 15_{17}^{17} \\ 12_{13}^{10} \\ \hline \\ - \\ - \\ 13_{15}^{17} \\ - \\ - \\ 48_{40}^{58} \\ 2.4_{2.0}^{2.8} \\ 8.9_{8.1}^{8.8} \\ 4.7_{4.3}^{6.2} \\ 5.4_{4.6}^{4.6} \\ 19_{11}^{21} \\ 3.3_{3.7}^{3.0} \\ 5.9_{5.7}^{5.7} \\ 6.3_{5.6}^{5.6} \\ 6.2_{5.4}^{7.1} \\ \hline - \\ 12_{14}^{14} \\ 12_{10}^{10} \\ - \\ 12_{14}^{14} \\ 12_{10}^{10} \\ - \\ 13_{16}^{16} \\ 13_{17}^{17} \\ - \\ 16_{19}^{19} \\ 14_{11}^{16} \\ 12_{17}^{17} \\ 16_{19}^{19} \\ 18_{15}^{17} \\ 17_{14}^{10} \\ 18_{15}^{17} \\ 17_{14}^{10} \\ 18_{15}^{17} \\ 18_{15}^{17} \\ \end{array}$	-
	2249	1996-10-31 09:17:13	1887.75	-P-	1	0	0	0	1		_	_	$7.9_{6.8}^{9.3}$
SAX J1750.8-2900	2717	2001-04-12 14:20:31	599.00-600.75	RP-	2	1	1	1	1	$20^{23}_{17}$	$23_{20}^{28}$	$6.4_{5.5}^{7.5}$	$4.3_{3.7}^{4.9}$
IGR J17511-3057	3858	2009-09-14 07:54:43	244.50-245.00	RPT	12	0	9	6	6	_	18 <sup>20</sup> <sub>16</sub>		$29_{25}^{35}$
G10 011011 0001	3859	2009-09-15 17:17:24	244.75-245.00	RP-	6	0	3	4	4	_	$18_{16}^{21}$	$15_{12}^{17}$	$16_{14}^{19}$
	3860	2009-09-17 06:33:27	244.75-245.00	RP-	3	0	2	3	3	_	$20_{17}^{16}$	$\begin{array}{c} 2.0\mathrm{s} \\ 2.0\mathrm{s} \\ \hline \\ -123_{84}^{164} \\ 54_{44}^{65} \\ -\\ -\\ 20_{15}^{25} \\ \hline \\ -\\ -\\ 81_{105}^{505} \\ \hline \\ 11_{13}^{13} \\ 7.6_{6.4}^{9.0} \\ -\\ -\\ -\\ 6.4_{5.5}^{7.5} \\ \hline \\ 12_{14}^{14} \\ 15_{17}^{17} \\ 12_{13}^{10} \\ -\\ -\\ 13_{15}^{15} \\ -\\ -\\ 48_{40}^{58} \\ 2.4_{2.0}^{2.8} \\ 8.9_{8.8}^{8.1} \\ 4.7_{4.3}^{5.2} \\ 5.9_{5.2}^{5.2} \\ 6.3_{5.6}^{7.0} \\ 6.2_{5.4}^{7.1} \\ -\\ 12_{14}^{14} \\ 12_{17}^{14} \\ 12_{17}^{15} \\ -\\ 13_{16}^{16} \\ 12_{17}^{14} \\ 12_{17}^{14} \\ 12_{17}^{14} \\ 12_{17}^{14} \\ 12_{17}^{14} \\ 12_{17}^{14} \\ 12_{17}^{14} \\ 12_{17}^{15} \\ 17_{17}^{15} \\ 17_{15}^{17} \\ 17_{15}^{17} \\ 17_{15}^{17} \\ 17_{15}^{17} \\ 17_{15}^{17} \\ 17_{15}^{17} \\ 17_{15}^{17} \\ 17_{15}^{17} \\ 17_{15}^{17} \\ 17_{17}^{17} \\ 18_{15}^{17} \\ 17_{15}^{17} \\ 17_{15}^{17} \\ 17_{15}^{17} \\ 17_{15}^{17} \\ 17_{15}^{17} \\ 17_{15}^{17} \\ 17_{15}^{17} \\ 17_{17}^{17} \\ 18_{15}^{17} \\ 17_{15}^{17} \\ 18_{15}^{17} \\ 17_{15}^{17} \\ 18_{15}^{17} \\ 17_{15}^{17} \\ 18_{15}^{17} \\ 17_{15}^{17} \\ 18_{15}^{17} $	$12_{10}^{14}$
	3861	2009-09-17 14:48:42	244.75-245.00	-P-	4	0	1	2	4	_	$17_{14}^{20}$	$14_{12}^{16}$	$16_{14}^{19}$
	3862	2009-09-20 14:50:31	244.00-245.00	RP-	8	1	8	6	4	$9.9_{8.4}^{11.8}$	$13_{11}^{14}$	$12_{10}^{12}$	$8.9_{7.9}^{10.0}$
	3863	2009-09-23 14:27:07	244.75-245.00	-P-	3	0	1	0	3	-	$11_{10}^{13}$		$11_{10}^{13}$
	3867	2009-09-25 07:31:36	244.00-245.00	-PT	12	3	8	6	7	$13_{11}^{15}$	$19_{16}^{\overset{10}{23}}$	$13_{11}^{15}$	$19_{16}^{23}$
	3868	2009-09-26 15:11:22	244.75	-P-	1	0	0	0	1	-	-		$11_{9}^{12}$
	3869	2009-09-27 06:57:22	244.75-245.00	-P-	3	0	0	1	3	_	_	$9.1_{7.7}^{10.6}$	$11_{9}^{13}$
IGR J17597-2201	3227	2004-09-14 13:23:11	390.00	-P-	1	0	1	0	0	_	$19_{16}^{23}$		_
	3227	2004-09-14 13:23:11	1529.00	—Т	1	0	0	1	0	_	-	$48^{58}_{40}$	_
SAX J1808.4-3658	3040	2002-10-19 10:14:33	8.00	-P-	1	1	1	1	0	$5.6_{4.9}^{6.4}$	$4.3_{3.8}^{4.8}$	$2.4^{2.8}_{2.0}$	_
	3037	2002-10-15 09:55:37	400.00-402.00	RPT	4	2	2	1	3	$8.0_{7.1}^{9.0}$	$9.2_{8.3}^{10.2}$	$8.9^{\overset{2.0}{9.8}}_{8.1}$	$5.7_{5.2}^{6.2}$
	3038	2002-10-17 07:19:24	401.00	-P-	4	0	4	3	2		$5.2_{4.6}^{5.8}$	$4.7_{4.2}^{5.2}$	$4.5_{4.2}^{4.8}$
	3039	2002-10-18 04:25:21	397.00-402.00	RPT	7	2	3	5	5	$15^{18}_{13}$	$15_{12}^{17}$	$5.4_{4.6}^{6.3}$	$24_{20}^{28}$
	3040	2002-10-19 10:14:33	399.00-401.00	RP-	7	2	4	6	5	$35_{29}^{13}$	$38_{32}^{12}$	$19_{18}^{21}$	$5.1_{4.5}^{\overline{5.8}}$
	3290	2005-06-05 15:19:04	401.00	-P-	3	0	1	3	2	_	$4.0_{3.5}^{4.6}$	$3.3_{3.0}^{3.7}$	$3.1_{2.8}^{3.4}$
	3769	2008-09-23 16:59:43	400.00-401.00	RP-	3	1	1	2	3	$6.7_{5.8}^{7.8}$	$6.0_{5.3}^{6.8}$	$5.9_{5.2}^{6.7}$	$3.4_{3.0}^{3.8}$
	3770	2008-09-24 20:14:25	400.00-404.00	RP-	4	2	3	2	3	$16_{13}^{19}$	$7.4_{6.4}^{8.5}$	$6.3_{5.6}^{7.0}$	$3.4_{2.9}^{4.0}$
SAX J1810.8-2609	3586	2007-08-20 21:01:37	531.75-532.00	-P-	1	0	0	1	1	_	-		$4.9^{5.4}_{4.4}$
XTE J1814-338	3084	2003-06-06 00:58:31	314.25	-P-	1	0	0	0	1	_	_		$11_{10}^{13}$
	3086	2003-06-07 21:12:22	314.00-314.50	RP-	7	0	1	6	5	_	$12_{10}^{14}$	$12_{11}^{14}$	$10_{9}^{11}$
	3087	2003-06-09 04:42:35	314.00-314.50	RP-	9	1	3	7	7	$13_{11}^{16}$	$11_{9}^{13}$		$11_{10}^{13}$
	3088	2003-06-10 02:23:00	314.00 – 314.50	RPT	11	0	3	7	9	_	$12_{11}^{14}$	$15_{12}^{17}$	$13_{11}^{15}$
	3089	2003-06-11 00:42:03	314.25	-P-	1	0	0	0	1	_	_	_	$13_{11}^{15}$
	3091	2003-06-12 11:11:37	314.00 - 314.50	RPT	16	0	4	12	12	_	$16^{18}_{13}$	$16^{19}_{14}$	$13_{11}^{15} \\ 22_{19}^{26} \\ 11_{10}^{13}$
	3092	2003-06-12 13:31:07	314.25	-P-	1	0	0	0	1	_	-		$11_{10}^{13}$
	3093	2003-06-13 01:25:31	314.50	RP-	2	0	0	2	2	_	_	$13_{11}^{16}$	$10_{9}^{12}$
	3094	2003-06-13 17:37:13	314.00 – 314.50	RPT	15	1	1	15	11	$16^{19}_{14}$	$12_{10}^{14}$		$17^{19}_{15}$
	3095	2003-06-14 00:20:54	314.00 – 314.50	RPT	15	1	5	10	11	$17^{20}_{15}$	$14_{12}^{16}$	$16^{19}_{14}$	$15^{18}_{13}$
	3096	2003-06-15 18:56:50	314.00 – 314.50	RPT	16	2	4	11	12	$19_{17}^{23}$	$18^{21}_{15}$	$18^{22}_{15}$	$18_{16}^{21}$
	3098	2003-06-16 17:56:22	314.00 – 314.50	RPT	12	1	2	10	9	$22_{19}^{26}$	$18_{16}^{21}$	$39_{34}^{45}$	$25_{22}^{29} \\ 19_{16}^{22}$
	3099	2003-06-16 19:37:54	314.50	RP-	3	0	0	2	2	-	_	$27^{32}_{23}$	$19_{16}^{22}$
	3100	2003-06-17 16:00:21	314.00 – 314.50	RP-	18	4	4	16	11	$27^{32}_{22}$	$21_{18}^{25}$	$19_{17}^{22}$	$17_{14}^{20}$
	3101	2003-06-18 19:05:19	314.00 – 314.50	RP-	8	1	1	8	6	$23_{20}^{27}$	$17^{19}_{14}$	$17^{20}_{14}$	$13_{11}^{14}$
	3102	2003-06-19 18:45:30	314.00 – 314.50	RP-	7	1	3	7	6	$20_{16}^{23}$	$15^{18}_{13}$	$16^{19}_{14}$	$12_{10}^{14}$
	3103	2003-06-20 01:38:10	314.00 – 314.50	RPT	19	5	10	9	11	$21_{18}^{25}$	$13_{11}^{15}$	$21_{18}^{24}$	$18_{16}^{21}$
	3104	2003-06-20 21:38:02	314.50	RP-	3	0	0	2	3	-	_	$18^{20}_{15}$	$14_{12}^{16}$
	3105	2003-06-21 15:20:59	314.00 – 314.50	RP-	10	2	2	10	8	$19_{16}^{22}$	$14_{12}^{17}$	$20_{17}^{23}$	$15^{17}_{13}$
	3106	2003-06-22 21:19:42	314.00 – 314.50	RP-	7	1	3	7	5	$16^{19}_{14}$	$13_{11}^{15}$	$17^{20}_{15}$	$13_{11}^{15}$
	3107	2003-06-23 11:15:00	314.00-314.50	RPT	20	2	6	11	17	$27_{22}^{32}$	$18_{16}^{22}$	$21_{17}^{24}$	$23_{20}^{26}$

 ${\bf Table~4~} (continued)$ 

1	2	3	4	5	6a Inde	6b epener	6c nt tim	6d ne win	6e dows	7a	7b Max FA	7c A (%)	$7\mathrm{d}$
Source	Entry	MINBAR TOA, UT	$^{\nu}_{\rm (Hz)}$	Where	any	$0.5\mathrm{s}$	$1.0\mathrm{s}$	$2.0\mathrm{s}$	$4.0\mathrm{s}$	$0.5\mathrm{s}$	$1.0\mathrm{s}$	$2.0\mathrm{s}$	$4.0\mathrm{s}$
	3108	2003-06-27 16:38:50	314.00-314.50	RPT	17	4	8	14	9	$18_{16}^{22}$	$22_{19}^{27}$	$16_{14}^{19}$	$17_{14}^{20}$
	3109	2003-06-27 21:12:02	314.00 – 314.50	RPT	12	1	2	9	8	$18_{15}^{22}$	$15_{13}^{17}$	$32_{27}^{38}$	$13_{11}^{16}$
	3110	2003-06-28 20:29:16	314.00 – 314.50	RP-	11	0	3	6	9	_	$17^{20}_{15}$	$14_{12}^{15}$	$20_{18}^{23}$
	3118	2003-07-08 19:02:33	314.00 – 314.50	RPT	16	0	2	5	16	_	$15_{12}^{17}$	$15^{18}_{13}$	$34_{29}^{39}$
	3121	2003-07-17 17:42:46	314.00 – 314.50	RP-	2	0	0	2	2	_	-	$7.8^{9.0}_{6.7}$	$8.1_{7.1}^{9.2}$
	3094	2003-06-13 17:37:13	1601.00	-T	1	0	1	0	0	_	$26^{31}_{22}$	_	_
	3086	2003-06-07 21:12:22	1858.00	-P-	1	1	0	0	0	$19_{16}^{22}$	_	$16_{14}^{19} \\ 32_{27}^{38}$	_
GX 17+2	8266	2011-10-20 06:58:52	457.00	-P-	1	0	1	0	0	_	$30_{25}^{36}$	_	_
	2261	1997-02-08 02:36:36	714.00	-P-	1	0	0	1	0	_	-	$13_{11}^{15}$	_
	2261	1997-02-08 02:36:36	860.00	-P-	1	0	1	0	0	_	$15^{18}_{13}$	-	_
	3200	2004-05-23 17:43:34	1320.00	-P-	1	1	0	0	0	$59_{48}^{72}$	-	$\begin{array}{cccccccccccccccccccccccccccccccccccc$	_
	2261	1997-02-08 02:36:36	1862.75	-P-	1	0	0	0	1	-	_		$9.5^{11.1}_{8.1}$
	2457	1998-11-18 08:51:25	1918.00	-P-	1	1	0	0	0	$97_{69}^{127}$	_	_	- 8.1
4U 1820-303	3231	2004-09-29 10:31:31	280.00	-P-	1	0	1	0	0	-	$5.8_{5.0}^{6.8}$	_	_
	8204	2011-03-06 18:33:57	1687.00	R—	1	0	1	0	0	_	$108_{74}^{143}$	_	_
GS 1826-24	2391	1998-06-08 04:11:45	34.50	-P-	1	0	0	1	0	_	-	5.96.9	
GD 1020 21	2630	2000-06-30 17:02:11	110.00	—Т	1	0	0	1	0	_	_	49 <sup>62</sup>	_
	2390	1998-06-07 16:48:28	133.00	—Т	1	0	1	0	0	_	$10_9^{12}$	37	
	3214	2004-07-20 11:47:45	220.00	—т —т	1	1	0	0	0	$80_{57}^{104}$	109		
	3392	2006-08-10 08:13:44	410.00	—т —Т	1	1	0	0	0	$87_{62}^{113}$			
	$\frac{3392}{2357}$	1997-11-05 18:18:19	471.50	—т —Т	1	0	0	1	0	61 62	_	- 8 19.6	
	2389	1998-06-07 05:31:28	790.00	-P-	1	1	0	0	0	$13_{11}^{15}$	_		_
	3119	2003-07-14 09:20:30	1099.25	-r - R	1	0	0	0	1	13 <sub>11</sub>	_		$4.7_{4.0}^{5.6}$
	3391			т— —Т	1	0	0	1	0	_	_		4.74.0
		2006-08-10 04:54:36	1105.50								_		- - c8.9
	3012	2002-07-29 13:36:15	1142.50	–P– —T	1 1	0 1	0	0	$\frac{1}{0}$	- 2441	_		$7.6^{8.9}_{6.4}$
	3396	2006-08-12 07:06:24	1506.00				0			$34_{29}^{41}$	_		_
	3392	2006-08-10 08:13:44	1805.00	—T	1	0	0	1	0	- 227	_		_
	3078	2003-04-09 08:11:18	1844.00	-P-	1	1	0	0	0	$23_{19}^{27}$	- co77		_
G V 1	2392	1998-06-12 09:59:27	1863.00	<u>—T</u>	1	0	1	0	0		$62_{47}^{77}$		
Ser X-1	2332	1997-07-31 12:20:56	279.00	_T	1	0	0	1	0		6.9		
HETE J1900.1-2455	3667	2008-02-10 20:32:51	6.00	R—	1	0	1	0	0	_	$5.9_{5.0}^{6.9}$	_	- 27
	3960	2010-09-20 05:29:04	5.75	-P-	1	0	0	0	1	79	_	$ \begin{array}{cccccccccccccccccccccccccccccccccccc$	$2.3_{2.0}^{2.7}$
	3667	2008-02-10 20:32:51	12.00	R—	1	1	0	0	0	$64_{52}^{78}$	-		-
	3818	2009-04-02 08:57:54	376.25	-P-	1	0	0	0	1	_	_	_	$4.5^{5.2}_{3.8}$
Aql X-1	3270	2005-04-17 00:08:27	156.25	-P-	1	0	0	0	1	-	-	-	$6.5^{7.6}_{5.5}$
	2552	1999-07-06 16:40:08	252.25	-T	1	0	0	0	1	-	-	_	$22_{18}^{26}$
	2560	1999-08-18 17:19:13	271.50	-T	1	0	0	0	1	-	-		$15^{18}_{13}$
	2266	1997-03-01 23:26:36	548.00 - 550.00	-P-	4	2	3	3	2	$5.8_{4.9}^{6.9}$	$5.8_{5.0}^{6.8}$	$6.3_{5.3}^{7.4}$	$5.1_{4.5}^{5.8}$
	2340	1997-09-05 12:33:57	548.50 - 549.50	-P-	1	0	0	1	0	_	-	$3.9_{3.3}^{4.6}$	_
	2537	1999-06-03 18:43:03	547.50 - 549.50	RP-	2	2	2	1	1	$6.3_{5.5}^{7.2}$	$6.1_{5.3}^{7.0} \\ 6.1_{5.2}^{7.2}$	$5.7^{6.4}_{5.2}$	$2.8_{2.4}^{3.2}$
	2694	2000-11-08 03:45:56	549.00 - 550.00	-P-	2	1	2	2	2	$6.9_{5.9}^{8.2}$	$6.1_{5.2}^{7.2}$	$6.7^{7.5}_{6.0}$	$5.0_{4.5}^{5.5}$
	2966	2002-02-19 23:46:23	547.50 - 550.00	RP-	4	1	2	4	3	$6.1_{5.4}^{7.0}$	$6.8_{5.9}^{8.0}$	$4.3_{3.7}^{5.1}$	$5.1_{4.6}^{5.6}$
	3601	2007-09-22 19:22:12	548.75 - 549.00	-P-	1	0	0	1	1	-	-	$4.0_{3.4}^{4.7}$	$5.1_{4.6}^{5.6}$ $3.2_{2.8}^{3.7}$
	3880	2009-11-22 03:20:46	549.00	-P-	1	0	1	1	0	_	$5.5_{4.7}^{6.5}$	$4.5_{3.9}^{5.2}$	_
	3964	2010-10-03 18:18:40	548.75 - 549.25	-P-	1	0	1	1	1	-	$5.1_{4.3}^{6.0}$	$5.6_{4.7}^{6.5}$	$4.2_{3.6}^{4.8}$
	2688	2000-10-01 19:02:43	590.00	-P-	1	0	0	0	1	_	_		$5.4_{4.6}^{6.4}$
	2690	2000-10-03 12:30:35	908.00	-T	1	1	0	0	0	$39^{48}_{31}$	_	-	-
	3265	2005-04-12 04:54:49	1212.00	-T	1	1	0	0	0	$28^{33}_{23}$	_	-	_
	3162	2004-02-21 02:51:12	1221.00	-P-	1	0	0	0	1	_	_	-	$3.1_{2.6}^{3.6}$
	3533	2007-05-27 16:11:20	1305.00	R	1	0	1	0	0	_	$5.8_{4.9}^{6.8}$	_	_
	3539	2007-06-08 05:56:56	1331.00	R	1	0	1	0	0	_	$4.9_{4.2}^{5.7}$	_	_
	3528	2007-05-24 12:10:03	1388.00	—Т	1	0	1	0	0	_	$52_{43}^{63}$	_	_
	3203	2004-05-25 22:05:25	1418.00	-T	1	1	0	0	0	$36^{43}_{29}$	-	_	_
	2743	2001-07-01 14:18:37	1462.25	-P-	1	0	0	0	1	-	_	_	$8.8_{7.5}^{10.4}$
	3350	2005-12-16 03:49:48	1670.00	—Т	1	1	0	0	0	$27^{33}_{23}$	_	$14_{12}^{15} \\ 15_{13}^{18} \\ 7.86.7 \\ - \\ - \\ - \\ 13_{11}^{15} \\ - \\ - \\ - \\ - \\ - \\ - \\ - \\ - \\ - \\ $	-
XB 1916-053	2811	2001-10-01 20:41:44	6.50	-P-	1	0	0	1	0	- 23	_	$5.1_{4.2}^{6.0}$	_
		1996-10-29 06:57:52		RP-	1	0	0		0			4.3	

 $Table\ 4\ continued$ 

1	2	3	4	5	6a	6b	6c	6d	6e	7a	7b	7c	$7\mathrm{d}$
					Indepenent time windows					Max FA (%)			
Source	Entry	MINBAR TOA, UT	$_{ m (Hz)}^{ u}$	Where	any	0.5 s	1.0 s	2.0 s	4.0 s	$0.5\mathrm{s}$	1.0 s	2.0 s	4.0 s
	2404	1998-07-23 05:30:55	21.00	R—	1	0	1	1	0	_	$8.2^{9.6}_{7.0}$	$5.9_{5.0}^{6.9}$	_
	2408	1998-08-01 18:23:49	270.00 – 271.75	-P-	2	0	1	2	1	_	$9.1_{7.8}^{10.6}$	$7.4_{6.3}^{8.7}$	$5.3_{4.5}^{6.2}$
	2741	2001-06-30 17:10:07	1588.00	-P-	1	1	0	0	0	$18_{15}^{22}$	-	-	-
XTE J2123-058	2397	1998-06-29 16:25:20	122.50	R—	1	0	0	1	0	_	-	$65^{81}_{50}$	_
Cyg X-2	2221	1996-03-27 14:29:08	16.00	-P-	1	1	0	0	0	$15_{12}^{17}$	_	_	_
	3335	2005-11-01 07:49:56	48.00	-P-	1	0	1	1	0	_	$19_{16}^{23}$	$13_{11}^{15}$	_
	3739	2008-07-01 11:18:14	1713.00	R—	1	0	0	1	0	_	-	$33_{26}^{41}$	_

Table 4 (continued)

NOTE—Table 4 columns: (1) source name; (2) burst entry # in MINBAR database; (3) burst TOA in MINBAR database; (4) frequency range of candidates from a particular frequency group; (5) region of occurence (R – rise, B – burst, T – tail); (6) number of independent window detections, (6a) of any T<sub>win</sub>, (6b-6e) in four window sizes separately; (7) Maximum FA in time windows of four sizes (7a-7d).

### B. INDIVIDUAL SOURCES

## B.1. Individual sources with previously detected TBO

### B.1.1. EXO 0748-676

Galloway et al. (2010) reported on two strong TBO candidates from the rise of two bursts out of 157 bursts searched. The candidates (with the powers of 59.68 and 48.26) were detected in one independent time window per burst at the frequencies of 552 and 552.5 Hz. The estimate of the significance of the pair of candidates separated by < 1 Hz was based on the conservative number of trials and led to  $6.3\sigma$  significance.

Earlier, Villarreal & Strohmayer (2004) had reported a  $5.35\sigma$ -equivalent 45-Hz oscillation in the stacked spectra of 38 bursts. This candidate does not show up in the larger burst sample of Galloway et al. (2010), and its origin is unclear.

Our sample consists of 159 bursts, the majority with long tails ( $\sim 90\,\mathrm{s}$ ). We detect candidates at 551.5–552.5 Hz from the same two bursts as Galloway et al. (2010). In both bursts the candidates come from a few time windows, all of them dependent (e.g. Fig. 19). The sub-threshold candidates hint to a frequency evolution. The highest powers of candidates in 551.5–552.5 Hz frequency range are 57.5 and 51.4 (56.8 and 49.2 on nonnormalized data, respectively), whereas maximum  $P_{\rm m}$  outside this frequency region is 43.6. None of the simulations had the same  $P_{\rm m}$  as the strongest candidate, however, we did not make a significance estimate for the pair of candidates close in frequency.

Our analysis procedure does not find TBO candidates in the 552–554 Hz frequency region from the two fainter bursts mentioned in Galloway et al. (2010) (even subthreshold).

EXO 0748-676 is remarkable as a prolific source of type II low-frequency. Low-frequency candidates come from 2–14.5 Hz. Sometimes they are confined to 2-3 Hz, sometimes they chaotically occupy all frequencies up to

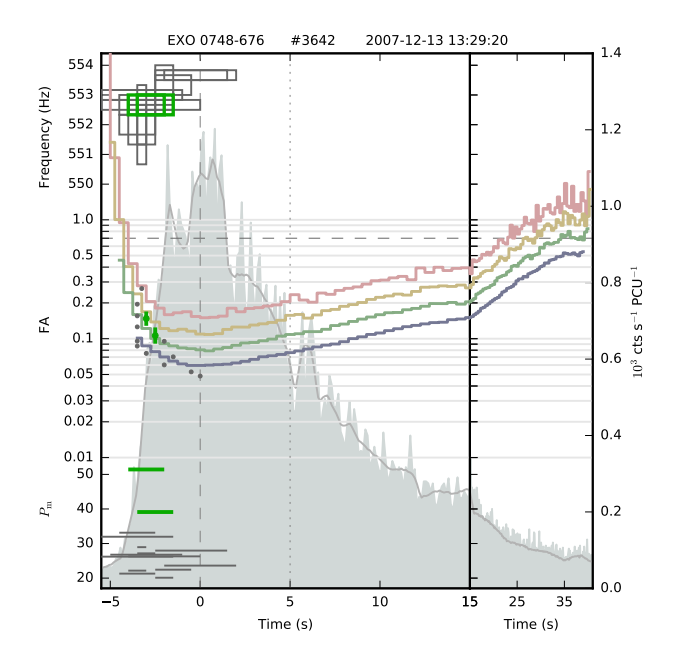


Figure 19. Oscillation candidate from EXO 0748-676.

 $13\,\mathrm{Hz}$ , and sometimes they occur at distinctly separate frequencies, e.g. 5 or  $9\,\mathrm{Hz}$ .

The source yielded a few dozen (glimmer) candidates with p=0.01, none of them close to the 45 Hz of Villarreal & Strohmayer (2004). Some of the candidates at widely separated frequencies come from the same burst, sometimes even from the same time windows.

### B.1.2. 4U 1608-522

TBOs from 4U 1608-522 have been detected at  $619\,\mathrm{Hz}$  in multiple bursts in the rise and after the burst peak by Galloway et al. (2008). The authors report large gradual frequency drifts, and FAs of 5-15%.

Our sample has 52 bursts, some of them very strong, suffering from data gaps and reduced average noise power (going down to 1.6). TBOs were detected at 616–620 Hz in seven bursts (e.g. Fig. 20). Two bursts had TBO signals in one independent time window (one of

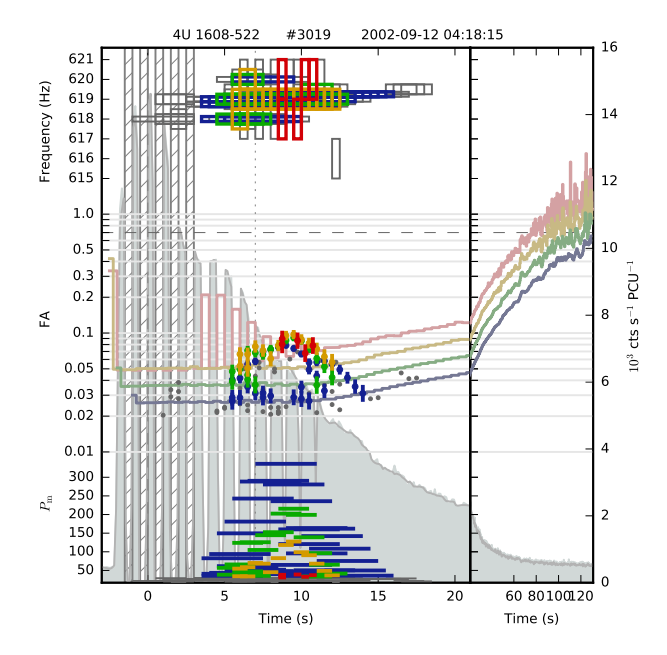


**Figure 20.** Burst from 4U 1608-522, with strong oscillation signal. The data is marred by gaps.

them had more sub-threshold candidates). The oscillations are mostly detected in the B region; one burst has TBOs starting in the rise. The gradual frequency drift throughout the TBO duration and FAs of 3-12% are consistent with Galloway et al. (2008) and Ootes et al. (2017).

In addition to TBOs, we record several type I low-frequency and about a dozen glimmer candidates (p = 0).

## B.1.3. 4U 1636-536

4U 1636-536 is one of the most prolific and best-studied TBO sources. Our sample contains 368 bursts from 4U 1636-536, forming the largest sample among the 57 sources that we have in total. Some of the bursts are quite bright, with average noise power dropping as low as 1.7.

TBOs at 576–582 Hz were detected from 75 bursts, most of them in the RB regions (the only detection in the T region is at its left edge). About 30% of the TBO detections are in one independent time window. FAs on the order of 5–15%, can reach up to 50% on the rise (Fig. 21). The same large FAs on the rise were previously reported by Strohmayer et al. (1998). The FAs that we find broadly coincide with the values reported in Ootes et al. (2017), Galloway et al. (2008), and Miller (2000).

In addition to TBO candidates, we detect a few low-frequency candidates and a large, but insignificant number of noise candidates (p=1). Miller (1999) reported a significant signal at 290 Hz from the sum of 0.75-s intervals on the rise of five bursts. None of our noise candidates were close to 290 Hz.

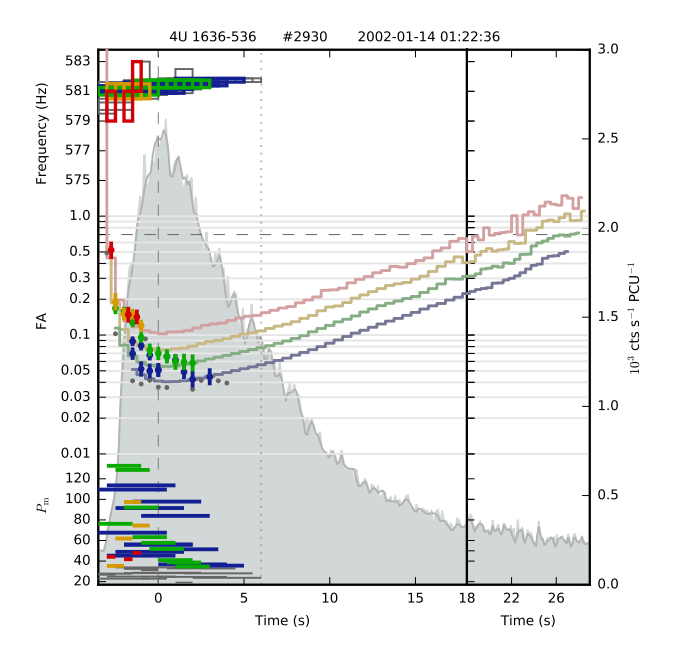


Figure 21. Example of a burst from 4U 1636-536 with a high-FA candidate on the burst rise.

### B.1.4. MXB 1658-298 (X 1658-298)

TBOs at 567 Hz were discovered by Wijnands et al. (2001), who detected them in six bursts out of 14 observed. The TBOs had small (0.5–1 Hz) frequency drift and FAs on the order of 10%. A larger sample of bursts was later explored by Galloway et al. (2008).

Our sample yielded 26 bursts, four of them with TBO candidates in the 566.75–567.25 Hz frequency range. The candidates are rather weak, with peak powers of 35–45, in one independent time window per burst. Some of them occur on the rise, some a few seconds after the burst peak. Formally, two TBOs are labeled as coming from the tail region, but those bursts had a sharp intensity drop, so that the B region was narrow. FAs on the order of 10% are broadly consistent with the values reported in Wijnands et al. (2001) and Galloway et al. (2008) for all bursts except for burst #2519. There, we have FAs 3 times smaller (consistent with Wijnands et al. (2001)).

Interestingly, there is a discrepancy in burst detections. Galloway et al. (2008) does not confirm one burst with a detection reported in Wijnands et al. (2001), but has one more burst with a detection from 2001. We do not have any noticeable sub-threshold candidates in three of the bursts with detections reported in these two papers.  $FA_{\rm up}$  are similar to or even lower than the reported detections.

The standard threshold does not yield any low-frequency candidates. A small number of noise candidates is not statistically significant.

Wijnands et al. (2001) reported a burst (#2519) with oscillations reappearing at a frequency larger by about

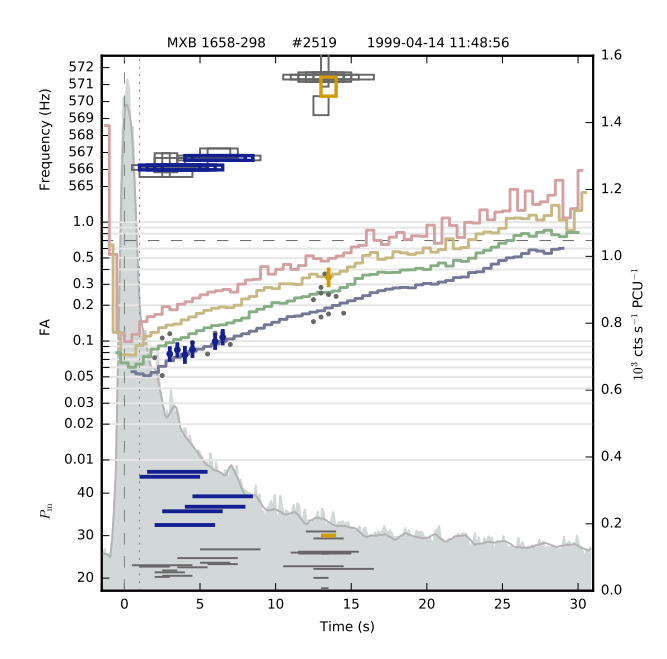


Figure 22. The burst with a TBO frequency step reported in Wijnands et al. (2001). On this figure the tail panel was merged with the burst panel to keep the time scale uniform. The threshold probability was increased by a factor of 3.7 for this plot; otherwise the candidate around 571 Hz lies below the selection threshold. This candidate is detected in one independent time window and may be a fortuitous noise spike or glimmer, not connected to TBOs earlier in the burst.

5 Hz (571.5 Hz), with similar signal strength (maximum  $P_{\rm m}=32$  for 2-s sliding windows with 0.25-s offset using the  $Z^2$  statistic). This candidate does not exceed our detection threshold (corresponding to  $P_{\rm m}=33.62$  for 2-s windows), however we do detect a bunch of subthreshold candidates in the same region. The candidate with the smallest probability has  $P_{\rm m}=30$  in 1-s window at 571 Hz (30.2 on non-normalized data). It is definitely not as strong as the TBOs earlier in the burst (Fig. 22). The discrepancy between our values and those of Wijnands et al. (2001) can be readily explained by the different choice of FFT windows and using FFT vs.  $Z^2$ .

None of the remaining bursts yielded candidates within the 10 Hz region of the TBO frequency range. It is hard to tell whether the 571-Hz candidate is related to TBOs. Two outcomes are possible: a) it is a TBO, as is stated in Wijnands et al. (2001); b) it is a glimmer candidate. Wijnands et al. (2001) estimate its significance taking into account only trials in the 10-Hz frequency region around the TBOs. However, it is unclear whether this is a correct choice, since this region was picked after the candidate was found on a broader search from 100 to 1200 Hz. Our analysis with the probability threshold multiplied by a factor of 3.7 yields nine more candidates, eight of them below 1000 Hz and one above. Some of these candidates are stronger than the

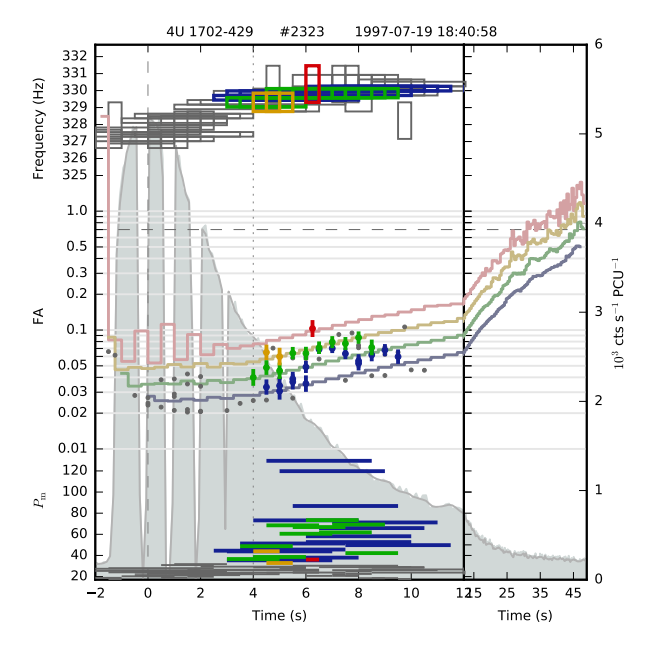


Figure 23. Example of a burst from 4U 1702-429 with multiple sub-threshold candidates.

571-Hz one. The simulated data does not have, on average this many candidates: only one simulation run had as many as 10 candidates (p=0.01). Thus, it is possible that MXB 1658–298 has glimmer candidates, and the peak at 571-Hz is one of them. It is also worth noting that this candidate has a softer spectrum than the TBOs earlier in the burst Wijnands et al. (2001).

The most solid way to prove that step candidate is a TBO would be to detect it once again at the same frequency preferably with larger power.

Oscillations around 329 Hz were discovered by Markwardt et al. (1999) in 5 out of 6 bursts observed at the time. The TBO frequency was gradually increasing during all bursts, and the reported FAs ranged from a few % up to 18%,

Our sample contains 50 bursts from this source, some of them with gaps and noise power as low as 1.8. Among these, 32 yielded TBO signals at  $326.00-330.5\,\mathrm{Hz}$  in the R and B regions.

FA of approximately 3–15% broadly match the valued reported by Ootes et al. (2017) and Galloway et al. (2008). Some of the bursts have detections in one independent window, with or without multiple sub-threshold detections in independent windows. There are also many sub-threshold detections from bursts with strong TBOs (e.g. Fig. 23). We see large gradual frequency rises; however some of this frequency evolution may be biased by the rapid variation of the count rate during the burst rise or gaps.

In addition to TBOs, our burst sample yielded some type I low-frequency candidates at 2–3 Hz due to the

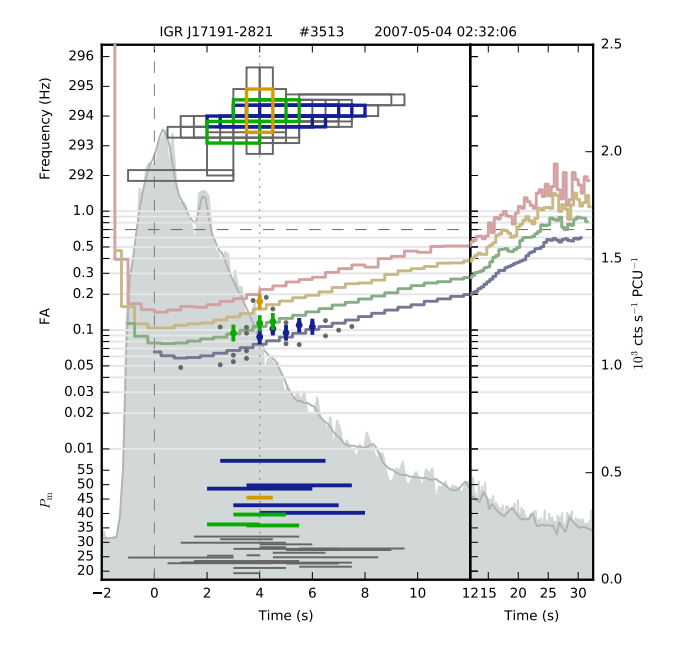


**Figure 24.** An example of TBOs from IGR J17191–282 with their typical large and gradual frequency evolution.

unmodeled spikes on the rise of several bursts, and statistically insignificant number of noise candidates.

### B.1.6. IGR J17191-2821

TBOs at 294 Hz were discovered by Altamirano et al. (2010b) in three bursts out of five observed (one of them showed significant oscillations only in part of the energy band). Two bursts exhibited a large gradual frequency drift, 2–3 Hz over about 10 s. The authors reported 5–10% rms amplitude in the 2–17 keV energy range.

Our sample consists of the same bursts as in Altamirano et al. (2010b). We detect TBOs in two bursts at the same frequency in the B region. The burst with the weakest TBOs from Altamirano et al. (2010b) had sub-threshold candidates in the TBO frequency range. The FAs of the detections are broadly similar to the ones measured by Altamirano et al. (2010b), despite the differences in time window sizes and energy cuts. For burst #3513 (Fig. 24), we do not record TBOs closer to the burst rise, having only one sub-threshold candidate there.

In addition to TBOs, one type I low-frequency candidate was detected.

## B.1.7. 4U 1728-34

TBOs from 4U 1728–34 were discovered by Strohmayer et al. (1996) at 363–364 Hz. The oscillations are characterized by a gradual few-Hz upward frequency drift and FAs as as large as 10%. A larger sample of bursts were subsequently searched for TBOs by van Straaten et al. (2001), Galloway et al. (2008), and Ootes et al. (2017).

Our sample contains 141 bursts from this source. Some of them have data gaps and average noise power

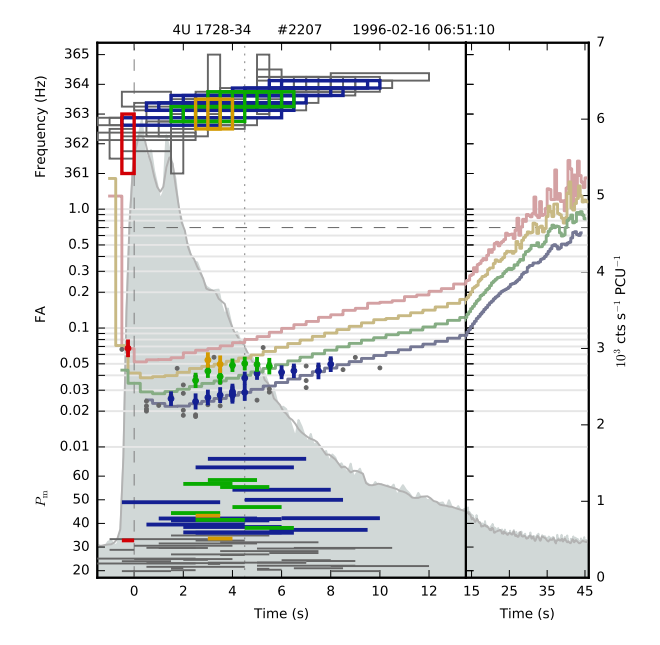


**Figure 25.** Example of TBOs from 4U 1728-34, showing typical gradual frequency drift.

as low as 1.8. Thirty-four bursts yielded TBO candidates in the frequency range of 362–364 Hz. All TBO candidates except one were detected in the R and B regions. The only one from the T region is on its left edge. Some of the bursts show detections in multiple independent time windows with gradual frequency drift over the course of the TBO train (Fig. 25). Sometimes the frequency evolution is biased by data gaps. Some of the bursts have fainter detections in one independent time window, on the rise or in the B region.

FAs of the TBO candidates are broadly comparable to the values reported in Galloway et al. (2008) and Ootes et al. (2017), but are consistently smaller than the ones in van Straaten et al. (2001), by a factor of about 1.5 although the FA evolution throughout the burst is similar. This is explained by the differences in data processing: van Straaten et al. added power from several frequency bins in 4-Hz windows around maximum power.

In addition to TBO candidates, our analysis yielded multiple low-frequency candidates, both type I and type II, and statistically insignificant number of noise candidates.

### B.1.8. KS 1731-260

Oscillations at 523.93 Hz were discovered by Smith et al. (1997) in the single burst observed at the time. Later, Galloway et al. (2008) searched for TBOs in 26 more bursts and found them in three bursts. Ootes et al. (2017), using different window sizes, also found oscillations in six bursts out of 27.

Because of the GTI requirement, our sample consisted of 26 bursts. TBOs were detected in three of them, at frequencies of 523.5–524.25 Hz, all of them right af-

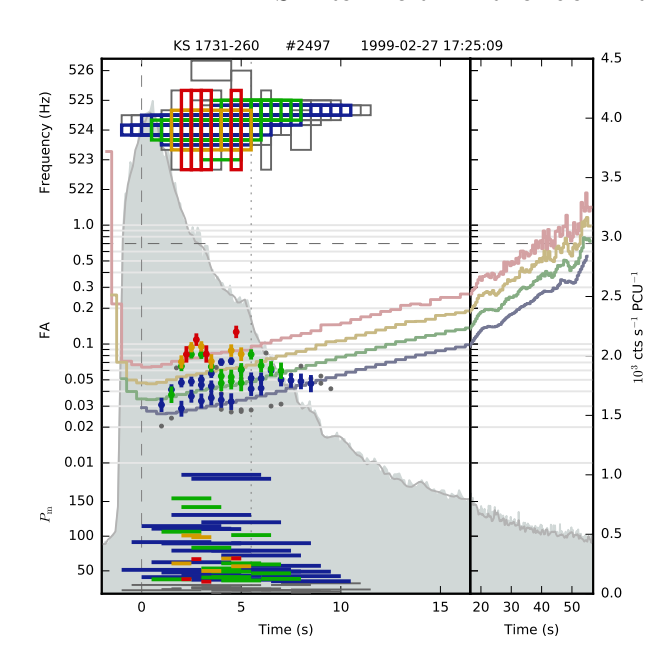


**Figure 26.** The burst with the strongest TBOs from KS 1731–260.

ter the burst peak (e.g. Fig. 26). Two bursts yielded detections in multiple independent time windows, one in a single time window but with more independent sub-threshold candidates on the rise. One more burst had sub-threshold candidates only. FAs of 4–14% are broadly consistent with the values reported by Galloway et al. (2008) and Ootes et al. (2017).

The source yielded also a small, statistically insignificant number of noise candidates.

## B.1.9. GRS 1741.9-2853

Strohmayer et al. (1997a) reported on 589-Hz TBOs in three bursts from GRS 1741.9–2853. The FA of detections were up to 13%, but these were for favorable energy cuts and custom time window intervals. The source was not in outburst again before the end of the RXTE mission. In 2013, Barrière et al. (2015) observed GRS 1741.9–2853 with NuSTAR. Unfortunately, the 2.5-ms dead time of NuSTAR hindered TBO detection. No oscillations were found, with the upper limits from simulations of the injected signals being higher than the detections in Strohmayer et al. (1997a).

Our sample consists of seven bursts. We detected TBO candidates at 589.00–589.75 Hz. For both bursts, the candidates came from the B region, with FA of about 5%, broadly comparable with the values reported in Galloway et al. (2008). In one burst, candidates were detected in two independent time windows, but of different length and not at the same frequency (Fig. 27). The other burst yielded a detection in one independent window and another independent sub-threshold candidate. The third burst with TBOs from Strohmayer et al. (1997a) was not covered by GTI.

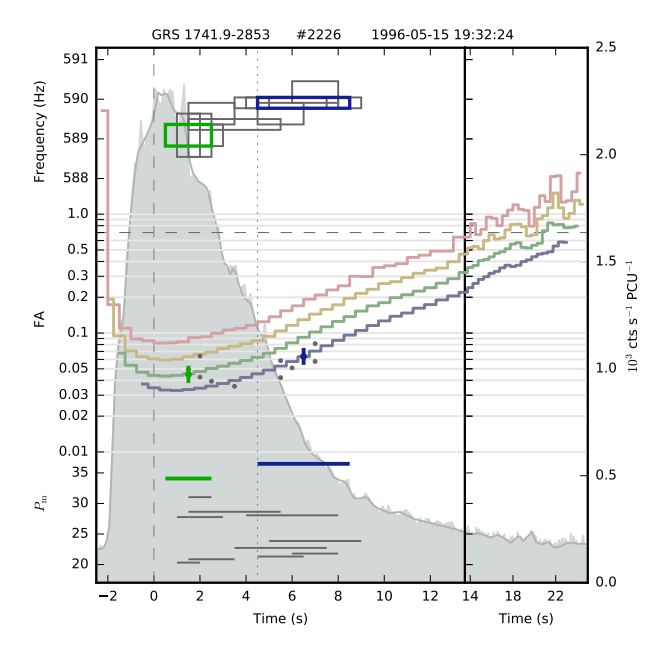


Figure 27. Example of oscillations from a faint TBO source GRS 1741.9-2853.

The candidates aroung 589.5 Hz are not strong, with  $P_{\rm m} < 40$ . All three independent-window candidates come from different frequencies, but the spread is smaller than 1 Hz. For the strongest candidate, 5% of simulations yielded the same or a larger number of candidates with equal or larger  $P_{\rm m}$ . However, selecting all candidates above threshold yields p=0. The fact that the candidates are grouped in frequency speaks in favor of their TBO nature, however a strict estimate of the significance of this grouping is beyond the scope of this paper.

In addition to TBO candidates, GRS 1741.9–2853 has some type II low-frequency candidates in the 2–4 Hz range, and one noise candidate (p=0.3) at 1829.25 Hz.

### B.1.10. IGR J17480-2446

TBOs from an unusually slowly spinning accreting pulsar IGR J17480–2446 were discovered by Cavecchi et al. (2011). Very strong 11-Hz oscillations were detected in one burst, with FAs of 30% and no frequency drift. The remaining 230 bursts explored by Cavecchi et al. (2011) also yielded TBOs in FFT windows from 10 to 300 s, with FAs down to 3%. The search was conducted on barycentered data using the APP ephemeris.

Our sample contained 297 bursts, with median peak S/N of only 6.4. Most of the times for the on-burst windows were set manually and were short, of about 5 s. Our FFT windows are shorter and the upper limits on FA are consequently much larger than in Cavecchi et al. (2011); we find characteristic upper limits on the FA on the order of 70%. Using our analysis procedure, only two bursts had candidates in the range of 10–11 Hz. Similarly to XTE J1814–338 and IGR J17511–3057,

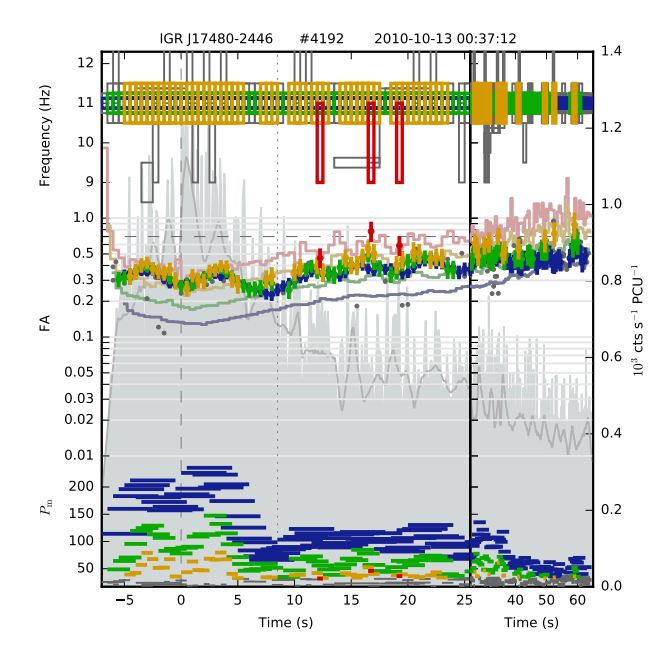


**Figure 28.** A burst with strong TBOs from IGR J17480-2446. The constant frequency and roughly constant FAs make these oscillations similar to the ones from accreting MSPs XTE J1814-338 and IGR J17511-3057, although those pulsars spin an order of magnitude faster.

the range of TBO frequencies reflects the coarseness of the Fourier grid, with detections at  $10\,\mathrm{Hz}$  coming from 0.5-s windows.

One of the bursts (#4192) had strong oscillations throughout the entire on-burst window (Fig. 28), with typical FA of 30%, maximum up to 90%. The average FA on 10–20-s timescales would have matched the one reported in Cavecchi et al. (2011). Another yielded a relatively faint ( $P_{\rm m}\approx 40$ ) detection in a single independent 4-s window (more if one considers sub-threshold candidates), For this burst, calculated FAs of  $\sim 90\%$  are most probably affected by an overestimated pre-burst background level.

Burst #4192 had several low-frequency (2–3 Hz) candidates of type II. Overall, the burst sample yielded a large but statistically insignificant number of noise candidates.

### B.1.11. IGR J17498-2921

IGR J17498-2921 is an accreting MSP with TBOs at 401 Hz discovered by Linares et al. (2011). Chakraborty & Bhattacharyya (2012) analysed 12 bursts from IGR J17498-2921 and detected TBOs from two bursts in averaged 1-s spectra. The PCA field of view contains several other bursters and the ten bursts without oscillations may be from another source, however the authors argue that this is unlikely.

The MINBAR catalogue lists only two bursts from IGR J17498-2921. From both bursts we detected TBOs in the B region, without frequency drift. There were also

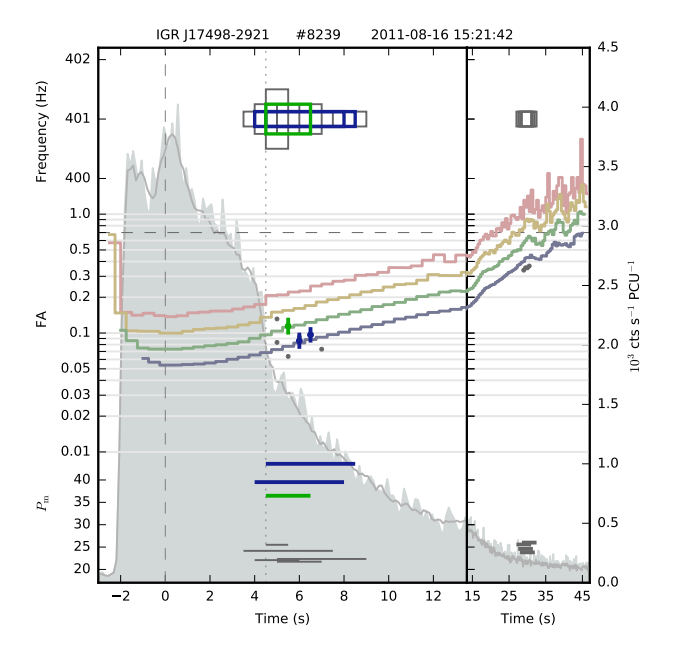


Figure 29. Oscillations from a rather faint TBO source, the accreting millisecond pulsar IGR J17498-2921.

some sub-threshold candidates on the tail. The FAs of 10% were consistent with Chakraborty & Bhattacharyya (2012). One burst had two independent-window detections, the other only one independent detection, but with sub-threshold candidates at the same frequency in the tail (FA of 30%, Fig. 29). In addition to TBOs, only one low-frequency candidate was detected.

### B.1.12. SAX J1750.8-2900

TBOs at 601 Hz were discovered by Kaaret et al. (2002) in one of the four bursts studied. The authors used merged event lists from the event and burst catcher modes, without any energy selection and searched for signal in 4-s windows overlapping by 0.125 s in the frequency range between 200 and 1200 Hz. TBOs were found in both the rise and decay, with a maximum power of 49.3 five seconds after the burst rise. No fractional amplitudes were reported.

We detected TBOs from the same burst in two independent time windows, with similar maximum power, five seconds after the burst rise. Similarly to Kaaret et al. (2002), we record frequency drift and the disappearance of the TBO signal during the burst peak. TBOs on the rise occur in shorter windows and have larger FAs than TBOs right after the burst peak (Fig. 30).

Galloway et al. (2008) found TBOs on the rise of two more bursts. These bursts have only sub-threshold candidates in our analysis, with FA similar to the ones measured by Galloway et al. (2008). The first burst has frequency behavior similar to Burst #2717, whilst TBOs from the second one do not have noticeable frequency drift and also appear at burst peak.

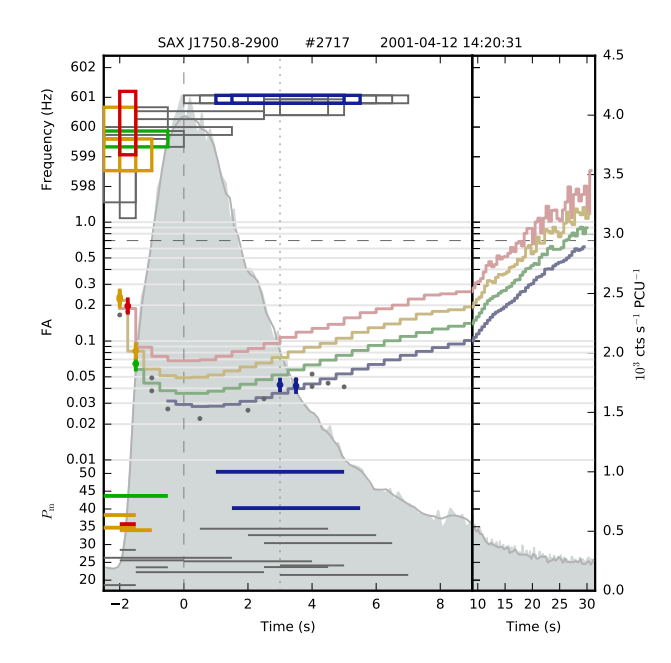


Figure 30. The only burst from SAX J1750.8-2900 with TBOs above the detection threshold.

In 2008, SAX J1750.8—2900 went into outburst again, adding two more bursts to the MINBAR sample. No TBO candidates were recorded from these bursts, even at the sub-threshold level.

For the strongest candidate, none of the simulations have candidates of similar strength. For both candidate groups, before and after the burst peak the peak power was over 40. The highest  $P_{\rm m}$  outside the frequency region around 600 Hz was smaller than 30. Despite the absence of candidates detected in independent time windows at the same frequency, the power of the candidates, the close proximity of their frequencies and the presence of sub-threshold candidates in two more bursts speak in favour of these candidates being TBOs.

No low-frequency or noise candidates were detected from this source.

## B.1.13. IGR J17511-3057

IGR J17511-3057 is an accreting MSP with TBOs at 245 Hz discovered by Altamirano et al. (2010a). Burst oscillations were seen in all bursts in the sample. For fainter bursts, the oscillations are detected earlier in the burst. For brighter bursts, TBOs often disappear at the burst peak. The authors note small (0.1 Hz) frequency drift on the rise and report FAs of 5-12%, with FAs on the tail larger than on the rise and peak.

The MINBAR database lists 9 bursts for this source, all of them with TBOs in the same regions as in Altamirano et al. (2010a). One of the bursts has TBOs in one independent time window only. We do not observe any frequency drift on the rise, although our Fourier frequency resolution is rather coarse. Similarly to XTE

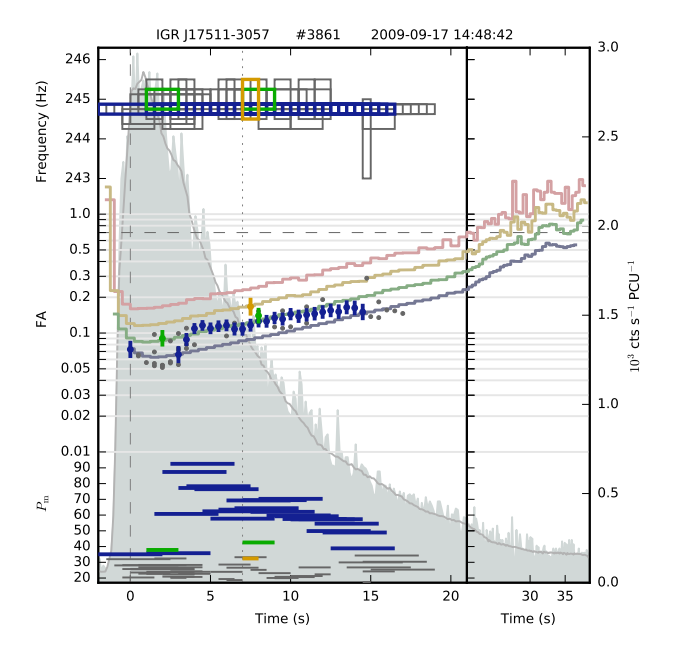


Figure 31. An example of TBOs from IGR J17511-3057, showing the main features of its TBOs: constant frequency and dip in FAs during the burst peak.

J1814-338, the frequency range of the detections reflects the coarseness of the Fourier frequency grid.

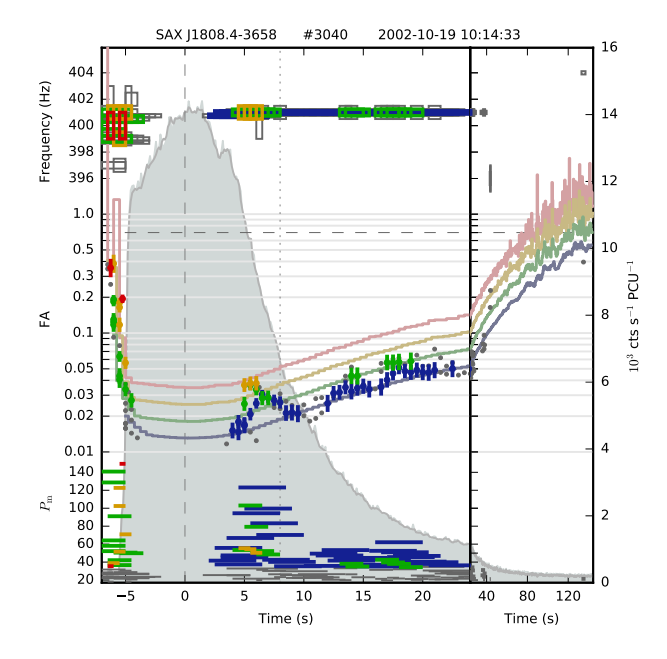
Like Altamirano et al. (2010a), we note a dip in FAs during burst peaks (Fig. 31), although in a smaller number of bursts than they do. Our FAs are also consistent with Altamirano et al. (2010a).

No low-frequency or noise candidates were detected from this source.

### B.1.14. SAX J1808.4-3658

SAX J1808.4—3658 is an accreting MSP with APPs and TBOs at 401 Hz (Wijnands & van der Klis 1998; Chakrabarty et al. 2003).

Minbar catalogue lists 9 Type I bursts, three of which have not been analysed for TBO behaviour before. We find TBOs in seven bursts. The source is very bright and some observing sessions suffer from data gaps. Typical behavior is as follows: TBOs start at the burst onset and rapidly drift in frequency up or down by a few Hz within a single FFT window of 0.5–1s (the amount of perceived drift may be biased by frequency covariance). The FAs on the rise are on order of 10–40%. Oscillations disappear during the burst peak, even accounting for the dead time which lowers the noise power to 1.6. Then oscillations reappear at frequencies slightly higher or lower and are fairly stable in frequency with wave-like variations of FAs, which at the same time increase slightly on the tail. The FAs after burst rise are on the order of few %. One burst did not show oscillations on the rise, another had only sub-threshold candidates on the rise. Such TBO properties are consistent with ones reported



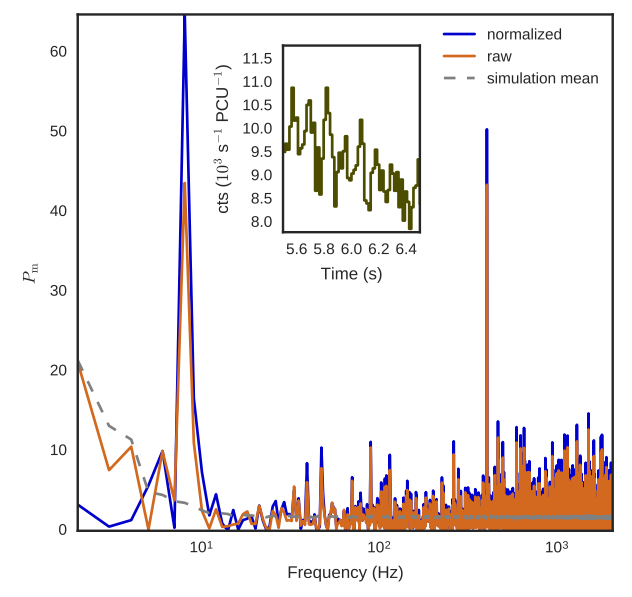


**Figure 32.** Top: TBOs from J1808.4–3658, showing rapid frequency drift at burst onset, disappearance at burst peak and stable frequency at the burst tail. Bottom: 1-D power spectrum in 1-s windows starting  $\sim 5.5 \, \mathrm{s}$  after burst peak in the same burst. In addition to the TBO, a strong glimmer candidate is evident at 8 Hz. The inset shows the LC in the same 1-s window. The oscillation with 8 periods per second is visible. The consistent offset between the normalized and raw PS is due to the large influence of dead time.

previously (Chakrabarty et al. 2003; Bhattacharyya & Strohmayer 2006, 2007; Galloway et al. 2008)

One of the bursts has type II low-frequency noise, a strong TBO, and a peculiar low-frequency glimmer candidate at 8 Hz, with peak power exceeding 60 (Fig. 32).

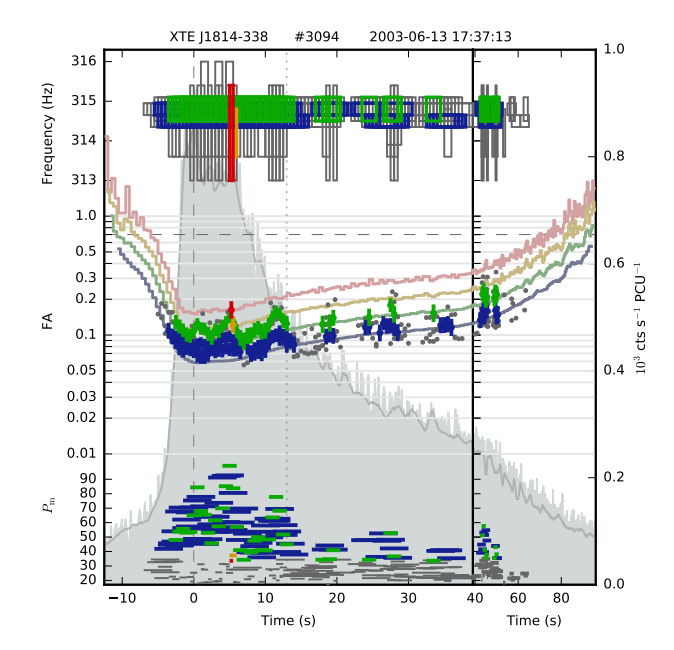


Figure 33. An example of TBOs from XTE J1814–338, showing the common features of its TBOs: constant frequency, presence throughout the tail, large-scale FA constancy and small-scale wave-like variations in FAs.

Note that the standard detection threshold yields p=0.22, however the power of glimmer candidate is much larger than any power in simulated datasets. The oscillation profile folded with 8-Hz frequency has a sinusoidal shape.

### B.1.15. XTE J1814-338

The accreting millisecond pulsar XTE J1814–338 is one of the best studied TBO sources (Strohmayer et al. 2003; Watts et al. 2005; Watts & Strohmayer 2006; Watts et al. 2008). Our sample consisted of 28 bursts, all of which have been studied before. We detect TBOs with power above the threshold in 26 bursts. The two remaining bursts did not have GTI coverage during the burst rise and peak, but had weak sub-threshold candidates during the tail.

The oscillation frequency (314 Hz) does not change by more than the Fourier frequency resolution during the burst; the apparent frequency range in Table 4 reflects the coarseness of the Fourier frequency grid.

The oscillations do not disappear during the burst peak and are often present in the burst tail. There are also many sub-threshold candidates. FAs tend to be roughly constant throughout the duration of the oscillation, until it disappears under the rising  $FA_{up}$  (Fig. 33). On top of the constant level, there are e vident wave-like variations of FAs. In general, our measurements of FAs of  $\sim 10\%$  are broadly consistent with Galloway et al. (2008); Watts et al. (2008).

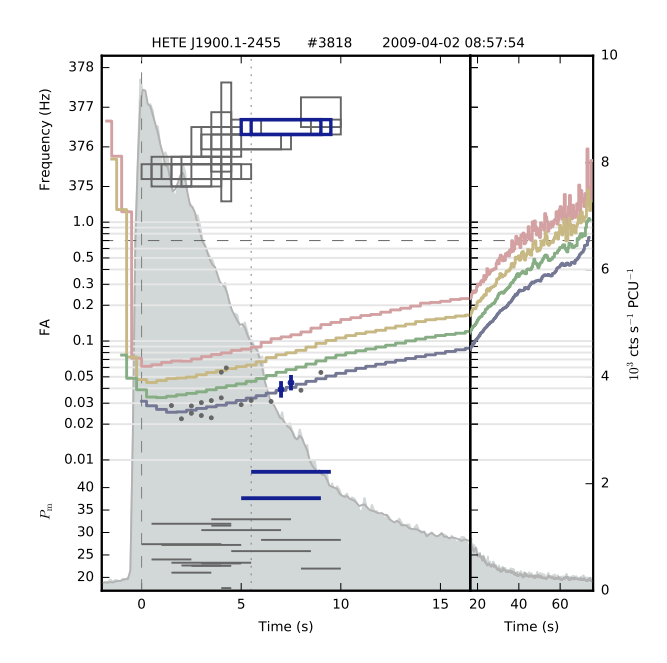


**Figure 34.** The only known burst with oscillations from the accreting MSP HETE J1900.1–2455. This candidate would not be significant by our blind (broad frequency range) search.

### B.1.16. HETE J1900.1-2455

HETE J1900.1–2455 is an accreting MSP with spin frequency of  $\sim 377\,\mathrm{Hz}$  (Patruno 2012). TBOs in a single burst were discovered by by Watts et al. (2009). The authors detected significant signal in four consecutive independent 2-s windows for 2–30 keV photons. The reported FAs were 3.5% in the same energy range.

Our sample consisted of 8 bursts, one of them with data gaps. The bursts are quite bright and during the peak the mean noise power drops to 1.7. Despite accounting for the influence of dead time, our search did not result in any new TBO detections – relatively faint TBO candidates were detected at 376.25 Hz only in the same burst as in Watts et al. (2009). Only one independent time window yielded  $P_{\rm m}$  above the detection threshold (Fig. 34), although sub-threshold candidates extend longer both in time and the frequency maps the same frequency evolution as in Watts et al. (2009). The FA was 4.5%, comparable to the value in Watts et al. (2009), noting that we have made different choices of windows and energy ranges.

HETE J1900.1–2455 is a good illustration of the advantages of using external information to narrow down the frequency range searched. TBOs at  $376.25\,\mathrm{Hz}$  would have been deemed insignificant by our broad frequency range analysis – 3% of our simulation runs had at least one candidate with probability equal to or smaller than the probability of the TBO candidate.

The source also has some low-frequency noise and an insignificant number of noise candidates.

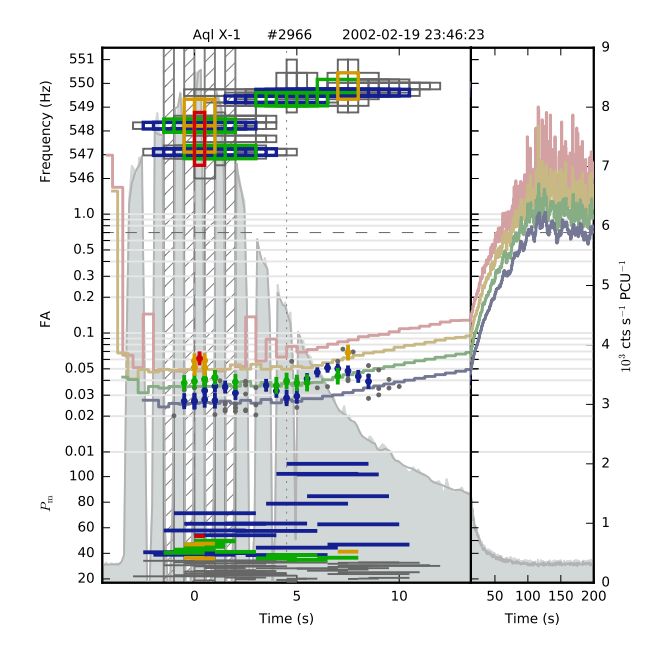


**Figure 35.** Example of a burst from Aql X-1, with data gaps distorting the observed TBO frequency evolution.

## B.1.17. Aql X-1

TBOs at 549 Hz were discovered by Zhang et al. (1998) in RXTE Burst Catcher data. Later, Casella et al. (2008) reported on strong ( $P_{\rm m}=120$ ) APPs at 550.27 Hz in a single 150-s time window which was not close to any burst.

Our sample consisted of 73 bursts, about half of them suffering from data gaps (e.g. Fig. 35). Noise power at the burst peak often drops to as low as 1.7. TBOs were detected in 8 bursts in the R and B regions in the frequency range  $547.4–550\,\mathrm{Hz}$ .

For several bursts, TBOs were detected in one independent window only. For brighter TBOs, there is a hint of a gradual frequency drift ( $\sim 1\,\mathrm{Hz}$  over few seconds), although gaps in the data have a large adverse effect on the observed frequencies. FAs of TBOs are on the order of 4–7%, broadly consistent with the values reported in Zhang et al. (1998), Galloway et al. (2008) and Ootes et al. (2017).

In addition to TBO candidates, we detected multiple low-frequency candidates at 2–6 Hz and an insignificant number of noise candidates.

# B.2. Individual sources with tentative TBO detections reported by previous papers

In this Section we discuss sources for which TBO detections have been claimed, or tentatively claimed, by previous works and which were classified as tentative in the review article by Watts (2012). There are 8 sources in this category: 4U 0614+09, 4U 1254-69 (XB 1254-690), MXB 1730-335 (Rapid Burster), XTE

J1739-285, 1A 1744-361, SAX J1748.9-2021, GS 1826-24 and XB 1916-053 (X 1916-53, 4U 1916-053).

### B.2.1. 4U 0614+09

Strohmayer et al. (2008) found a 415-Hz signal in a 10-s window in the tail of one of the two bursts in their sample. The bursts were detected in 2006 and 2007 with Swift Burst Alert Telescope (BAT). The oscillations had FAs of 12.3% and occurred in the 13–20 keV energy range, in one of the 10-s windows. The signal has  $4\sigma$  significance assuming a conservative number of trials.

The RXTE sample consists of only one burst, different to those observed by Strohmayer et al. (2008). The burst was extremely bright, resulting in the telemetry rate being heavily saturated, which caused large data gaps. The burst started with a very bright sub-second spike, followed by a gap, which is an indication of PRE. This spike was not included in the on-burst window although it is part of the real burst rise. Our LC modeling did not reproduce a short gap at about 4s from the burst start, thus all candidates from the time windows covering that moment were discarded. We detected no candidates above the specified threshold. Our count rates imply much stronger upper limits on FA, around 2%.

Our non-detection does not challenge the TBO claim of Strohmayer et al. (2008), since even sources with strong TBO records have bursts that are apparently devoid of oscillations. However, it remains the case that TBOs were detected essentially only in one independent time window, from one burst. Detecting the oscillations at similar frequencies from more bursts would strengthen the conclusion.

## B.2.2. 4U 1254-69 (XB 1254-690)

Bhattacharyya (2007) reported on a tentative 95 Hz candidate from the rising phase of one of the five bursts recorded. The  $P_{\rm m}=24.3$  TBO candidate was found in the first 1-s interval after the burst start and had FA of  $0.31\pm0.07$ . The signal was confined to a 1 s time window and no significant frequency evolution was found, according to the authors. The significance was estimated to be 95%, considering the number of harmonics and windows searched.

We have two more bursts compared to Bhattacharyya (2007). Using our formal detection criterion, our analysis did not yield any candidates in the same data. However we did confirm similar powers ( $P_{\rm m}$  of about 25.5) at the same frequency of 95 Hz. The sub-threshold candidates at this frequency are strongest in 1-s windows; there are less significant sub-threshold candidates at other window sizes, but not in independent windows. The FA of the maximum-power signal is similar to the one in Bhattacharyya (2007).

Lowering the detection threshold to 25.43 on 1 s window and correspondingly at other windows (multiplying the threshold probability by a factor of 30), we get

five additional noise candidates (p=0.3), both below and above 1000 Hz, all in the bursts analysed by Bhattacharyya (2007). Bhattacharyya (2007) did not find any significant oscillations in other bursts up to 2048 Hz, however our data suggest otherwise. This may be explained by differences in the choice of windows and oversampling factor.

Some of our sub-threshold candidates also occur in 1-s time windows and are stronger than the power reported by Bhattacharyya (2007). We conclude there is not enough evidence to classify the 95-Hz oscillation candidate as TBO and not as a noise candidate.

### B.2.3. MXB 1730-335 (Rapid Burster)

Fox et al. (2001) described a tentative 306.5 Hz TBO candidate in the sum of spectra from the rising part of 31 bursts, with 1.8% of it being a chance detections according to their simulations. According to the authors, various tweaks to the data selection parameters affected the detection significance in different ways. The candidate was not detected in single bursts, and was not confirmed in two subsequent outbursts.

Our sample consists of 57 bursts, some of them with data gaps. We did not detect any candidates at frequencies close to 306.5 Hz. The source yielded some type II low-frequency candidates within 2–6 Hz, and a large, but not significant number of noise candidates (p=0.16). One of the candidates (at 18.25 Hz) is quite strong, with  $P_{\rm m}=46.5$  (Fig. 14). This candidate has a power of 44.52 on non-normalized data. Only 2% of simulation runs have one or more candidates of the same or larger significance.

### B.2.4. XTE J1739-285

A tentative sub-ms oscillation from XTE J1739–285 was found by Kaaret et al. (2007). The authors reported a 1122-Hz candidate in one of the six bursts examined. The authors used a different energy cut for PCU0 compared to the other PCUs in order to to minimize background, since PCU0 had recently lost its propane layer. Kaaret et al. used 4-s FFTs with a 0.125-s step. The maximum candidate power was 42. The significance of the candidate (equivalent to 3.97 $\sigma$  of normal distribution) was estimated with simulations based on LC modeling, taking into account dead time. The candidate was not confirmed by Galloway et al. (2008), who used nonoverlapping 4-s windows and potentially different energy cuts.

Our sample had the same bursts as in Kaaret et al. (2007) and Galloway et al. (2008). We do not find any candidates from this source, having, on average 0.29 candidates from our simulation runs.

The maximum power from the burst in Kaaret et al. (2007) is 29.5 in a 4-s window at the same frequency in a similar place during the burst tail. Increasing the detection threshold probability by a factor of 16.5 to

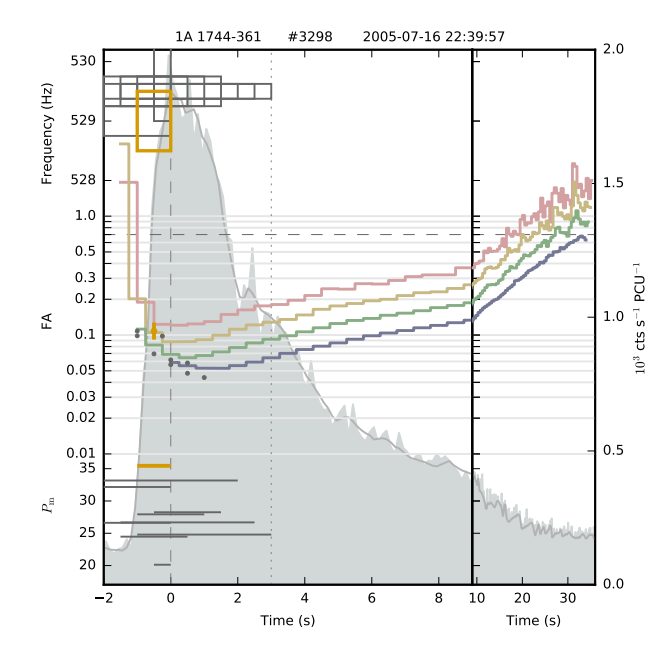


**Figure 36.** A TBO candidate from 1A 1744–361, previously reported by Bhattacharyya et al. (2006). The short duration, moderate power, but at the same time potential frequency drift make it hard to classify this candidate either as noise or a TBO.

match  $P_{\rm m}=29.5$  (29.9 on non-normalized data) in 4-s windows yielded 5 additional candidates (p=0.6), some of which were more significant than the 1122-Hz one. Thus, in our analysis there is not enough evidence to classify the 1122-Hz candidate as a TBO and not a noise candidate.

The tentative detection of Kaaret et al. (2007) presents an interesting case since it is rather strong, its significance was established using simulations but it was not confirmed using different energy cuts and window overlap. It may be possible that the custom energy cuts Kaaret et al. (2007) were more sensitive to potential oscillations. However, it also may be the case that their noise model was not entirely correct (no analysis of model applicability was given) or that the detection is not related to TBOs (e.g. a glimmer candidate).

Detection of the 1122-Hz signal in more bursts in the future would serve as the strongest corroboration of its TBO nature. It is also worth re-examining the existing RXTE data, investigating the influence of energy cuts on the 1122-Hz candidate's power and the distribution of  $P_{\rm m}$  in general.

## B.2.5. 1A 1744-361

A burst oscillation candidate was found by Bhattacharyya et al. (2006) in the single burst observed by RXTE. The signal appeared at  $\sim 529\,\mathrm{Hz}$  in the rise of burst # 3298. Splitting the peak into 4-s power spectra, and using a  $Z^2$  spectrum, indicated a small (< 0.5 Hz) step in frequency. The highest rms FAs were 10.3% in

the > 3 keV band and 15% for > 8 keV. The candidate was also found by Galloway et al. (2008), who reported FA of  $11.3\pm1.8\%$ .

Our analysis on a sample of three bursts yielded exactly one candidate, matching the one from Bhattacharyya et al. (2006). The candidate was at 529 Hz, with  $P_{\rm d}=35.4$  (34.24 on non-normalized data) in one 1-s window (Fig. 36). There are also sub-threshold candidates with different FFT windows. The sub-threshold detections are somewhat later and higher in frequency, but none of them occurs in an independent time window. The associated FA is similar to that reported previously:  $11\pm2\%$ . Our sample contains two more bursts compared to the previous analysis. The additional bursts are a factor of a few fainter, and the upper limits on FA are about three times larger than the FA of detection.

For the simulation runs, 10% of them have one or more candidates above the detection threshold. For the higher threshold corresponding to P=35 in 1-s windows, only 1% of simulations had one or more candidate.

Based on the power alone, the 529-Hz candidate is not strong enough to classify as a TBO in our analysis. However, the presence of sub-threshold candidates hinting at frequency drift makes this candidate interesting. A definitive answer requires the detection of candidates at similar frequencies from future bursts.

### B.2.6. SAX J1748.9-2021

Kaaret et al. (2003) reported on a  $P_{\rm m}=38.7~{\rm TBO}$ candidate at 409.7 Hz in one of the 15 bursts observed. The authors used merged photon TOA lists from event and burst catcher modes and computed FFTs in 3-s successive time windows with 0.25-s steps. The oscillations lasted for about 4s and did not show any obvious frequency evolution. The significance of the detection was estimated to be equivalent to  $4.4\sigma$  of the normal distribution, however the number of time windows searched was not taken into account. Later, Altamirano et al. (2008) found intermittent APPs at 442.36 Hz in the persistent emission, with Leahy-normalized power as large as 100 with favorable data selection. The authors repeated the analysis of Kaaret et al. (2003), but without window overlap. Taking into account the number of time windows searched, the significance of the 409.7-Hz candidate dropped to  $\leq 2.5\sigma$ .

Our sample consisted of 29 bursts from the 2001 and 2010 outbursts. One low-frequency and two noise candidates were detected, none of them close to 409 or 442 Hz. For the same burst as Kaaret et al. (2003), we detected at 409.75 Hz a maximum power of 33.2 in a 4-s window.

Multiplying the detection probability by a factor of 2.5 to match  $P_{\rm m}=33.2$  in 4-s windows yielded two more candidates, some of which were more significant than the 409.75-Hz one. About half of the simulation runs have the same or a larger number of candidates.

The weakness of 409.7-Hz candidate, and, more importantly the detection of a strong pulsation signal at a

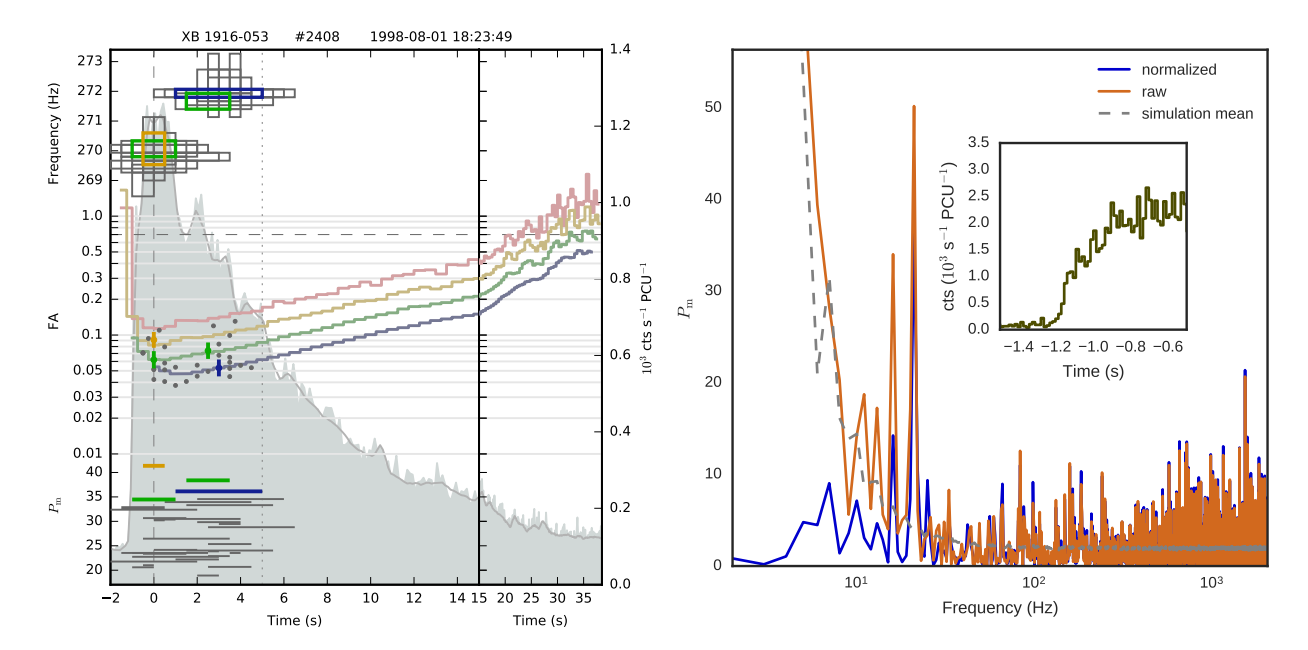


**Figure 37.** Left: TBO candidate from XB 1916–053, previously reported by Galloway et al. (2001). Right: 1D PS spectrum featuring a strong 21-Hz candidate during the rise of another burst. After renormalization, the signal power drops from 50.19 to 37.28.

distinct frequency by Altamirano et al. (2008) leads us to conclude that the candidate reported by Kaaret et al. (2003) was a spurious detection.

### B.2.7. GS 1826-24

Thompson et al. (2005) reported on a 4.7-sigma detection of 611-Hz oscillations in the summed spectra of three burst tails during their simultaneous observations with Chandra. The authors searched for oscillations in FFT windows of several sizes and used different energy cuts. The signal was detected in part of the RXTE energy band, in 0.25 time windows.

Our sample contained 77 bursts which are rather long (2 min on average). Some of bursts were not covered by GTI or suffered from data gaps. Our analysis yielded several type II low-frequency candidates during the burst tails and a large, but not significant (p=0.63) number of noise candidates, none of them around 611 Hz.

### B.2.8. XB 1916-053 (X 1916-53, 4U 1916-053)

Galloway et al. (2001) searched for TBOs in six bursts from XB 1916–053. The search was carried out in power spectra made from 0.5-s sliding windows overlapping by 0.25 s. Power spectra were oversampled in frequency by a factor of 8. The authors reported TBOs at 269.4 Hz with a single-trial significance equivalent to  $4.6\sigma$  of normal distribution; the significance accounting for the number of time windows searched and frequency oversampling was not given. After its onset, the signal becomes weaker and drifts in frequency by about  $1.5 \, \text{Hz}$  over the next second, then disappears and reappears  $\sim 1 \, \text{s}$  later about  $0.5 \, \text{Hz}$  higher, with the first 0.25-s

window yielding two peaks 3 Hz apart. Galloway et al. (2008) did not find any additional TBO candidates from the same frequency range on a larger sample of bursts.

The MINBAR catalogue lists 14 bursts from XB 1916-053 which were suitable for our analysis. Like Galloway et al., we detect candidates at  $\sim 271\,\mathrm{Hz}$  in burst #2408. The candidates appear in two independent time windows, of different size and separated by 1.75 Hz (see Fig. 37, left). Overall, we record 11 candidates above the adopted threshold, at frequencies between 6.5 and 1588 Hz. Six of them come from the independent time windows. For the strongest candidate, the one in 2-s window at 270 Hz, 2\% of the simulation runs had the same or larger number of candidates of at least the same power. Adjusting the power threshold to match the power of second (third and so on) candidate results in p=0. Five out of 11 candidates have frequencies not higher than 21 Hz and their  $P_{\rm m}$  changed substantially after renormalization due to large mean values of Fourier coefficients (see Fig. 37, right). One of these five candidates is stronger than the one at 271.5 Hz.

The highest-power candidate alone is marginally significant on our analysis. The presence of another candidate close in frequency and time makes its TBO nature more likely, however the quantitative estimate of it is beyond the scope of this work.

### B.3. Sources without previously detected TBOs

## B.3.1. Unremarkable sources

The following twelve sources yielded no TBO candidates in our analysis: 4U 2129+12, Cir X-1, GRS 1747-312, KS 1741-293, SLX 1735-269, SAX J1747.0-2853,

XB 1832–330, XTE J1709–267, XTE J1739–285, XTE J1810–189, GX 3+1, and SAX J1806.5–2215. All of these sources had < 30 bursts with total burst duration of < 15 min per source. The median peak S/N of the bursts differed by two orders of magnitude, from 8 to 580, and the median upper limits on FAs in 1-s time windows at the burst peaks (hereafter, *characteristic* FA<sub>up</sub>) were anywhere from 5% to 81%. The average number of candidates from simulated bursts ranged from 0.02 to 1.1. Of these sources, GX 3+1 and SAX J1806.5–2215 each had type I low-frequency candidates in one burst.

2S 0918–549, 4U 0513–40, IGR J17597–2201, and Ser X-1 also had a relatively small number of bursts (< 20), with parameters comparable to the previous groups and a similar  $\sim 1$  average number of simulated candidates per source. These sources yielded some type I low-frequency candidates and one or two noise candidates. A significant fraction of simulation runs (p=0.16–0.5) had the same or a larger number of candidates. All noise candidates from real data had powers relatively close to the selection thresholds.

The following group of sources yielded type II low-frequency candidates at frequencies of 2–4 Hz: 4U 0836–429, 4U 1323–62, and 4U 1705–44. Those sources had longer total observing bursting durations (18–70 min), moderate median peak S/N ratios ( $\sim 50$ ) and characteristic FA<sub>up</sub> of about 10%. Several noise candidates recorded had a large chance of being due to random noise fluctuations, with p ranging from 0.4 to 0.8.

1A 1742–294, XTE J1701–462, 4U 1735–444, 4U 1746–37, and XTE J2123–058 yielded a small number of noise candidates each and no low-frequency candidates. The number of bursts, total duration, median peak S/N and characteristic FA varied by a factor of few within this group, however for all sources the large fraction of simulated bursts (p of 0.13–0.83) had the same or a larger number of noise candidates. A negative result from TBO searches from 4U 1746–37 was reported previously in Ootes et al. (2017).

GX 17+1 had unusually long bursts (average duration 4.5 min). Six candidates were detected with p=0.7. About two thirds of our sample was previously examined by Kuulkers et al. (2002): who did not find any signal beyond  $P_{\rm m}=42.8$  in time windows of 0.25 and 2 s, For all bursts in the sample, the maximum power above 10 Hz did not exceed 37.5.

# B.3.2. Sources with somewhat larger number of noise or low-frequency candidates

The relatively faint sources XTE J1710-281 and SLX 1744-300 had a marginally significant number of noise candidates per source (p of 0.02 and 0.01, respectively). None of the candidates were particularly strong, and their frequencies were scattered between

20 and 1980 MHz. No low-frequency candidates were recorded.

A stronger source, 4U 1722-30, yielded a rather strong single candidate. The candidate was recorded at 22 Hz at burst peak in a 0.5-s time window covering a small dip in the LC. This dip was well modeled and had no low-frequency type I candidates assosiated with it. The candidate had a power of 36.49, with an unnormalized power of 33.59. Only 1 out of 100 simulations yielded 1 or more candidates with the same or larger power. A similarly strong candidate coming from a 1-s time window with a data gap was recorded from 4U 1820-303 at 280 MHz. The candidate had  $P_{\rm m} = 39.7$  (34.69 in unnormalized data) and p = 0.02. It is worth mentioning that NICER has observed PRE bursts from this source recently, and no oscillations have been detected (Keek et al. 2018). Overall, although these candidates are rather strong, their power depends greatly on proper LC modeling.

Two other faint sources, EXO 1745–248 and Cyg X-2 had remarkably numerous and strong low-frequency candidates (type II). For EXO 1745–248, these candidates were recorded within most of the on-burst windows at multiple frequencies between 2 and 12 Hz. Sometimes the candidates were grouped in time, similarly to IGR J17473–2721. Only one noise candidate (p=0.4) was detected from this source, at 14.5 Hz, with multiple low-frequency candidates from the same time windows at 2–8 Hz.

The low-frequency candidates from Cyg X-2 exhibited various behavior: during some bursts they were confined to a single frequency, during others they were spread chaotically within  $2-12\,\mathrm{Hz}$  or occurred at two separate frequencies (e.g. 3 and  $9\,\mathrm{Hz}$ ). Few glimmer candidates were recorded, with p=0.01.

## B.3.3. IGR J17473-2721: an interesting pair of candidates

IGR J17473–2721 generated an interesting pair of candidates at 602 and 605 Hz occurring few seconds apart in the same burst (Fig. 38). The first candidate came from a 0.5-s window on the burst rise, had  $P_{\rm m}=31.3$  (29.3 on non-normalized data), and FA of 13%. The second candidate came from a 1-s window right after the burst peak and had  $P_{\rm m}$  of 36.8 (33.8 on non-normalized data) and FA of 4%. The other 43 bursts did not have any candidates at similar frequencies.

The moderate power (more than half of simulations had the same or larger number of candidates of at least the same significance) and the lack of detections in multiple time windows or bursts do not allow us to classify these candidates as TBOs, however the other properties (candidates framing burst peak for the PRE burst, second candidate being few-Hz higher than the first one) are similar to confirmed TBOs (cf. e.g. SAX J1750.8–2900).

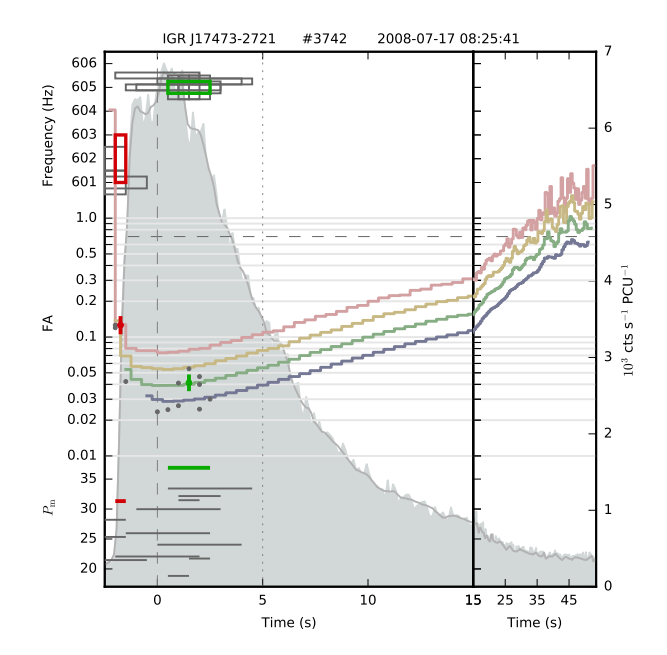


Figure 38. An interesting pair of oscillation candidates from IGR J17473-2721. The candidates are rather faint and not significant based on their power alone. However, the occurrence within the burst (marked as PRE in the MINBAR catalogue) and frequency separation resemble typical TBO behavior.

IGR J17473-2721 also had many low-frequency candidates at frequencies of  $2-6.25\,\mathrm{Hz}$ . Sometimes low-frequency candidates were spread uniformly throughout an on-burst window, sometimes they formed distinct groups.

### B.3.4. SAX J1810.8-269: new TBO source

The MINBAR catalogue lists six bursts from SAX J1810.8–269. The bursts are relatively bright and some of them have data gaps. Strong oscillations ( $P_{\rm m}=78.58$ , 74.28 on the non-normalized data) were discovered at  $\sim 531\,{\rm Hz}$  in the B region of one of the bursts (Fig. 39). For the adopted detection threshold, the signal is present in one independent 4-s time window. None of the simulations had a signal with similar power. Subthreshold candidates with  $P_{\rm m}\gtrsim 24$  are detected in two consecutive 4-s windows, for the significance estimates of that see Bilous et al. (2018), which reports this discovery in more detail.

No low-frequency or noise candidates were detected from this source.

## REFERENCES

Altamirano, D., Casella, P., Patruno, A., Wijnands, R., & van der Klis, M. 2008, ApJL, 674, L45

Altamirano, D., Watts, A., Linares, M., et al. 2010a, MNRAS, 409, 1136

Altamirano, D., Linares, M., Patruno, A., et al. 2010b, MNRAS, 401, 223

Arzoumanian, Z., Gendreau, K. C., Baker, C. L., et al. 2014, in Proc. SPIE, Vol. 9144, Space Telescopes and Instrumentation 2014: Ultraviolet to Gamma Ray, 914420

Barrière, N. M., Krivonos, R., Tomsick, J. A., et al. 2015, ApJ, 799, 123

Bhattacharyya, S. 2007, MNRAS, 377, 198

Bhattacharyya, S., & Strohmayer, T. E. 2006, ApJL, 642, L161

—. 2007, ApJ, 656, 414

Bhattacharyya, S., Strohmayer, T. E., Markwardt, C. B., & Swank, J. H. 2006, ApJL, 639, L31

Bilous, A. V., Watts, A. L., Galloway, D. K., & in 't Zand, J. J. M. 2018, ApJL, 862, L4

Buccheri, R., Bennett, K., Bignami, G. F., et al. 1983, A&A, 128, 245

Casella, P., Altamirano, D., Patruno, A., Wijnands, R., & van der Klis, M. 2008, ApJL, 674, L41

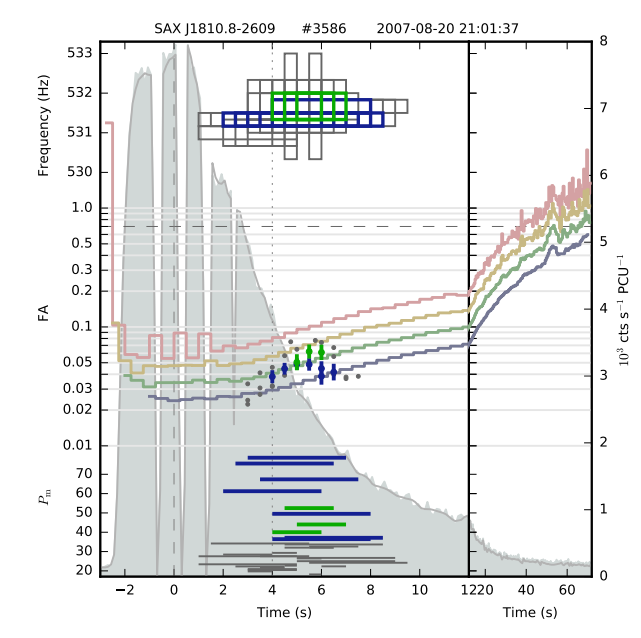


**Figure 39.** TBOs from a new oscillation source SAX J1810.8–269.

Cavecchi, Y., Patruno, A., Haskell, B., et al. 2011, ApJL, 740, L8

- Chakrabarty, D., Morgan, E. H., Muno, M. P., et al. 2003, Nature, 424, 42
- Chakraborty, M., & Bhattacharyya, S. 2012, MNRAS, 422, 2351
- Fox, D. W., Lewin, W. H. G., Rutledge, R. E., et al. 2001, MNRAS, 321, 776
- Galloway, D. K., Chakrabarty, D., Muno, M. P., & Savov, P. 2001, ApJL, 549, L85
- Galloway, D. K., Lin, J., Chakrabarty, D., & Hartman, J. M. 2010, ApJL, 711, L148
- Galloway, D. K., Muno, M. P., Hartman, J. M., Psaltis, D., & Chakrabarty, D. 2008, ApJS, 179, 360
- Garcia, F., Chambers, F. R. N., & Watts, A. L. 2018, ArXiv e-prints, arXiv:1806.10679
- Groth, E. J. 1975, ApJS, 29, 285
- Haensel, P., Zdunik, J. L., Bejger, M., & Lattimer, J. M. 2009, A&A, 502, 605
- Heyl, J. S. 2004, ApJ, 600, 939
- in't Zand, J. 2017, in 7 years of MAXI: monitoring X-ray
   Transients, held 5-7 December 2016 at RIKEN, ed.
   M. Serino, M. Shidatsu, W. Iwakiri, & T. Mihara, 121
- Jahoda, K., Markwardt, C. B., Radeva, Y., et al. 2006, ApJS, 163, 401
- Jahoda, K., Swank, J. H., Giles, A. B., et al. 1996, in Proc. SPIE, Vol. 2808, EUV, X-Ray, and Gamma-Ray Instrumentation for Astronomy VII, ed. O. H. Siegmund & M. A. Gummin, 59–70
- Kaaret, P., in 't Zand, J. J. M., Heise, J., & Tomsick, J. A. 2002, ApJ, 575, 1018
- —. 2003, ApJ, 598, 481
- Kaaret, P., Prieskorn, Z., in 't Zand, J. J. M., et al. 2007, ApJL, 657, L97
- Keek, L., Arzoumanian, Z., Chakrabarty, D., et al. 2018, ApJ, 856, L37
- Kuulkers, E., Homan, J., van der Klis, M., Lewin, W. H. G., & Méndez, M. 2002, A&A, 382, 947
- Leahy, D. A., Elsner, R. F., & Weisskopf, M. C. 1983, ApJ, 272, 256
- Linares, M., Altamirano, D., Watts, A., et al. 2011, The Astronomer's Telegram, 3568
- Mahmoodifar, S., & Strohmayer, T. 2016, ApJ, 818, 93
- Markwardt, C. B., Strohmayer, T. E., & Swank, J. H. 1999, ApJL, 512, L125
- Matsumoto, M., & Nishimura, T. 1998, ACM Trans. Model. Comput. Simul., 8, 3
- Miller, M. C. 1999, ApJL, 515, L77
- —. 2000, ApJ, 531, 458
- Muno, M. P., Chakrabarty, D., Galloway, D. K., & Psaltis, D. 2002a, ApJ, 580, 1048

- Muno, M. P., Özel, F., & Chakrabarty, D. 2002b, ApJ, 581, 550
- Ootes, L. S., Watts, A. L., Galloway, D. K., & Wijnands, R. 2017, ApJ, 834, doi:10.3847/1538-4357/834/1/21
- Patruno, A. 2012, ApJL, 753, L12
- Piro, A. L., & Bildsten, L. 2005, ApJ, 629, 438
- Ray, P. S., Arzoumanian, Z., Brandt, S., et al. 2018, in Society of Photo-Optical Instrumentation Engineers (SPIE) Conference Series, Vol. 10699, Space Telescopes and Instrumentation 2018: Ultraviolet to Gamma Ray, 1069919
- Smith, D. A., Morgan, E. H., & Bradt, H. 1997, ApJL, 479, L137
- Strohmayer, T. E., Jahoda, K., Giles, A. B., & Lee, U. 1997a, ApJ, 486, 355
- Strohmayer, T. E., Markwardt, C. B., & Kuulkers, E. 2008, ApJL, 672, L37
- Strohmayer, T. E., Markwardt, C. B., Swank, J. H., & in't Zand, J. 2003, ApJL, 596, L67
- Strohmayer, T. E., Zhang, W., & Swank, J. H. 1997b, ApJL, 487, L77
- Strohmayer, T. E., Zhang, W., Swank, J. H., et al. 1996, ApJL, 469, L9
- Strohmayer, T. E., Zhang, W., Swank, J. H., White, N. E., & Lapidus, I. 1998, ApJL, 498, L135
- Thompson, T. W. J., Rothschild, R. E., Tomsick, J. A., & Marshall, H. L. 2005, ApJ, 634, 1261
- van der Klis, M. 1989, in NATO Advanced Science Institutes (ASI) Series C, Vol. 262, NATO Advanced Science Institutes (ASI) Series C, ed. H. Ögelman & E. P. J. van den Heuvel, 27
- van der Klis, M. 2006, Rapid X-ray Variability, ed. W. H. G. Lewin & M. van der Klis, 39–112
- van Straaten, S., van der Klis, M., Kuulkers, E., & Méndez, M. 2001, ApJ, 551, 907
- Verdhan Chauhan, J., Yadav, J. S., Misra, R., et al. 2017, ApJ, 841, 41
- Villarreal, A. R., & Strohmayer, T. E. 2004, ApJL, 614, L121
- von Neumann, J. L. 1951, Nat. Bureau Standards, 12, 36 Watts, A. L. 2012, ARA&A, 50, 609
- Watts, A. L., Patruno, A., & van der Klis, M. 2008, ApJL, 688, L37
- Watts, A. L., & Strohmayer, T. E. 2006, MNRAS, 373, 769
- Watts, A. L., Strohmayer, T. E., & Markwardt, C. B. 2005, ApJ, 634, 547
- Watts, A. L., Altamirano, D., Linares, M., et al. 2009, ApJL, 698, L174
- Wijnands, R., Strohmayer, T., & Franco, L. M. 2001, ApJL, 549, L71

Wijnands, R., & van der Klis, M. 1998, Nature, 394, 344

Worpel, H., Galloway, D. K., & Price, D. J. 2013, ApJ, 772, \$94\$

 $--.\ 2015,\ ApJ,\ 801,\ 60$ 

Zhang, S., Santangelo, A., Feroci, M., et al. 2019, Science China Physics, Mechanics, and Astronomy, 62, 29502Zhang, W., Jahoda, K., Kelley, R. L., et al. 1998, ApJL, 495, L9

Zhang, W., Jahoda, K., Swank, J. H., Morgan, E. H., & Giles, A. B. 1995, ApJ, 449, 930